

January 2015

# Synthesis and Fabrication of Graphene/ Conducting Polymer/Metal Oxide Nanocomposite Materials for Supercapacitor Applications

Mohamad Khawaja

University of South Florida, mkhawaja@mail.usf.edu

Follow this and additional works at: <http://scholarcommons.usf.edu/etd>

 Part of the [Electrical and Computer Engineering Commons](#), and the [Materials Science and Engineering Commons](#)

## Scholar Commons Citation

Khawaja, Mohamad, "Synthesis and Fabrication of Graphene/Conducting Polymer/Metal Oxide Nanocomposite Materials for Supercapacitor Applications" (2015). *Graduate Theses and Dissertations*.  
<http://scholarcommons.usf.edu/etd/5715>

This Dissertation is brought to you for free and open access by the Graduate School at Scholar Commons. It has been accepted for inclusion in Graduate Theses and Dissertations by an authorized administrator of Scholar Commons. For more information, please contact [scholarcommons@usf.edu](mailto:scholarcommons@usf.edu).

Synthesis and Fabrication of Graphene/Conducting Polymer/Metal Oxide Nanocomposite  
Materials for Supercapacitor Applications

by

Mohamad K. Khawaja

A dissertation submitted in partial fulfillment  
of the requirements for the degree of  
Doctor of Philosophy  
Department of Electrical Engineering  
College of Engineering  
University of South Florida

Co-Major Professor: Elias Stefanakos, Ph.D.  
Co-Major Professor: G. Yogi Goswami, Ph.D.  
Manoj K. Ram, Ph.D.  
Arash Takshi, Ph.D.  
Sarath Witanachchi, Ph.D.

Date of Approval:  
June 30, 2015

Keywords: Specific Capacitance, Energy Density, Electrode Deposition, Electrolytes,  
Electrochemical Characterization

Copyright © 2015, Mohamad K. Khawaja

## ACKNOWLEDGMENTS

I would like to thank the Clean Energy Research Center (CERC) and my advisors, Drs. Elias Stefanakos and Yogi Goswami, for affording me the great opportunity to work on their research team and for their constant guidance throughout this work. I would like to thank my committee members for their time and help. I would especially like to thank Drs. Arash Takshi and Manoj Ram for their tremendous help and support.

Special thanks to all the CERC and Department of Electrical Engineering staff and colleagues who made my time and my research at USF experience pleasurable and memorable.

## TABLE OF CONTENTS

LIST OF TABLES .....	iv
LIST OF FIGURES .....	v
ABSTRACT .....	viii
CHAPTER 1: INTRODUCTION .....	1
1.1 Objectives of the Dissertation .....	4
1.2 Organization of the Dissertation .....	5
CHAPTER 2: OVERVIEW OF SUPERCAPACITORS .....	7
2.1 Introduction .....	7
2.2 Supercapacitor's Storage Mechanism .....	8
2.2.1 Electric Double Layer Capacitance (EDLC) .....	10
2.2.2 Pseudocapacitance .....	13
2.3 Supercapacitors Electrode Materials .....	14
2.3.1 EDLC Electrode Materials .....	14
2.3.1.1 Carbon Nanotubes (CNTs).....	16
2.3.1.2 Graphene .....	17
2.3.2 Pseudocapacitors Electrode Materials .....	20
2.3.2.1 Transition Metal Oxides (TMOs).....	20
2.3.2.2 Conducting Polymers (CPs).....	21
2.3.2.2.1 Polyaniline (PANI).....	23
2.3.3 Composite Materials .....	24
2.4 Design of Supercapacitors .....	26
2.4.1 Electrolytes .....	27
2.4.1.1 Aqueous Electrolytes .....	28
2.4.1.2 Organic Electrolytes .....	29
2.4.1.3 Other Electrolytes .....	29
2.4.2 Current Collectors .....	30
2.4.3 Separators .....	31
2.5 Electrochemical Measurement Techniques .....	31
2.5.1 Cyclic Voltammetry (CV).....	32
2.5.2 Constant Current Charge/Discharge (CCCD).....	33
2.5.3 Electrochemical Impedance Spectroscopy (EIS).....	34
2.6 Supercapacitor Performance Evaluation .....	35

<b>CHAPTER 3: METHODOLOGY AND APPROACH FOR ELECTRODE MATERIAL DEPOSITION .....</b>	<b>38</b>
3.1 Introduction .....	38
3.2 Preparation of G <sub>c</sub> Electrodes .....	39
3.2.1 G <sub>c</sub> /PVDF Electrodes .....	39
3.2.2 Binder-Free G <sub>c</sub> Electrodes .....	40
3.2.3 Gel Electrolyte.....	41
3.3 Electrochemical Characterizations .....	42
3.4 Discussion .....	44
3.5 Conclusions .....	45
<b>CHAPTER 4: BARIUM STRONTIUM TITANATE AS A HIGH DIELECTRIC BLOCKING LAYER TO REDUCE THE SUPERCAPACITOR SELF-DISCHARGE..</b>	<b>47</b>
4.1 Introduction .....	47
4.2 Preparation of Supercapacitor Electrodes .....	48
4.2.1 BST Electrophoresis Deposition .....	48
4.2.2 BST Synthesis .....	49
4.3 Electrode Characterizations .....	51
4.3.1 Morphology .....	51
4.3.2 Electrochemical Characterizations .....	53
4.4 Conclusions .....	59
<b>CHAPTER 5: SOL-GEL SYNTHESIS OF RUTHENIUM OXIDE-GRAPHENE NANOCOMPOSITES AS ELECTRODE MATERIAL FOR SUPERCAPACITORS ....</b>	<b>60</b>
5.1 Introduction .....	60
5.2 Experimental .....	60
5.2.1 Material Synthesis .....	60
5.2.2 Characterization.....	61
5.2.3 Electrode Preparation .....	61
5.2.4 Electrochemical Measurements.....	62
5.3 Results and Discussion .....	62
5.4 Conclusions .....	67
<b>CHAPTER 6: THE EFFECTS OF VARYING THE MASS LOADING ON MoS<sub>2</sub>-PANI SUPERCAPACITOR ELECTRODES.....</b>	<b>69</b>
6.1 Introduction .....	69
6.2 Experimental .....	71
6.2.1 Synthesis of MoS <sub>2</sub> -PANI.....	71
6.2.2 Characterization.....	71
6.2.3 Electrode Preparation .....	71
6.2.4 Electrochemical Measurements.....	72
6.3 Results and Discussion .....	73
6.4 Conclusions .....	82

CHAPTER 7: CONCLUSIONS AND RECOMMENDATIONS FOR FUTURE WORK ....	84
7.1 Conclusions .....	84
7.2 Recommendations for Future Work .....	85
REFERENCES .....	88
APPENDIX A: COMMERCIAL BARIUM STRONTIUM TITANATE DATASHEET ....	102
APPENDIX B: COPYRIGHT PERMISSIONS FOR FIGURES AND TABLES .....	103

## LIST OF TABLES

Table 2.1 EDLC and pseudocapacitance comparison .....	10
Table 2.2 Comparison EDCL vs. batteries .....	13
Table 2.3 Properties and characteristics of various carbon and carbon-based materials as supercapacitor electrode materials.....	14
Table 2.4 The properties of graphene compared to other carbon allotropes .....	18
Table 2.5 Reported work on TMOs as supercapacitor electrode materials .....	20
Table 2.6 CPs supercapacitor electrodes based on synthesis method .....	22
Table 2.7 Reported work on composite materials as electrodes for supercapacitors .....	25
Table 2.8 Ion sizes of inorganic electrolytes and aqueous solutions' ionic conductivity.....	28
Table 2.9 Ion sizes of some organic electrolytes and organic solvents' properties .....	29
Table 2.10 The nomenclature to identify different types of specific capacitance .....	36
Table 3.1 Specific capacitance values obtained from CV .....	42
Table 3.2 Circuit model parameters' values .....	42
Table 4.1 $C_g$ , $C_a$ and the percentage of drop in specific capacitance after $BST_c$ deposition.....	55
Table 4.2 EIS fitting parameters' values .....	57
Table 6.1 Evaluation of $MoS_2$ -PANI electrodes with varying mass loading.....	76
Table 6.2 List of $MoS_2$ and $MoS_2$ -composites as electrode materials for supercapacitors ...	81

## LIST OF FIGURES

Figure 1.1 Specific power against specific energy, also called a Ragone plot, for various electrical energy storage devices .....	2
Figure 2.1 (a) Simplified schematic of capacitor design .....	8
Figure 2.2 Types of supercapacitors grouped by their dominating charge storage mechanism and the typical materials used.....	9
Figure 2.3 Charge accumulation on the electrolyte leading to the adsorption of electrolyte ions on the surface of the anode and cathode .....	10
Figure 2.4 Models of the electrical double layer at a positively charged surface.....	11
Figure 2.5 The double layer equivalent capacitance, $C_{dl}$ , is the series combination of the Helmholtz capacitance and the diffuse layer capacitance .....	12
Figure 2.6 Properties and applications of graphene spheres, CNTs, and graphene sheets and visualization of their structural formation .....	19
Figure 2.7 Chemical structure of some of the main CPs.....	22
Figure 2.8 PANI's oxidation states at $y = 0.5$ (E), $y = 0$ (P), and $y = 1$ (L).....	24
Figure 2.9 (a) A cross-sectional view of a typical three-electrode supercapacitor cell .....	27
Figure 2.10 The electrical conduction through an electrode material with and without a conductive substrate .....	30
Figure 2.11 A typical CV signal where the potential is scan from initial voltage to a final voltage and the back to the initial voltage .....	32
Figure 2.12 The equivalent circuits of (a) EDLC, and (b) pseudocapacitor .....	34
Figure 2.13 Digital image of the Radiometer Analytical Voltalab 40 that was used for all the electrochemical characterizations .....	35
Figure 2.14 An illustration of key performance metrics, test methods, major affecting factors for the evaluation of supercapacitors .....	36



Figure 3.1 Two $G_c$ :PVDF electrodes on graphite with PVA- $H_3PO_4$ gel electrolyte sandwiched in the middle .....	39
Figure 3.2 Doctor blade used to smooth the surface of the electrodes .....	40
Figure 3.3 Deposition stages of binder-free $G_c$ using an alumina membrane .....	41
Figure 3.4 Electrochemical characterization of $G_c$ /PVDF .....	43
Figure 3.5 Electrochemical characterization of $G_c$ .....	43
Figure 3.6 Films of different graphene-CPs composites and CPs completely break before they can be deposited onto a substrate.....	45
Figure 4.1 $BST_c$ deposition process on ITO-PET substrates .....	49
Figure 4.2 $BST_s$ sol-gel synthesis structure.....	50
Figure 4.3 TGA of the sol-gel synthesized $BST_s$ powder .....	51
Figure 4.4 SEM images .....	52
Figure 4.5 Aqueous electrolyte detaching the $G_c$ film from the ITO-PET substrate .....	53
Figure 4.6 Gravimetric (a-b) and areal (c-d) CVs of $G_c$ / $BST_c$ at different deposition times at $50 \text{ mV s}^{-1}$ scan rate .....	54
Figure 4.7 (a) gravimetric and areal CVs of D2 and D3 supercapacitors at $50 \text{ mV s}^{-1}$ scan rate.....	56
Figure 4.8 (a) uniform blocking layer model and (b) $G_c$ / $BST_c$ model .....	56
Figure 4.9 (a) and (b) measured and fitted EIS of $G_c$ and $G_c$ / $BST_c$ at different deposition times .....	57
Figure 4.10 Open circuit potentials of $G_c$ and $G_c$ / $BST_c$ (4 min) over a 12 hour period.....	58
Figure 5.1 Morphology images of different synthesized powders .....	63
Figure 5.2 EDS peaks .....	64
Figure 5.3 XRD diffraction peaks of $RuO_2$ -G at a 10:1 ratio .....	64
Figure 5.4 (a) CV of synthesized $RuO_2$ , $RuO_2$ -G 10:1 ratio, and $RuO_2$ -G 1:1 ratio in $2M H_2SO_4$ at $20 \text{ mV s}^{-1}$ scan rate .....	66

Figure 5.5 EIS of the synthesized RuO <sub>2</sub> , RuO <sub>2</sub> -G at the 10:1 ratio, and RuO <sub>2</sub> -G at the 1:1 ratio in 2M H <sub>2</sub> SO <sub>4</sub> .....	67
Figure 6.1 The graphite substrates and deposition micro-needle (inset) .....	72
Figure 6.2 (a) FT-IR and (b) XRD peaks of synthesized MoS <sub>2</sub> -PANI.....	73
Figure 6.3 SEM images of MoS <sub>2</sub> -PANI electrodes .....	74
Figure 6.4 CV of MoS <sub>2</sub> -PANI electrodes .....	75
Figure 6.5 CCCD of MoS <sub>2</sub> -PANI electrodes .....	77
Figure 6.6 The stability of MoS <sub>2</sub> -PANI over 100 cycles at 100 mV s <sup>-1</sup> scan rate .....	77
Figure 6.7 EIS of MoS <sub>2</sub> -PANI electrodes .....	78
Figure 6.8 MoS <sub>2</sub> -PANI electrodes' specific capacitance as a function the mass loading .....	81
Figure 7.1 Supercapacitor devices .....	86
Figure A1 BST datasheet .....	102

## ABSTRACT

The rising energy consumption worldwide is leading to significant increases in energy production with fossil fuels being the major energy source. The negative environmental impact of fossil fuel use and its finite nature requires the use of alternative sources of energy. Solar energy is a clean alternative energy source; however, its intermittent nature is a major impediment that needs to be reduced or eliminated by the development of cost effective energy storage. Thermal storage in tanks filled typically with molten salt at elevated temperatures is widely used in concentrating solar power plants to generate electricity during periods of low daytime solar radiation or night time. Similarly, electrical storage in batteries, etc. is used in conjunction with photovoltaic solar power plants.

Electrochemical supercapacitors can be effectively used for electrical storage, either alone or in a hybrid configuration with batteries, for large scale energy storage as well as in electric vehicles and portable electronics. Unlike batteries', supercapacitor electrodes can be made of materials that are either less toxic or biodegradable and can provide almost instantaneous power due to their unique charge storage mechanism similar to conventional capacitors found in most electronics. Unfortunately, the same storage mechanism prevents supercapacitors from having high energy density. The purpose of this dissertation is to investigate organic and inorganic electrode materials that can increase the specific capacitance and energy density of supercapacitors. Additionally, certain types of supercapacitor electrode

materials store the charges at the electrode/electrolyte interface preventing any deformation of the material and thus increasing its cycle life by two to three orders of magnitude.

Transition metal oxides, layered transition metal chalcogenides, and their composites with graphene and conducting polymers have been synthesized, characterized, and their electrochemical performances evaluated for suitability as electrode materials for supercapacitor applications. Morphology and crystalline structure characterization methods used, such as scanning electron microscopy (SEM), transmission electron microscopy (TEM), energy dispersive spectroscopy (EDS), X-ray diffraction (XRD), and Fourier transform infrared spectroscopy (FT-IR), were used throughout this work. Electrochemical characterization involved cyclic voltammetry (CV), constant current charge and discharge (CCCD), and electrochemical impedance spectroscopy (EIS) in two and three electrode configuration using aqueous and organic electrolytes.

Ruthenium oxide-graphene ( $\text{RuO}_2\text{-G}$ ) electrodes were tested in the two-electrode cell configuration and exhibit an areal capacitance of  $187.5 \text{ mF cm}^{-2}$  in  $2\text{M H}_2\text{SO}_4$  at a  $\text{RuO}_2\text{:G}$  ratio of 10:1. Due to  $\text{RuO}_2$  high toxicity, scarcity, and high cost, manganese oxide-graphene ( $\text{MnO-G}$ ) was used as an alternative but its low specific capacitance remains a major stumbling block.

The electrodes' mass loading was studied in detail to understand the effects of thickness on the measured specific capacitance. Layered transition metal chalcogenides are structurally similar to graphene but possess different characteristics. Molybdenum sulfide ( $\text{MoS}_2$ ) is a two-dimensional material that has lower conductivity than graphene but larger sheet spacing making it easy for other materials to intercalate and form composites such as molybdenum sulfide-polyaniline ( $\text{MoS}_2\text{-PANI}$ ).  $\text{MoS}_2\text{-PANI}$  electrodes, with different thicknesses, were measured in a three-electrode cell configuration resulting in gravimetric capacitance of  $203 \text{ F g}^{-1}$  for the

thinnest electrode and areal capacitance of  $358 \text{ mF cm}^{-2}$  for the thickest electrode; all measurements performed using  $1\text{M H}_2\text{SO}_4$  aqueous electrolyte.

Attempts were also made to reduce the supercapacitor self-discharge by depositing on the electrode a blocking thin layer of barium strontium titanate (BST). The results were rather inconclusive because of the large thickness of the deposited BST layer. However, they strongly suggest that a very thin BST layer could improve the overall capacitance because of the very large dielectric constant of the BST material. Additional work is required to determine its effects on self-discharge.

## CHAPTER 1: INTRODUCTION

Energy production and supply is the main catalyst in the modernization of our civilization over the past two centuries. The finite nature of the global energy sources, mainly fossil fuels in the form of natural gas, petroleum, and coal, prompts the immediate attention into looking elsewhere for sources of energy that can complement the current supply with a view of overtaking them in the future. Renewable energy sources consisting mainly of hydroelectric, solar, wind, and biomass are considered clean alternatives to conventional energy production sources; however, according to the U.S. Energy Information Administration (EIA) in its primary energy overview of 2014, renewables accounted for less than 10% of the total energy production. While the utilization of renewable energy is low, it is a step in the right direction as the challenge is not only in finding alternatives to diminishing energy sources but also in protecting the environment from carbon dioxide (CO<sub>2</sub>) emission resulting for burning carbon fossil fuels [1].

The intermittency of renewable energy, especially wind and solar, prevents it from seriously competing against fossil fuels but regulating its supply by means of energy storage could vastly improve its usability and integration for mass production. Energy storage importance is not only for the regulation of otherwise a fluctuating energy production but also, on a smaller scale, for electronic devices and transportation.

Batteries, fuel cells, and supercapacitors (also known as electrochemical capacitors (ECs), electrochemical supercapacitors (ESs), or ultracapacitors) are electrochemical storage devices that are capable of storing charges through different mechanisms. Supercapacitors are of

particular interest due to their high power density and cycle life, compared to batteries. Supercapacitors are considered as one of the main elements in the future of energy storage according to the technology roadmap of the International Energy Agency (IEA). The BCC Research, in its 2011 report (title: Supercapacitors: Technology Developments and Global Markets) estimates the 2010 supercapacitors market was valued at \$470 million and will be reaching \$1.2 billion in 2015.

Comparison of specific power and specific energy (also known as the Ragone plot [2]) of storage devices is shown in Figure 1.1. As it can be seen conventional capacitors possess large power density but very low energy density while the opposite is true for batteries and fuel cells. Supercapacitors attempt to bridge the gap between conventional capacitors and batteries. The times shown in Figure 1.1 indicate the time constant of the devices obtained by dividing the energy density by the power density.

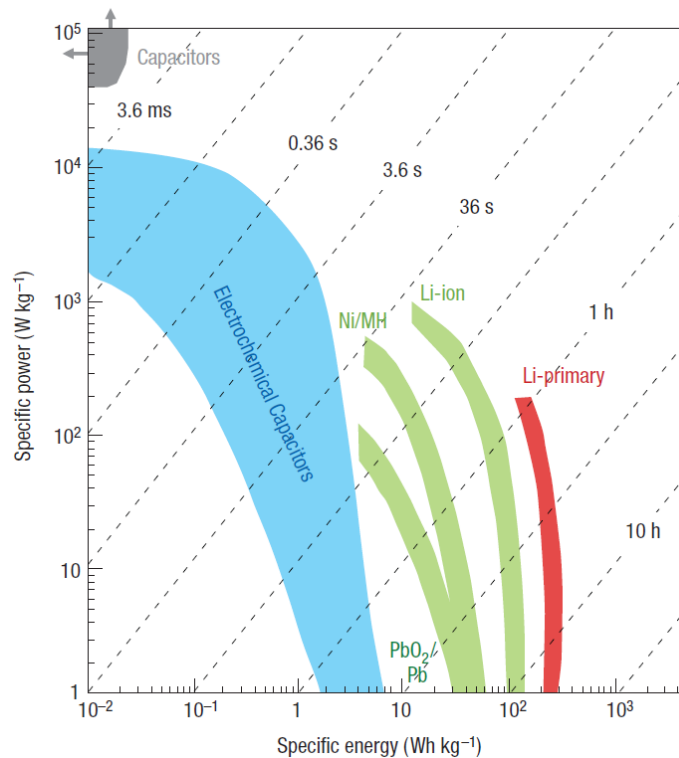


Figure 1.1 Specific power against specific energy, also called a Ragone plot, for various electrical energy storage devices [2].

Supercapacitor electrodes are fabricated with unique materials that possess very high surface area such as activated carbon (AC), graphene, and carbon nanotubes (CNTs). The high surface area enables the supercapacitor to store more charges at the electrode/electrolyte interface than at the metal plate/dielectric layer of conventional capacitors. In addition to the high surface area of graphene and CNTs electrodes, their high electric conductivity and charge retention after multiple cycles (>100000) make them attractive for energy storage. Pseudocapacitors, another form of supercapacitors, can store charges in a mechanism that is analogous to that seen in batteries through the oxidation and reduction (redox) of organic (conducting polymers (CPs)) and inorganic (transition metal oxides (TMOs) or metal sulfides) electrode materials. CP electrodes have not been able to achieve high charge retention but their use in composites with graphene and CNTs have shown notable improvement in their stability as well as increase in their charge storage capabilities.

The major drawbacks in supercapacitors are their low energy density, even though it is higher than in conventional capacitors, it is an order of magnitude lower than that of batteries. The low energy density is attributed to the limited operation voltage window due to thermodynamic limitations in the electrolytes. Aqueous electrolytes are limited to 1 V while organic electrolytes can reach up to 2.7 V which still does allow the energy density of supercapacitors to be comparable to batteries. Ionic liquids and gel electrolytes can increase the operating voltages to 4 V but their low conductivity at room temperature and over a short amount of time, respectively, is a stumbling block in enhancing the energy density of supercapacitors. Increasing the charge storage capabilities by developing next-generation electrode materials can improve the energy density while maintaining the high power density of these devices.



Self-discharge is another major flaw of supercapacitors. The recombination of charges through Faradaic reactions when the supercapacitor is idle leads to a reduction in its shelf life. Depositing a thin layer of an insulating material, while it will reduce the overall capacitance, it can reduce the self-discharge. A compromise between the charge storage capability and self-discharge has to be carefully considered to make supercapacitors that can still perform as desired.

### **1.1 Objectives of the Dissertation**

The work of this dissertation is focused on supercapacitors. The main objectives are to address the fundamental problems with supercapacitors: (i) reduce the self-discharge, and (ii) improve the charge storage capabilities which will in turn enhance the energy density.

To reach the first objective of reducing self-discharge, a blocking layer of a high dielectric insulating material, barium strontium titanate (BST), is applied to graphene electrodes. The open circuit potential is measured after charging the electrodes for a long time with and without BST. The equivalent circuits are carefully considered to understand the effect of BST on the overall performance of supercapacitors.

The second objective is to develop the next-generation electrode materials than can enhance the capacitance and energy of supercapacitors. To reach this objective, ruthenium oxide ( $\text{RuO}_2$ ) is synthesized and compared to the synthesized composites of graphene and ruthenium oxide (G- $\text{RuO}_2$ ).  $\text{RuO}_2$  electrodes have yielded high capacitance values compared to other MOs and CPs but their high cost and scarcity prevents their commercial use. The integration of graphene at different weight ratios can provide an alternative to using pure  $\text{RuO}_2$  electrodes thus reducing the cost of making  $\text{RuO}_2$  based supercapacitors.

Additionally, molybdenum sulfide and polyaniline (MoS<sub>2</sub>-PANI) is another composite electrode material investigated for enhanced supercapacitor electrodes performances; the structural similarity of MoS<sub>2</sub> to graphene gives it a particular interest while PANI's previous use in graphene composites makes it an excellent candidate for this study. The thickness of the electrode material is also considered to further understand the effect it has on the performance of supercapacitors.

The materials developed are tested through electrochemical measurements and their morphology is imaged by scanning electron microscopy (SEM) and transmission electron microscopy (TEM). The structure is identified by X-ray diffraction (XRD), energy dispersive spectroscopy (EDS), and Fourier transform infrared spectroscopy (FT-IR).

## **1.2 Organization of the Dissertation**

The structure of the dissertation can be summarized as follows.

Chapter 1 describes the motivation behind the investigation of different composite materials that can be used as supercapacitor electrodes as well as investigation of self-discharge and the effects of depositing a blocking layer on electrode surface.

Chapter 2 is dedicated for the overview of supercapacitors explaining the two different storage mechanisms involved, the various parts included in the design and fabrication of supercapacitors with emphasis on the electrode materials and composites, measurements techniques, and literature background of pervious work in carbon materials, TMOs, and CPs.

Chapter 3 illustrates the deposition methods used to apply the electrode material on the substrates: (i) the use of a binder to ensure complete adhesion and its effects on the electrode material, and (ii) the use of alumina membrane as an alternative deposition technique to eliminate the use of binders to deposit the electrode material on the substrates.

Chapter 4 examines the deposition of BST through the electrophoresis technique on the surface of graphene electrodes to evaluate the effects on specific capacitance and self-discharge and to attempt to understand the role of the high dielectric constant of BST on the storage mechanism of supercapacitors.

Chapter 5 investigates the effects of varying the weight ratio of graphene to RuO<sub>2</sub> on the specific capacitance of supercapacitors in various electrolytes and describes the synthesis process of RuO<sub>2</sub> and composite G-RuO<sub>2</sub>.

Chapter 6 evaluates the electrochemical behavior of composite MoS<sub>2</sub>-PANI as an electrode material and studies the effects of electrode's mass loading on the overall performance of supercapacitors while also discussing the different methods in the evaluation of supercapacitors.

Chapter 7 concludes the dissertation stating the major findings and addressing the aforementioned objectives also proposing future work to continue the investigation of new electrode materials that can enhance the overall capacitance and electrolytes than can work with a large potential window to allow for the highest energy density possible.

## CHAPTER 2: OVERVIEW OF SUPERCAPACITORS

### 2.1 Introduction

Supercapacitors are energy storage devices that can store charges electrostatically at the electrode/electrolyte interface[3] or in the electrochemically active electrode layers by means of reversible reduction and oxidation (redox) reactions[2].

In 1745 the Leyden (Leiden) jar was discovered by German cleric Ewald George von Kleist and simultaneously by Dutch scientist Pieter van Musschenbroek [4-5]. The Leyden jar consisted of two metal foils wrapped around the inner and outer surfaces of a glass jar filled with aqueous acidic solution. The metal foils acted as electrodes while the glass jar acted as the dielectric between the inner and outer electrodes as shown in Figure 2.1. This was the concept of the first capacitor that was earlier referred to as a condenser. When the planar parallel plates of the condenser were polarized, equal charges of opposite magnitudes accumulated on the surface of each plate inducing a potential difference. The relationship between the charge and potential (voltage) is defines as:

$$Q = CV \quad (2.1)$$

where Q is the summation of the absolute values of charges on the parallel plates, V is the induced potential difference, and C is the proportionality constant that is referred to as the capacitance of the condenser. The term condenser was later dropped in favor of a new term to describe this device, capacitor. From Equation 2.1, the capacitance can be described as the charge accumulated on the surface of the plates divided by the potential of the capacitor:

$$C = \frac{Q}{V} = \frac{\epsilon_r \epsilon_o A}{d} \quad (2.2)$$

where  $\epsilon_r$  is the dielectric constant of the parallel plates' separation layer,  $\epsilon_o$  is the dielectric constant of free space,  $d$  is the charge separation distance, and  $A$  is the surface area of the plates.

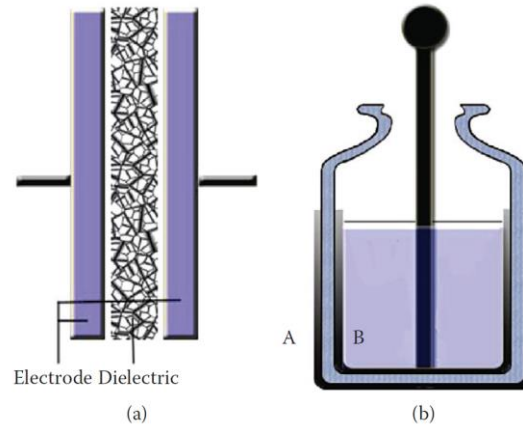


Figure 2.1 (a) Simplified schematic of capacitor design. (b) Cross-sectional schematic of Leyden jar (water-filled glass jar with metal foil electrodes on its inner and outer surfaces, denoted A and B) [5].

## 2.2 Supercapacitor's Storage Mechanisms

Similar to the aforementioned dielectric capacitor, a supercapacitor consists of a dielectric material separating the two parallel plates. However, supercapacitor plates are made of porous materials that have large specific surface area (SSA) and referred to as electrodes instead of planar plates. The dielectric materials separating the supercapacitor electrodes are mainly liquids known as electrolytes that allow for the deep penetration of their ions into the porous structure of the electrodes to utilize the large SSA.

The charge storage mechanism of the Leyden jar was not well understood until the nineteenth century when Herman von Helmholtz suggested a model of the ion distribution at the electrode/electrolyte interface [6]. Later, Gouy [7], Chapman [8], Stern [9], and Grahame [10] all contributed in modifying the original model to better understand and describe the theory behind the charge storage mechanism. H. I. Becker, from General Electric Company, was the first to file

a patent for an electric double layer capacitor consisting of porous carbon electrodes in an aqueous electrolyte operating at 2.5 V or less [11]. B. E. Conway developed the first pseudocapacitor in his laboratory which has a different charge storage mechanism than the one described in Becker's patent [12-13].

The two types of supercapacitors that are being heavily investigated, fabricated, evaluated, and commercially produced are: (i) the electric double layer capacitors (EDLC), and (ii) redox based pseudocapacitors; the fundamental difference between these two types is the way they store electric charges. The former uses a non-Faradaic process which relies on the electrostatic accumulation of charges at the electrode/electrolyte interface while the latter utilizes Faradaic redox reactions in which charges pass across the double layer giving rise to a Faradaic current passing through the cell. The taxonomy of supercapacitors is shown in Figure 2.2 and a comparison between EDLC and pseudocapacitance is shown in Table 2.1.

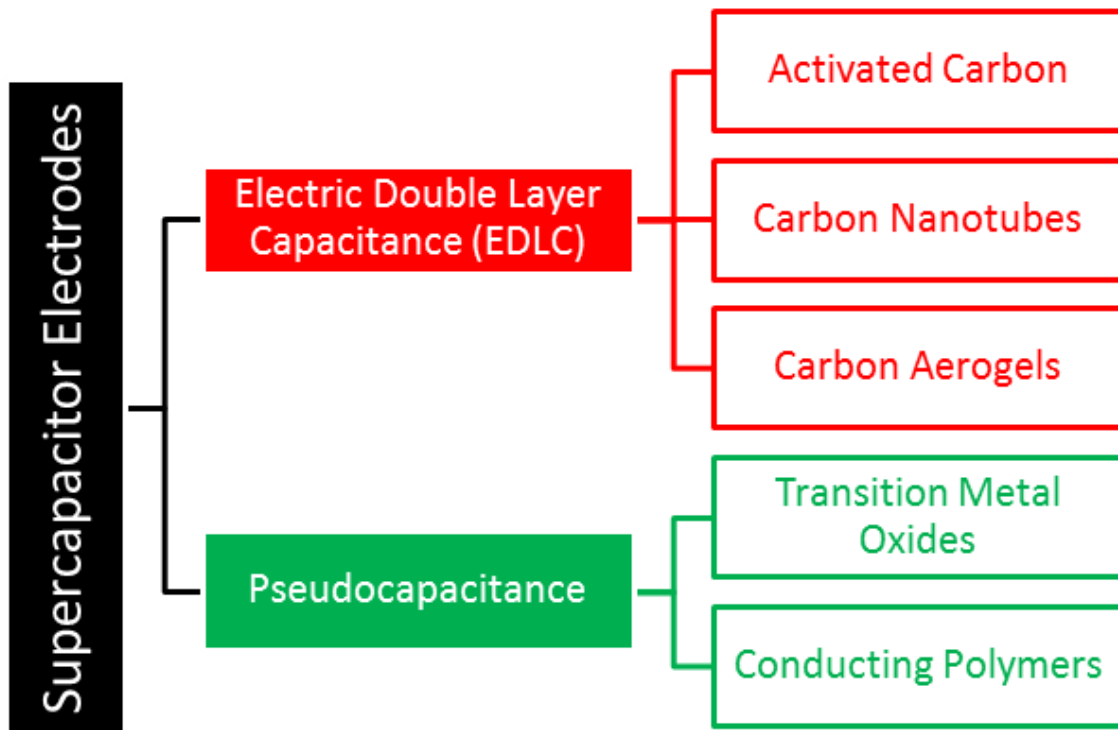


Figure 2.2 Types of supercapacitors grouped by their dominating charge storage mechanism and the typical materials used.

Table 2.1 EDLC and pseudocapacitance comparison [14].

EDLC	Pseudocapacitance
Non-Faradaic	Involves Faradaic process(es)
20-50 $\mu\text{F}/\text{cm}^2$	2000 $\mu\text{F}/\text{cm}^2$ for a single-state process; 200-500 $\mu\text{F}/\text{cm}^2$ for multi-state, overlapping process
C fairly constant with potential, except through the potential of zero charge	C fairly constant with potential for $\text{RuO}_2$ ; for single state process, exhibits marked maximum
Highly reversible charging/discharging	Can exhibit several maxima for overlapping, multi-state processes, as for H at Pt; quite reversible but has intrinsic electrode kinetic rate limitation determined by the Faradaic leakage resistance
Has restricted voltage range (contrast to non-electric electrostatic capacitor)	Has restricted voltage range
Exhibits mirror-image voltammograms	Exhibits mirror-image voltammograms

### 2.2.1 Electric Double Layer Capacitance (EDLC)

The charge in an EDLC is electrostatically accumulated at the electrode/electrolyte interface due to the electrolyte ions adsorption onto the surface of the electrode material. Negative charges accumulate on the cathode attracting electrolyte cations while the absence of electrons on the anode attracts the electrolyte anions as long as the EDLC is polarized by a potential that does not exceed the voltage window (breakdown voltage) of the electrolyte as shown in Figure 2.3.

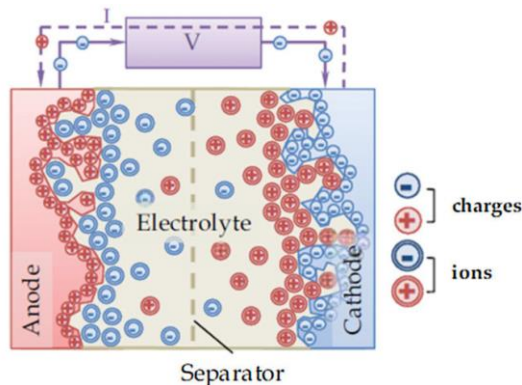


Figure 2.3 Charge accumulation on the electrolyte leading to the adsorption of electrolyte ions on the surface of the anode and cathode [15].

Helmholtz, first, attributed the capacitance to the accumulation of charges only at the electrode/electrolyte interface [6]. Later, the Gouy-Chapman model suggested that the charges were not only present at the electrode/electrolyte interface but also scattered in the diffuse layer of the electrolyte[7-8]. Stern [9] then combined the Helmholtz and the Gouy-Chapman models and expressed the double layer capacitance as the result of two arrays: (i) the charge accumulation of the Helmholtz layer at a thickness equal to the size of the solvent molecule, and (ii) the diffuse layer where charges are scattered due to thermal fluctuation [5] of the electrolyte. High free electron density causing charge density to be highly concentrated in the Thomas-Fermi screening distance leading to an overspill of electron density in the diffuse layer [4][16]. Stern was successful in correcting the Gouy-Chapman model that altered the original concept of the double layer capacitance as well as the overestimation of the values of the capacitance. Grahame, distinctly, concluded that due to the size difference between cations and anions, the Helmholtz layer thickness would not be uniform leading him to divide the Helmholtz layer into two regions, the inner Helmholtz and outer Helmholtz planes while maintaining the diffuse layer [10]. The representation of the EDLC models at one (positive) electrode is shown in Figure 2.4.

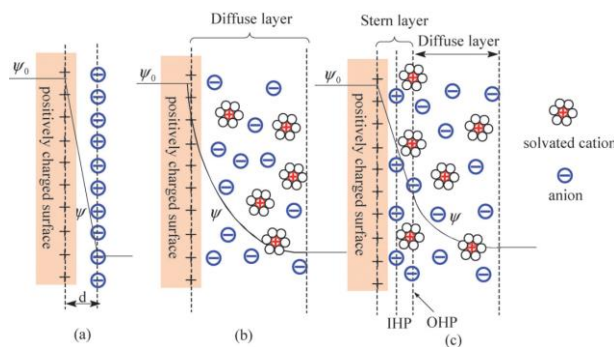


Figure 2.4 Models of the electrical double layer at a positively charged surface. (a) The Helmholtz model showing that the charge is only stored at the electrode surface with  $d$  as the double layer distance, (b) the Gouy-Chapman model introducing the diffuse layer and disregarding the Helmholtz region, and (c) the Stern-Grahame model showing that the charge is stored in the Helmholtz and the diffuse layer while also showing the Inner Helmholtz plane (IHP) and the Outer Helmholtz Plane (OHP).  $\psi_0$  is the electrode potential and  $\psi$  is the electrode/electrolyte potential [17].



The equivalent double layer capacitance at the electrode/electrolyte interface is the series combination of the Helmholtz, capacitance,  $C_H$ , and the diffuse layer capacitance,  $C_{diff}$ , as shown in Figure 2.5.

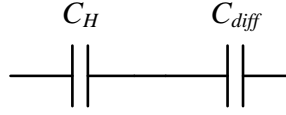


Figure 2.5 The double layer equivalent capacitance,  $C_{dl}$ , is the series combination of the Helmholtz capacitance and the diffuse layer capacitance.

The smaller capacitance between  $C_H$  and  $C_{diff}$  will always dominate the double layer capacitance and since the Helmholtz layer distance is smaller than the diffuse layer (the size of the solvent molecule in contrast to larger layer where excess ions disperse), while disregarding any change in the electrolyte's dielectric constant and temperature fluctuation,  $C_{diff}$  is bound to be smaller than  $C_H$  as indicated in the following equation:

$$\frac{1}{C_{dl}} = \frac{1}{C_H} + \frac{1}{C_{diff}} \quad \leftrightarrow \quad C_{dl} = \frac{C_H C_{diff}}{C_H + C_{diff}} \quad (2.3)$$

however, the concentration of the electrolyte is inversely proportional to the length of the diffuse layer, resulting is  $C_{diff}$  values closer to  $C_H$  [5].

Given the interfacial capacitance and atom density, the charge density along with Faraday's constant and Avogadro's number, the number of electrons stored per atom in an EDLC can be determined. For double layer materials, only a fraction of an electron is stored. Conversely one or multiple valence electrons per atom are involved in the redox reaction of batteries [4]. EDLC has no effect on the electrode material's structure and therefore can have very high number lifecycles compared to the batteries' electrochemical kinetics limitations as shown in Table 2.2.

Table 2.2 Comparison EDCL vs. batteries [18].

	EDLC	Batteries
Discharge time	0.3-30 s	0.3-3 h
Charge time	0.3-30 s	1-5 h
Energy density (Wh/kg)	1-10	10-100
Specific power (W/kg)	≈1000	50-200
Charge-discharge efficiency	0.85-0.98	0.7-0.85
Cycle life (years)	>100000 (30)	>500-2000 (5)

### 2.2.2 Pseudocapacitance

Pseudocapacitance is attributed to the Faradaic redox reaction of the electrochemically active electrode material. There are three types of Faradaic reaction processes [4] [5] [13] [19]: (i) reversible lithium intercalation, (ii) adsorption of hydrogen (H) or metal adatoms, known as underpotential deposition (UPD), on top of platinum (Pt) or gold (Au) electrode  $H^+ + e^- + Pt \leftrightarrow Pt - H_{ads}$ , and (iii) Faradaic redox reactions in the form of  $O_x + ne \leftrightarrow R_d$ , where  $O_x$  is the oxidant,  $R_d$  is the reductant, and  $n$  is the number of electrons involved in the reversible reaction and is best expressed by the Nernst equation:

$$E = E_{O_x/R_d}^0 + \frac{RT}{nF} \ln \left( \frac{C_{O_x}}{C_{R_d}} \right) \quad (2.4)$$

where  $E_{O_x/R_d}^0$  is the standard electrode potential of the reversible redox reaction,  $C_{O_x}$  and  $C_{R_d}$  are concentrations of  $O_x$  and  $R_d$  within the electrolyte ( $\text{mol cm}^{-3}$ ),  $R$  is the universal gas constant ( $8.314 \text{ J K}^{-1} \cdot \text{mol}^{-1}$ ),  $T$  is the temperature (K),  $F$  is the Faraday's constant ( $96485.3365 \text{ s.A mol}^{-1}$ ), and  $E$  is electrode potential that can be obtained using the theory of electrochemical thermodynamics governed by the Nernst equation. Assuming uniform concentrations, the Faradaic current flowing through the electrode can be shown as [20]:

$$i_F = nFd \frac{dC_{o_s}}{dt} \quad (2.5)$$

As the Faradaic current passes through the double layer region as well as the bulk of the electrode and if the pseudocapacitor has double layer capacitance contribution then the total capacitance at one electrode is the summation of the contribution of the pseudocapacitance,  $C_{pc}$ , and double layer capacitances:

$$C_{Total} = C_{dl} + C_{pc} \quad (2.6)$$

## 2.3 Supercapacitors Electrode Materials

### 2.3.1 EDLC Electrode Materials

The electrode's surface area is directly proportional to its capacitance, as seen in Equation 2.2. A wide range of carbon materials have been investigated as electrodes for supercapacitors [21]. Carbon fiber cloth [22-23], ACs [24-25], carbon aerogel [26-27], CNTs [28-29], and graphene[30-32] have all been synthesized and their supercapacitor performances evaluated. Table 2.3 lists some of the electrode properties of carbon materials.

Table 2.3 Properties and characteristics of various carbon and carbon-based materials as supercapacitor electrode materials [17] (Graphene is referenced separately).

Carbon materials	Specific surface area $m^2 g^{-1}$	Density $g cm^{-3}$	Aqueous electrolytes		Organic electrolytes	
			$F g^{-1}$	$F cm^{-3}$	$F g^{-1}$	$F cm^{-3}$
Commercial activate carbon (ACs)	1000-3500	0.4-0.7	< 200	< 80	< 100	< 50
Particulate carbon from SiC/TiC	1000-2000	0.5-0.7	170-220	< 120	100-120	< 70
Functionalized porous carbons	300-2200	0.5-0.9	150-300	< 180	100-150	< 90
Carbon nanotube (CNT)	120-500	0.6	50-100	< 60	< 60	< 30

Table 2.3 (Continued)

Carbon materials	Specific surface area $\text{m}^2 \text{g}^{-1}$	Density $\text{g cm}^{-3}$	Aqueous electrolytes		Organic electrolytes	
			$\text{F g}^{-1}$	$\text{F cm}^{-3}$	$\text{F g}^{-1}$	$\text{F cm}^{-3}$
Templated porous carbons (TC)	500-3000	0.5-1	120-350	< 200	60-140	< 100
Activated carbon fibers (ACF)	1000-3000	0.3-0.8	120-375	< 150	80-200	< 120
Carbon cloth	2500	0.4	100-200	40-80	60-100	24-40
Carbon aerogels	400-100	0.5-0.7	100-125	< 80	< 80	< 40
Graphene	> 2600 [33]	< 1 [34]	107 [35]	> 350 [36]	85 [35]	60 [31]

Depending on the activation method as well as the carbon precursors, surface area as high as  $3000 \text{ m}^2 \text{g}^{-1}$  was recorded with ranging pore sizes of macropores ( $> 50\text{nm}$ ), mesopores ( $2-50\text{nm}$ ), and micropores ( $< 2\text{nm}$ ) [17]. While large SSA is ideal for high performance supercapacitor electrodes, the recorded capacitance values are not always quite as large as those obtained from TMOs or CPs. The low density of carbon materials hinders their charge storage abilities in compact, battery-like, electrodes. The high volumetric capacitance of graphene in an aqueous electrolyte reported in the Table 2.3 was obtained by using a unique technique to dry the graphene hydrogel that condensed graphene and increased its density to  $1.58 \text{ g cm}^{-3}$  but reduced its SSA to  $370 \text{ m}^2 \text{g}^{-1}$  only while maintaining its porosity. This indicates that carbon materials, graphene especially, can be manipulated to perform favorably towards the desired outcome.

### 2.3.1.1 Carbon Nanotubes (CNTs)

CNTs are nearly one-dimensional (1D)  $sp^2$ -bonded single graphite layer wrapped in cylindrical structure that can be synthesized as single-walled nanotubes (SWNTs) or multi-walled nanotubes (MWNTs). MWNTs were first discovered by S. Iijima in 1991 and referred to as graphitic carbon needles that measured 4-30 nm in diameter and up to 1  $\mu\text{m}$  in length and were synthesized using the direct current arc-discharge carbon evaporation in an inert environment under vacuum [37]. Later in 1993, S. Iijima and T. Ichihashi modified the original synthesis process and produced SWNTs that measured 1 nm in diameter [38]. The conductivity of CNTs can vary from fractions to thousands of  $\text{S cm}^{-2}$  depending on their structure [39]. The mechanical strength (density adjusted) of SWNTs is, at least, an order of magnitude larger than that of steel [40].

Alternative synthesis processes for CNTs are CVD and high pressure carbon monoxide (HiPco) but the high energy demand for those processes makes them costly along with the high impurity content, bundling of CNTs leading low SSA, and low gravimetric and volumetric capacitance in comparison to ACs, limits CNTs supercapacitor investigation [5]. However, Hata et al were able to synthesize bundle-free SWNTs that measured up to 2.5 mm in length with 99.98% purity using water-assisted CVD [41]. The SSA of the new perfectly aligned SWNTs was measured reaching  $1100 \text{ m}^2 \text{ g}^{-1}$  and the capacitance obtained, in organic electrolyte, was larger than ACs' with SSA of  $1640 \text{ m}^2 \text{ g}^{-1}$  that was used for comparison [42]. Additionally, controlled oxidation of high SSA SWNT allowed for the removal of the nanotubes' lids doubling the SSA to over  $2200 \text{ m}^2 \text{ g}^{-1}$  that increased the capacitance, energy density, and power density further exceeding what was observed for high SSA ACs [43].

MWNTs properties have been investigated and their supercapacitor electrodes performances have been measured but they showed lower SSA and capacitance in comparison to SWNTs and ACs which is attributed to the bulky structure of the nanotubes reducing the electrolyte's ions accessibility [44]. In addition to using CNTs as an electrode material for supercapacitors, double-walled nanotubes (DWNTs), sandwiched between a 360 nm graphene film and a substrate, were used as current collectors for graphene-based flexible supercapacitors; compared to gold (Au) current collectors, DWNTs overall performance was almost identical [45].

CNTs, although they had a slow start, exhibit great mechanical, electrical, and electrochemical properties making them a viable option as electrode material or current collector for supercapacitor applications.

### 2.3.1.2 Graphene

Graphene, a two-dimensional (2D) planar sheet of  $sp^2$ -bonded carbon atoms, was discovered in 2004 by K.S. Novoselov and A.K. Geim [46]. Graphene is another form of carbon material but it deserves its own mention as it is presently the most widely researched material [47] for various applications. Some of the graphene characteristics are:

- High SSA ( $> 2600 \text{ m}^2 \text{ g}^{-1}$ ) [33]
- High charge mobility ( $> 200000 \text{ cm}^2 \text{ V}^{-1} \text{ s}^{-1}$ ) [48]
- High thermal conductivity ( $5000 \text{ W m}^{-1} \text{ K}^{-1}$ ) [49]
- Strong Young's modulus (1 TPa) [50]

Graphene's superior characteristics compared to other carbon allotropes are shown in Table 2.4. The high SSA and charge mobility make graphene an ideal material for supercapacitor electrodes. Graphene's high stress-strain tolerance, as evident by its strong Young's modulus,

allows it to be used in flexible supercapacitors [51-52] that can one day provide the necessary energy to power flexible electronic devices. The disadvantages of using graphene as an electrode material for supercapacitors is the agglomeration and restacking of graphene sheets eliminating the accessible pores without increasing its density resulting in a reduction of its capacitance. Synthesis of graphene composite with TMOs or CPs can prevent restacking; this will be covered later in this chapter (in section 2.3.3).

Synthesis of graphene, as described by Najafabadi [47], is divided into two categories; first, the top-down approach in which 2D graphene is extracted from the bulk three-dimensional (3D) graphite lattice by methods including, but not limited to, scotch tape exfoliation, wet chemical and electrochemical synthesis, or liquid phase exfoliation. The abundance of graphite makes this type of graphene synthesis cost effective and it can be produced as monolayers or multilayers making it appropriate for energy storage applications. The second graphene synthesis approach is the bottom-up where graphene is grown using chemical vapor deposition (CVD), plasma enhanced CVD (PECVD), or thermal decomposition of the surface of silicon carbide (SiC) wafers in vacuum among other synthesis processes.

Table 2.4 The properties of graphene compared to other carbon allotropes [34].

Carbon allotropes	Graphite	Diamond	Fullerene (C <sub>60</sub> )	Carbon nanotube	Graphene
Hybridized form	sp <sup>2</sup>	sp <sup>3</sup>	Mainly sp <sup>2</sup>	Mainly sp <sup>2</sup>	<b>sp<sup>2</sup></b>
Crystal system	Hexagonal	Octahedral	Tetragonal	Icosahedral	<b>Hexagonal</b>
Dimension	Three	Three	Zero	One	<b>Two</b>
Experimental specific surface area (m <sup>2</sup> g <sup>-1</sup> )	~10-20	20-160	80-90	~1300	<b>~1500</b>

Table 2.4 (Continued)

Carbon allotropes	Graphite	Diamond	Fullerene (C <sub>60</sub> )	Carbon nanotube	Graphene
Density (g cm <sup>-3</sup> )	3.09-2.23	3.5-3.53	1.72	>1	>1
Optical properties	Uniaxial	Isotropic	Non-linear optical response	Structure-dependent properties	<b>97.7% of optical transmittance</b>
Thermal conductivity (W m <sup>-1</sup> K <sup>-1</sup> )	1500-2000	900-2320	0.4	3500	<b>4840-5300</b>
Hardness	High	Ultrahigh	High	High	<b>Highest (single layer)</b>
Tenacity	Flexible non-elastic	-	Elastic	Flexible elastic	<b>Flexible elastic</b>
Electronic properties	Electrical conductor	Insulator, semi-conductor	Insulator	Metallic and semiconducting	<b>Semimetal, zero-gap semiconductor</b>
Electrical conductivity (S cm <sup>-1</sup> )	Anisotropic 2-3 x 10 <sup>4</sup>	-	10 <sup>-10</sup>	Structure-dependent	<b>2000</b>

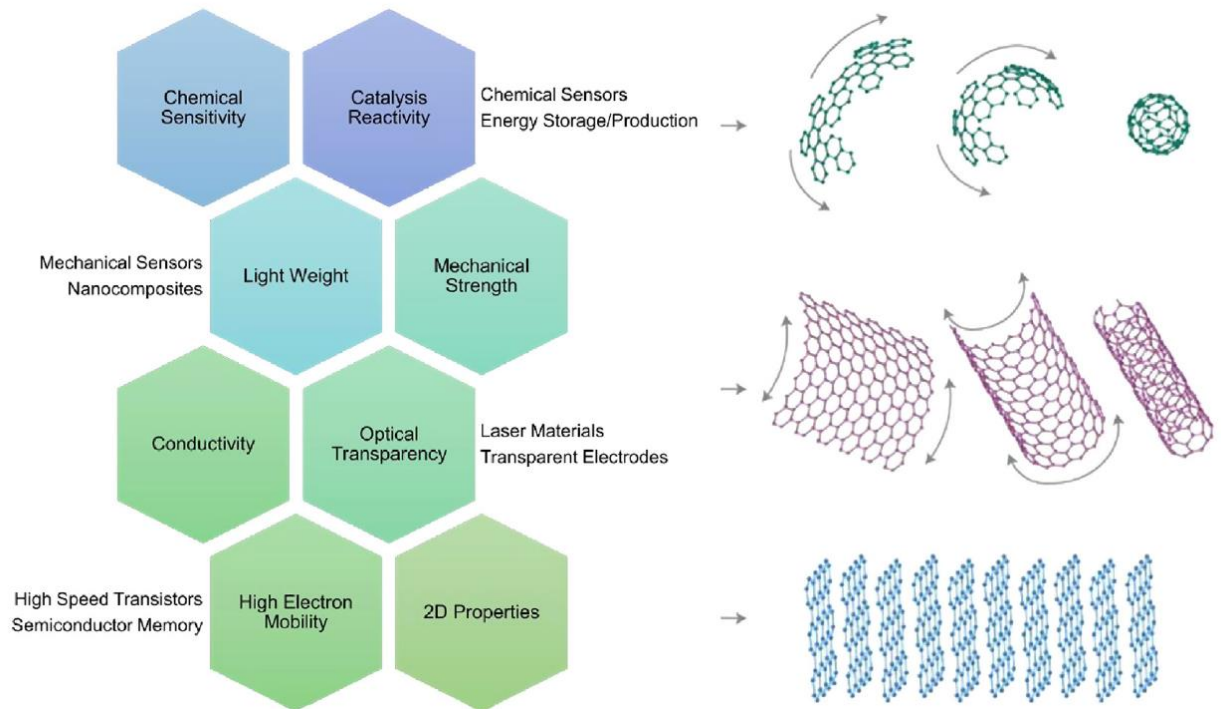


Figure 2.6 Properties and applications of graphene spheres, CNTs, and graphene sheets and visualization of their structural formation [47].



## 2.3.2 Pseudocapacitors Electrode Materials

### 2.3.2.1 Transition Metal Oxides (TMOs)

TMOs, especially RuO<sub>2</sub>, have been widely investigated as supercapacitor electrode materials. TMOs exhibit various oxidation states at different potentials and possess crystalline structures that allow high conductivity which enable charges to propagate within their lattice. For example, fast redox reactions coupled with high reversibility and cycle life (compared to batteries) make RuO<sub>2</sub> an excellent material for charge storage; its redox mechanism can be represented as:  $RuO_x(OH)_z + yH^+ + ye^+ \leftrightarrow RuO_{x-y}(OH)_{z+y}$  where y is the oxidation state. The toxicity, scarcity, and high cost of RuO<sub>2</sub> prevent its industrial integration.

Alternatives to RuO<sub>2</sub> have been proposed and their electrochemical properties tested, mainly MnO<sub>2</sub>, but their lower conductivity, agglomeration, and volume change compromises their commercial production as supercapacitor electrodes. Some of the popular electrode's deposition techniques and specific capacitance values are listed in Table 2.5.

Table 2.5 Reported work on TMOs as supercapacitor electrode materials.

Metal oxide	Deposition technique	Electrolyte	Film thickness	Specific capacitance	Ref
RuO <sub>2</sub>	Electrodeposition	0.5M H <sub>2</sub> SO <sub>4</sub> *	0.5-0.6 mg cm <sup>-2</sup>	552 F g <sup>-1</sup>	[53]
RuO <sub>2</sub>	Electrodeposition	0.5M H <sub>2</sub> SO <sub>4</sub> *	0.17 mg cm <sup>-2</sup>	786 F g <sup>-1</sup>	[54]
RuO <sub>2</sub>	Electrostatic spray deposition	0.5M H <sub>2</sub> SO <sub>4</sub> *	0.15-0.3 mg cm <sup>-2</sup>	650 F g <sup>-1</sup>	[55]
RuO <sub>2</sub>	Spray pyrolysis method	0.5M H <sub>2</sub> SO <sub>4</sub> *	490 nm	551 F g <sup>-1</sup>	[56]
RuO <sub>2</sub>	Chemical bath deposition	0.5M H <sub>2</sub> SO <sub>4</sub> *	260 nm	400 F g <sup>-1</sup>	[57]
RuSnO <sub>2</sub>	Sol-gel slurry	0.1M H <sub>2</sub> SO <sub>4</sub> *	0.3 mg cm <sup>-2</sup>	690 F g <sup>-1</sup>	[58]
RuO <sub>2</sub>	Dip coating	1M H <sub>2</sub> SO <sub>4</sub> *	0.0375-0.85 mg cm <sup>-2</sup>	620 F g <sup>-1</sup>	[59]

Table 2.5 (Continued)

Metal oxide	Deposition technique	Electrolyte	Film thickness	Specific capacitance	Ref
MnO <sub>2</sub>	Electrochemical anodization	1M NaCl*	0.02 mg cm <sup>-2</sup>	199 F g <sup>-1</sup>	[60]
MnO <sub>2</sub>	Electroplating	0.1M Na <sub>2</sub> SO <sub>4</sub> *	0.17-0.24 mg cm <sup>-2</sup>	230 F g <sup>-1</sup>	[61]
MnO <sub>2</sub>	Layer-by-layer deposition	2M KCl*	8 nm	288 F g <sup>-1</sup>	[62]
MnO <sub>2</sub>	Sol-gel dip coating	0.1M Na <sub>2</sub> SO <sub>4</sub> *	1.05 μg cm <sup>-2</sup>	698 F g <sup>-1</sup>	[63]
MnO <sub>2</sub>	PTFE bound	0.1M K <sub>2</sub> SO <sub>4</sub> *	100 μm	150 F g <sup>-1</sup>	[64]
Fe <sub>3</sub> O <sub>4</sub>	PTFE bound	0.1M K <sub>2</sub> SO <sub>4</sub> *	100 μm	75 F g <sup>-1</sup>	[64]
V <sub>2</sub> O <sub>5</sub>	PTFE bound	0.1M K <sub>2</sub> SO <sub>4</sub> *	100 μm	170 F g <sup>-1</sup>	[64]

\* Three electrode cell configuration

### 2.3.2.2 Conducting Polymers (CPs)

The conductivity increase of covalently bonded, semiconducting, polyacetylene, (CH)<sub>x</sub> by approximately four orders of magnitude through exposure to chlorine, bromine, or iodine vapor at room temperature in 1977 [65] was the catalyst for rapid development of CPs science and their applications. Electrochemical investigations of the newly transformed conducting organic polymer followed soon after [66-69]. Along with polyacetylene (PA), some of today's widely studied CPs are polypyrrole (PPy), polythiophene (Pth), poly(3,4-ethylenedioxythiophene) (PEDO), poly(p-phenylene vinylene) (PPV), and polyaniline (PANI); their chemical structures are shown in Figure 2.7.

The doping of a polymer results in the deprotonation of the polymer's centers, -COOH to -COO<sup>-</sup>, creating a conjugated polymer (polybase) that causes ionic charges interaction with the functional groups on polymer's edges changing its standard Gibbs energy allowing for existence of localized electronic states at lower energies than the band gap of the CP creating paths for the

charge to transfer along the backbone of the CP [4]. Vapor, solution, electrochemical, and self are the most widely used methods of doping.

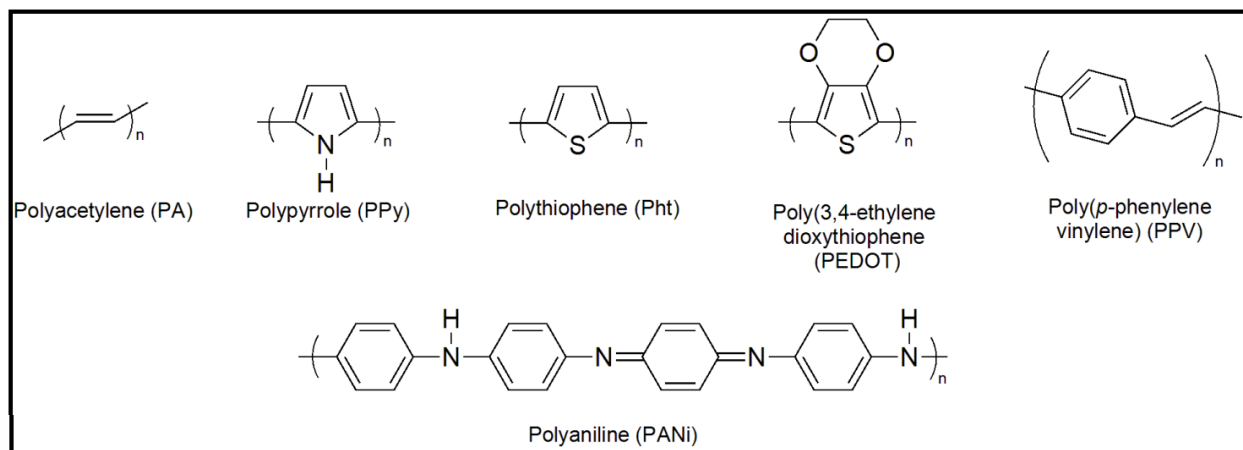


Figure 2.7 Chemical structure of some of the main CPs [70].

CPs can be synthesized in various ways some of which are: (i) chemical polymerization, (ii) electrochemical polymerization, (iii) photochemical polymerization, (iv) CVD, etc. Chemical polymerization is a widely used CPs synthesis process as it does not require any special equipment for the oxidation of monomers into radical ions that can covalently bond to form chains of polymers. This synthesis method was used in the making MoS<sub>2</sub>-PANI composite materials (discussed in detail in chapter 6).

Positive and negative charges can be introduced to the CPs redox reactions at certain potentials which allowed CPs to be used as supercapacitor electrodes. However, fast charging and discharging of CP electrodes causes it to swell and crack reducing its life cycles compared to that of carbon material electrodes. Table 2.6 lists some of the supercapacitor electrodes comprised only of CPs and their performances.

Table 2.6 CPs supercapacitor electrodes based on synthesis method.

CP	Synthesis Method	Electrolyte	Specific Capacitance	Ref
PEDOT nanotubes	Electrochemical polymerization*	1M LiClO <sub>4</sub> *	140 F g <sup>-1</sup> at 100 mV s <sup>-1</sup>	[71]

Table 2.6 (Continued)

CP	Synthesis Method	Electrolyte	Specific Capacitance	Ref
PPy	Pulse polymerization*	0.5M H <sub>2</sub> SO <sub>4</sub> * 0.5M H <sub>2</sub> SO <sub>4</sub> **	1100 F g <sup>-1</sup> 400 F g <sup>-1</sup>	[72]
PANI nanofibers	Chemical polymerization	1M H <sub>2</sub> SO <sub>4</sub> *	298 F g <sup>-1</sup> at 5 mV s <sup>-1</sup>	[73]
PANI	In situ chemical polymerization	0.5M H <sub>2</sub> SO <sub>4</sub> ** H <sub>2</sub> SO <sub>4</sub> -PVA <sup>a**</sup> (gel)	360 F g <sup>-1</sup> at 1 A g <sup>-1</sup> 332 F g <sup>-1</sup> at 1 A g <sup>-1</sup>	[74]
PANI nanowire arrays	Electrochemical polymerization*	1M HClO <sub>4</sub> *	950 F g <sup>-1</sup> at 1 A g <sup>-1</sup>	[75]
PANI films: Emeraldine Pernigraniline Leucoemeraldine	Electrochemical polymerization*	1M H <sub>2</sub> SO <sub>4</sub> *	258 F g <sup>-1</sup> 83 F g <sup>-1</sup> 32 F g <sup>-1</sup> at 10 mV s <sup>-1</sup>	[76]

<sup>a</sup> polyvinyl alcohol

\* Three-electrode cell configuration

\*\* Two-electrode cell configuration

### 2.3.2.2.1 Polyaniline (PANI)

H. Letheby reported a dark blue color that aniline acquired when influenced with nascent oxygen in 1862 [77]. This was the earliest stage at which aniline was oxidized and PANI was formed; however, it was not understood until the conductivity of organic polymers was enhanced in the twentieth century.

PANI is the product of polymerization of aniline monomer. The general formula of PANI is  $[(-B-NH-B-NH-)_y (-B-N=Q=N-)_{1-y}]$  where B and Q represent the C<sub>6</sub>H<sub>4</sub> benzenoid and quinonoid rings, respectively, and y corresponds to the neutral redox state [78]. PANI exists in multiple oxidation states (at different y values), pernigraniline (y = 0) fully oxides, leucoemeraldine (y = 1) fully reduced, and emeraldine (y = 0.5) partially oxidized that is the only

conductive form (protonation by aqueous acids) of PANI. The structure of some of PANI's oxidation states are shown in Figure 2.8.

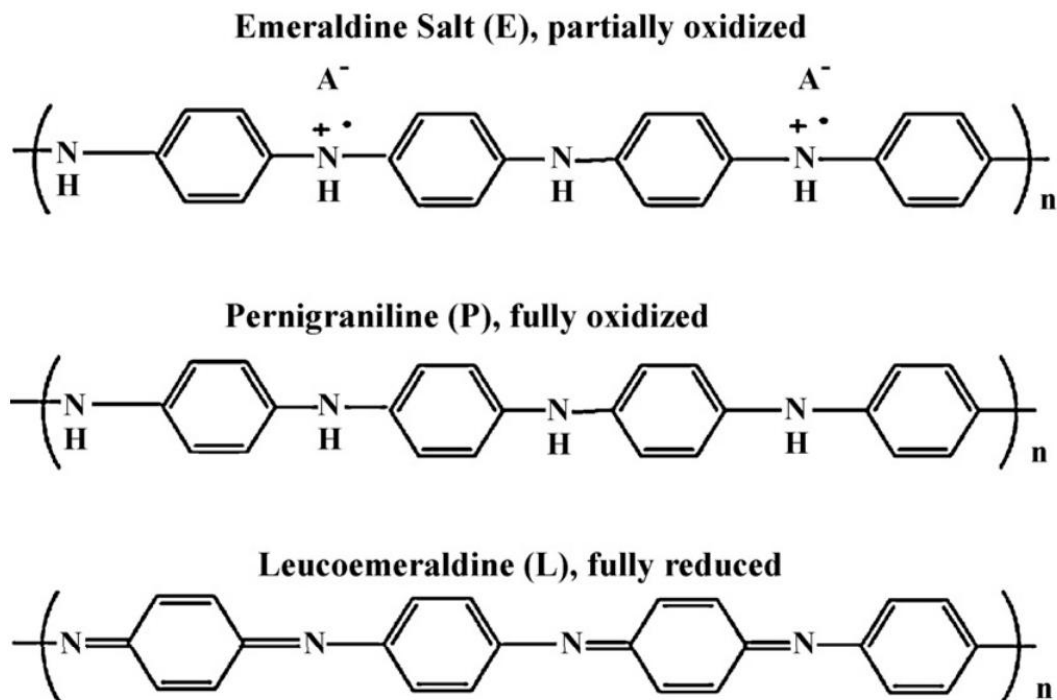


Figure 2.8 PANI's oxidation states at  $y = 0.5$  (E),  $y = 0$  (P), and  $y = 1$  (L) [76].

The various oxidation states of PANI make it interesting for electrochemical storage applications. Emeraldine salts based PANI, as expected, exhibit superior storage capabilities to other PANI forms due to its electrical conductivity. Some of the supercapacitor electrodes' performances are listed in Table 2.5.

### 2.3.3 Composite Materials

Composite supercapacitor electrodes are comprised of two or more different materials (from the aforementioned two types of supercapacitor materials). This combination aims to utilize the best each individual material has to offer. The synergistic effects are highly desirable for improved electrode materials. The advantages of using graphene-TMOs composites are the reduction in TMOs' volume expansion upon fast charge/discharge, preventing agglomeration of TMOs and restacking of graphene sheets, creating a highly conductive networks for improved

electron transport, and an overall improvement of electrochemical properties (capacitance, energy, and power) [34]. Similarity, graphene-CPs composites show improved electrical conductivity and mechanical strength reducing the swelling/shrinking of CPs, prolonging the life cycles, and improving charge storage capabilities [79].

Graphene is not the only material that enhances the supercapacitor composite electrodes; CNTs have been reported to do so as well. Also, composite electrode materials are not only EDLC/pseudocapacitance but can also be synthesized any combination; Table 2.7 lists some of the materials combinations used as electrodes for supercapacitors.

Table 2.7 Reported work on composite materials as electrodes for supercapacitors.

Nanocomposite material	Electrolyte	Specific capacitance	Ref
RuO <sub>2</sub> Graphene CNT 3D nickel	2M Li <sub>2</sub> SO <sub>4</sub> **	502.78 F g <sup>-1</sup>	[80]
RuO <sub>2</sub> Graphene	1M H <sub>2</sub> SO <sub>4</sub> *	570 F g <sup>-1</sup>	[81]
MnO <sub>2</sub> Graphitic petals	1M Na <sub>2</sub> SO <sub>4</sub> *	580 F g <sup>-1</sup>	[82]
MnO <sub>2</sub> Graphene	1M Na <sub>2</sub> SO <sub>4</sub> *	324 F g <sup>-1</sup>	[83]
Mn <sub>3</sub> O <sub>4</sub> Graphene	6M KOH*	256 F g <sup>-1</sup>	[84]
Mn <sub>3</sub> O <sub>4</sub> Graphene	1M Na <sub>2</sub> SO <sub>4</sub> *	175 F g <sup>-1</sup>	[84]
NiOOH MWCNT	1M KOH*	2436 F g <sup>-1</sup>	[85]
Co <sub>3</sub> O <sub>4</sub> Graphene	2M KOH**	472 F g <sup>-1</sup>	[86]
Fe <sub>3</sub> O <sub>4</sub> Graphene	1M H <sub>2</sub> SO <sub>4</sub> **	180F g <sup>-1</sup>	[87]
ZnO Graphene	1M KOH*	62.2 F g <sup>-1</sup>	[88]
TiO <sub>2</sub> Graphene	1M H <sub>2</sub> SO <sub>4</sub> **	60 F g <sup>-1</sup>	[87]
PEDOT Graphene	2M HCl**	304 F g <sup>-1</sup>	[89]
PEDOT Graphene	2M H <sub>2</sub> SO <sub>4</sub> **	261 F g <sup>-1</sup>	[89]
Ppy Graphene	1M H <sub>2</sub> SO <sub>4</sub> **	256 F g <sup>-1</sup>	[90]
POA Graphene	2M H <sub>2</sub> SO <sub>4</sub> *	380 F g <sup>-1</sup>	[91]
POT Graphene	2M H <sub>2</sub> SO <sub>4</sub> *	425 F g <sup>-1</sup>	[92]
POT Graphene	0.1M LiClO <sub>4</sub> *	235 F g <sup>-1</sup>	[92]

Table 2.7 (Continued)

Nanocomposite material	Electrolyte	Specific capacitance	Ref
POT Graphene	1M BMIM-PF <sub>6</sub> <sup>*</sup>	219 F g <sup>-1</sup>	[92]
PANI Graphene	1M H <sub>2</sub> SO <sub>4</sub> <sup>*</sup>	1126 F g <sup>-1</sup>	[93]
MnO <sub>2</sub> Ppy	0.5M Na <sub>2</sub> SO <sub>4</sub> <sup>*</sup>	620 F g <sup>-1</sup>	[94]

\* Three electrode cell configuration

\*\* Two electrode cell configuration

Asymmetric supercapacitors employ a different concept of using two materials. The electrodes in asymmetric types are not synthesized composites but are two different materials each deposited on one electrode resulting in asymmetric capacitance. The biggest advantage to this type of combination is the increase in operating voltage of the electrolyte. It has been reported that asymmetric capacitors composed of AC electrode and MnO<sub>2</sub> electrode improved the specific energy by over five folds than in symmetric MnO<sub>2</sub> supercapacitors [64] by increasing the operating voltage of an aqueous electrolyte.

## 2.4 Design of Supercapacitors

The electrodes are the most important component in the building block of supercapacitors and are discussed in detail in the next chapter. Nonetheless, the electrolyte, the current collector, and the separator are important parameters to consider for fabrication of a supercapacitor.

A few important design parameters should be considered for preparing the electrodes and electrolyte [15] [95]:

- Large electrode surface area to store maximum charges on the electrode/electrolyte interface
- High electrolyte conductivity
- High corrosion resistance

- Optimizing the electrode porosity to compliment the electrolyte's ion size in order to maximize the charge storage on the electrode/electrolyte interface

Supercapacitor test cells, whether for pseudocapacitors or EDLC evaluation, can be fabricated using the two-electrode cell configuration that best resembles an actual supercapacitor and are commercially available or a three-electrode cell configuration which is widely used in electrochemical research [96]. The schematics of both cell setups are shown in Figure 2.9.

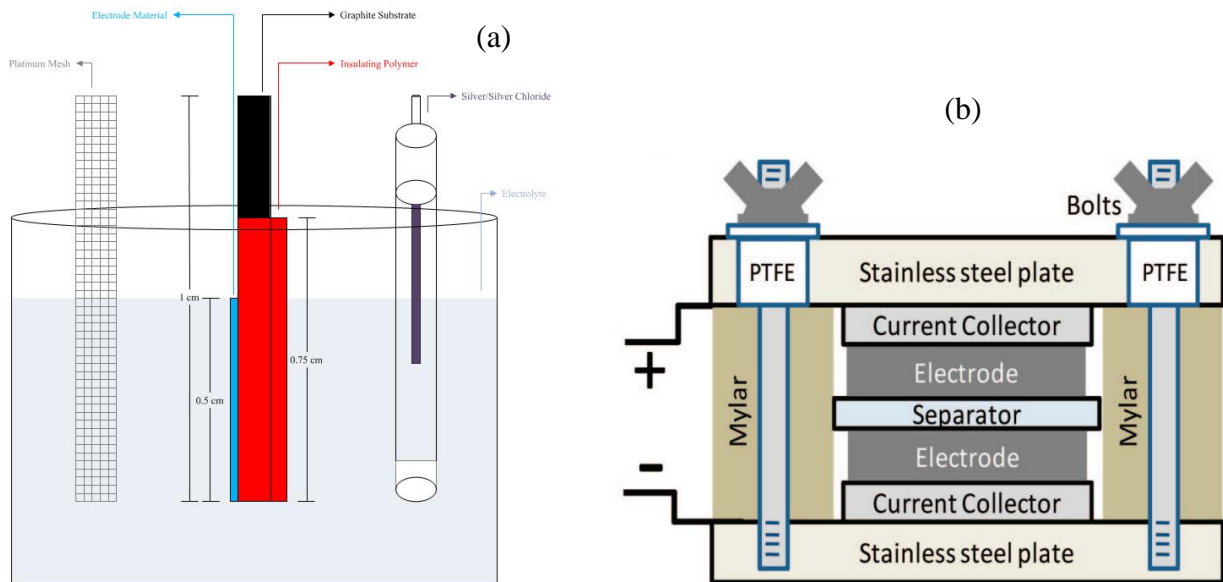


Figure 2.9 (a) A cross-sectional view of a typical three-electrode supercapacitor cell. It uses a reference electrode (e.g. Ag/AgCl) to record the voltage, a counter electrode to close the circuit, and an insulating polymer layer if the current collector is not inert, and (b) two-electrode supercapacitor cell [35] enclosed in stainless steel to prevent the electrolyte from leaking.

### 2.4.1 Electrolytes

Electrolytes are an essential part of supercapacitors and detrimental to their performance. The series resistance and the operating voltage are determined by the electrolytes. Exceeding the thermodynamic decomposition potentials of electrolytes can cause breakdown of the supercapacitors. Electrolytes' stability is crucial to maintain a large cycle life. Electrolytes' ions matching with the electrodes' pores is important to take advantage of the high surface area of electrodes.



The energy of supercapacitors (and capacitors in general) rely on operating voltage of the electrolyte

$$E = \frac{1}{2} CV^2 \quad (2.7)$$

where E is the energy, C is the capacitance, and V is the electrolyte's operating voltage. Similarly, the power of supercapacitors relies on V

$$P = \frac{V^2}{4R_s} \quad (2.8)$$

where P is the power and  $R_s$  is the equivalent series resistance of supercapacitors.

#### 2.4.1.1 Aqueous Electrolytes

Aqueous electrolytes are widely used in supercapacitor research due to their low cost associated with the plethora of ion sources such as acids ( $H_2SO_4$  and HCl), bases (KOH), and salts (KCl). The small ion sizes of inorganic electrolytes and high ionic conductivity, as seen in Table 2.8 make them favorable for producing high specific capacitance due to the small distance of separation of the solvated ions and the electrode's charges. However, aqueous electrolytes have an operating voltage window of just 1 V, less than that of other types of electrolytes, which makes them less attractive for commercial production due to their low energy densities.

Table 2.8 Ion sizes of inorganic electrolytes and aqueous solutions' ionic conductivity [5] [44].

Inorganic Electrolyte	Ion Size (nm)		Aqueous Electrolyte Solution	Conductivity ( $mS\ cm^{-1}$ )	$\Delta V$ (V)
	Cation	Anion			
$H_2SO_4$		0.533	KOH	540	1
KOH	0.26		KCl	210	1
$Na_2SO_4$	0.36	0.533	$H_2SO_4$	750	1
NaCl	0.36		$Na_2SO_4$	91.1	1
			$K_2SO_4$	88.6	1

### 2.4.1.2 Organic Electrolytes

Organic electrolytes are widely used in commercial supercapacitors due to their high operating voltage, compared to aqueous electrolytes, in the range of 2.5-3 V. Low ionic conductivity and large ion sizes increase the series resistance of supercapacitors and reduce their capacitive performance and power. However, the disadvantages of organic electrolytes are balanced by the quadratic effect of their large operation voltage range on the energy. The properties of some organic electrolytes and organic solvents are shown in Table 2.9.

Table 2.9 Ion sizes of some organic electrolytes and organic solvents' properties [44].

Organic Electrolyte	Ion Size (nm)		Solvent	Viscosity (Pa/s)	Dielectric Constant ( $\epsilon$ )
	Cation	Anion			
$(C_2H_5)_4N.BF_4(TEA^+BF_4^-)$	0.686	0.458	Acetonitrile	0.369	36.64
$(C_2H_5)_3(CH_3)N.BF_4(TEMA^+BF_4^-)$	0.654	0.458	$\gamma$ -Butyrolactone	1.72	39
$(C_4H_9)_4N.BF_4(TBA^+BF_4^-)$	0.83	0.458	Dimethyl ketone	0.306	21.01
$(C_6H_{13})_4N.BF_4(THA^+BF_4^-)$	0.96	0.458	Propylene carbonate	2.513	66.14

### 2.4.1.3 Other Electrolytes

Ionic liquids (IL), free of solvents, are highly concentrated viscous molten salts at room temperature. ILs biggest disadvantage is their low conductivity at room temperature causing the power density of supercapacitors to be lower than that of aqueous and organic electrolytes; however, they can operate at a potential window of 5 V which allows them to have superior energy densities [97], [98]. Room temperature ILs (RTILs) such as imidazolium, pyrrolidinium, tetraalkylammonium, pyridinium, piperidinium, and sulfonium combined with a variety of anions such as tetrafluoroborate ( $BF_4^-$ ), hexafluorophosphate ( $PF_6^-$ ), and trifluoromethanesulfonate ( $CF_3SO_3^-$ ) can have 6 V operation range [99].

Polymer-based gel electrolytes such as  $\text{H}_3\text{PO}_4\text{-PVA}$  [51] and  $\text{H}_2\text{SO}_4\text{-PVA}$  [74] have been used in the fabrication of flexible supercapacitors. The operating voltage of gel electrolytes can be stretched as high as 2 V but their low conductivity and its deterioration over short periods of time, compared to liquid-based organic electrolytes, impact their capacitive and power performances. Yet gel electrolytes remain a viable candidate for testing supercapacitor devices.

### 2.4.2 Current Collectors

Current collectors are conductive substrates upon which the supercapacitor electrode materials are deposited. Electrode materials, while exhibiting good capacitive performance, cannot be used as current collectors to feedback the current and voltage reposes from the testing equipment due to the high electronic conductivity along their structure. Current collectors allow electrons to travel in the direction of the electrode's thickness instead of along the electrode's length vastly reducing the charge transport distance as illustrated in Figure 2.10. Aluminum, platinum, and graphite are some of the commonly used current collectors. Current collectors with lower conductivity than platinum or graphite such as ITO coated polyethylene terephthalate (PET) (transparent paper) have been used due to their flexibility and used in testing flexible supercapacitor devices [100]. CNTs have also been used as highly conductive current collectors [45].

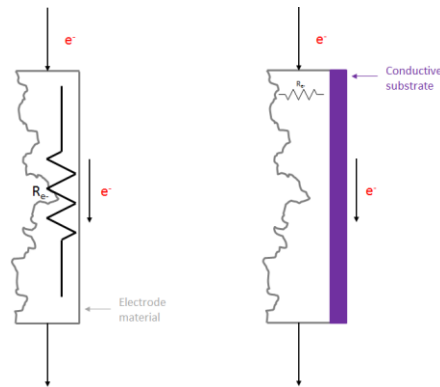


Figure 2.10 The electrical conduction through an electrode material with and without a conductive substrate.

### 2.4.3 Separators

Separators in supercapacitors are used to prevent the electrodes from physically contacting and shorting out. Separators must be [5]:

- Highly porous to allow high ionic conductivity
- Thin
- Mechanically stable to provide durability for the supercapacitor
- Preserve wettability to allow ion conduction

### 2.5 Electrochemical Measurement Techniques

A series of electrochemical tests must be carried out to evaluate the performance of a supercapacitor and to identify its specific capacitance, specific power, and specific energy.

As was shown in Figure 2.9, the supercapacitor behavior can be tested in either three-electrode or two-electrode cell configuration. It is important to perform the specific capacitance calculations depending on the type of cell used. In a three-electrode setup, the total capacitance is calculated from charges stores on the electrode. On the other hand, the two-electrode cell's total capacitance is a series combination of the contribution of each individual electrode. Taking the double layer capacitance, for example, the total capacitance is modeled as the contribution from the  $C_H$  and the contribution from  $C_{diff}$  and the equivalent capacitance is the series combination of individual contributions. The two-electrode cell setup uses the same concept as that of the double layer, as seen in Equation (2.3), to calculate the total capacitance. If the two electrodes connected exhibit only double layer capacitance then the total capacitance would be:

$$\frac{1}{C_{dl(Total)}} = \frac{1}{C_{dl(1)}} + \frac{1}{C_{dl(2)}} \quad \leftrightarrow \quad C_{dl(Total)} = \frac{C_{dl(1)}C_{dl(2)}}{C_{dl(1)} + C_{dl(2)}} \quad (2.9)$$

### 2.5.1 Cyclic Voltammetry (CV)

Cyclic voltammetry (CV) is a measure of the current as a function of a predetermined voltage range,  $V$ , using a reversible linear voltage sweep (known as the scan rate,  $\nu$ ). The voltage is applied between two supercapacitor electrodes (in the two-electrode cells) or between a working electrode and reference electrode (in the three-electrode cells). The potential in the CV starts at an initial voltage ( $E_i$ ) and increases linearly with respect to time until it reaches a final voltage ( $E_f$ ) the scan is then reversed and the potential moves from  $E_f$  to  $E_i$  at the same rate. The process is done for multiple cycles as shown in Figure 2.11.

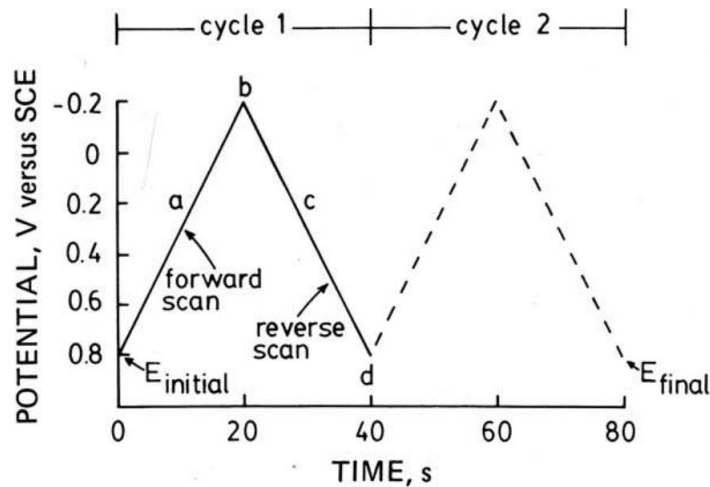


Figure 2.11 A typical CV signal where the potential is scan from initial voltage to a final voltage and the back to the initial voltage. The scan rate is the slope of the signal [101].

Once the desired potential range and the scan rate are selected and applied to the cell, the output of the CV is a graph of the measured current,  $i$ , versus  $V$ . For redox materials, the measured current is governed but the following equations:

$$i = nFAk_o C_{O_x/R_d} \quad (2.10)$$

$$i = nFAx \frac{\partial C_{O_x/R_d}}{\partial x} \quad (2.11)$$

where  $n$  is the number of electrons transferred per ion,  $F$  is Faraday's constant,  $A$  is the apparent area of the electrode,  $k_o$  is the reaction rate coefficient,  $C_{O_x/R_d}$  is the concentration of the oxidant

or reductant, and  $x$  is the distance of the  $C_{Ox/Rd}$  from the electrode. Equation 2.10 is true when the diffusion of  $O_x$  and  $R_d$  is fast and  $C_{Ox/Rd}$  is uniform at the surface and the bulk of the electrode material meaning that the current is kinetically controlled. On the other hand, Equation 2.11 is true when the kinetics of the redox reaction are fast and  $C_{Ox/Rd}$  is not uniform throughout the electrode material meaning that the current is diffusion controlled.

To determine the mechanism of the electrodes, CV can be used. If  $i$  and square root of  $v$  are linearly related, then the electrode reaction is diffusion controlled and the diffusion coefficient can be determined using the Randles-Sevcik equation:

$$i_p = 2.69 \times 10^{-5} n^{\frac{2}{3}} A D^{\frac{1}{2}} v^{\frac{1}{2}} \quad (2.12)$$

where  $i_p$  is peak current, and  $D$  is the diffusion coefficient.

The stored charge and potential window for CV measurements combined with the output current (that is a result of the stored charge) allow for the calculation of the cell's capacitance:

$$C = \frac{dQ}{dV} \rightarrow C = \frac{idt}{dV} \rightarrow C = \frac{i}{v} \quad (2.13)$$

### 2.5.2 Constant Current Charge/Discharge (CCCD)

CCCD, also known as galvanostatic charge/discharge or galvanic pulses, is another method of measuring the electrochemical behavior of a supercapacitor. In this technique, a constant current is applied to the circuit and the voltage response with respect to time is measured. The same but negative current is applied to discharge the supercapacitor under the same charging conditions. Similar to CV, the capacitance can be obtained from the predetermined charging/discharging current:

$$C = \frac{dQ}{dV} \rightarrow C = \frac{idt}{dV} \rightarrow C = \frac{i\Delta t}{\Delta V} \quad (2.14)$$

since  $i$  is applied discharge current (as opposed to the measured current in CV),  $\Delta V$  is the change in measured voltage over the change in the corresponding time  $\Delta t$ .

CCCD can also be used to calculate  $R_S$  from the instantaneous drop of voltage when the current is reversed at the start of discharging (also known as the IR drop) using Ohm's law.

### 2.5.3 Electrochemical Impedance Spectroscopy (EIS)

Electrochemical impedance spectroscopy (EIS) is a characterization technique of the electrode/electrolyte interface using alternating current over a large frequency sweep. The complex impedance of the cell is obtained as a function of the applied frequency. The Nyquist plot shows the imaginary versus the real components on the complex plain. Circuit models are used to estimate the values of  $C_{dl}$ ,  $R_S$ , parallel (leakage) resistance,  $R_P$ , and charge transfer resistance resulting from the Fradaic reactions,  $R_{CT}$ . The rather simplistic circuit model for EDLCs is shown in Figure 2.12(a) that is true for non-porous materials. However the response is not always ideal and the porosity of the electrode material complicates the equivalent circuit as shown in Figure 2.12(b) and observed in chapter 3. The constant phase element (CPE),  $Q_{CPE}$ , which is a non-ideal capacitor and its impedance reliant on the CPE admittance parameter,  $Y_o$ , the ideality constant,  $n$ , ( $0 < n < 1$ ), and the angular frequency  $\omega$  (reciprocal of the applied frequency) resulting from the capacitance and resistance of the pores and can be calculated as:

$$\bar{Z}_{CPE} = \frac{1}{Y_o (j\omega)^n} \quad (2.15)$$

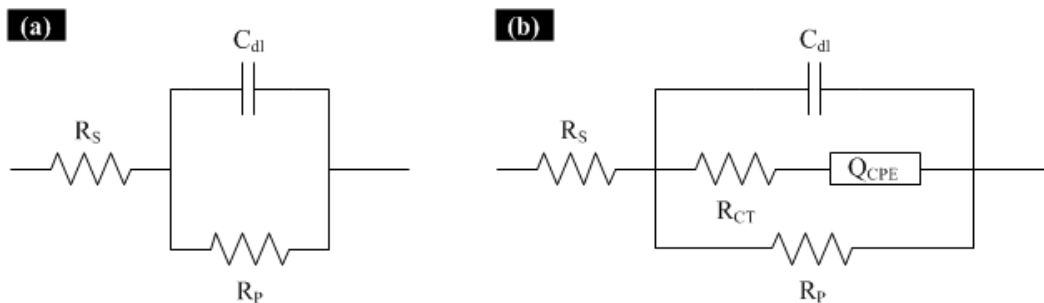


Figure 2.12 Equivalent circuits of (a) EDLC, and (b) pseudocapacitor.

Throughout the work of this dissertation, all the electrochemical measurements were performed using the Radiometer Analytical Voltalab 40 potentiostat shown in Figure 2.13.

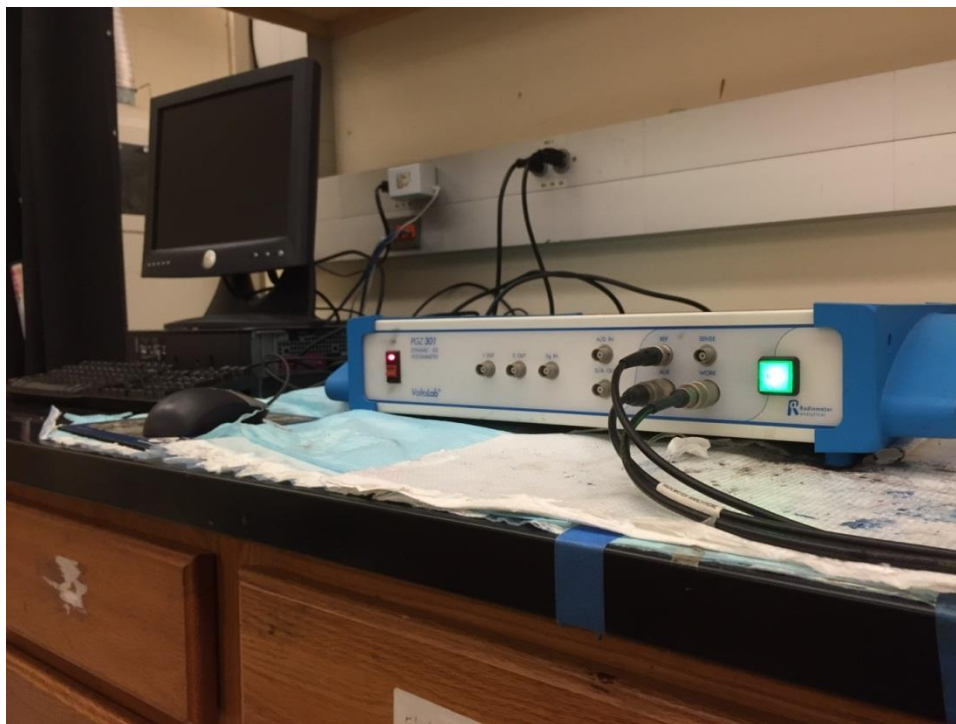


Figure 2.13 Digital image of the Radiometer Analytical Voltalab 40 that was used for all the electrochemical characterizations.

## 2.6 Supercapacitor Performance Evaluation

There are multiple dominating factors that can affect the evaluation of the supercapacitors' charge storage capabilities; these factors include, but are not limited, to the experimental setup, the electrolyte, the operating voltage, the electrode material, the density of the material, and the thickness of the electrode among others. Figure 2.14 shows the majority of the key metrics that affect the testing and evaluation of the performance of supercapacitors.

The specific capacitance refers to measured capacitance, independent of measurement technique, normalized to the electrode's mass, area, or volume. Table 2.10 identifies the nomenclature that will be used in this dissertation to describe the specific capacitance henceforth. Similarly, the energy density and power density refer to the normalized values.



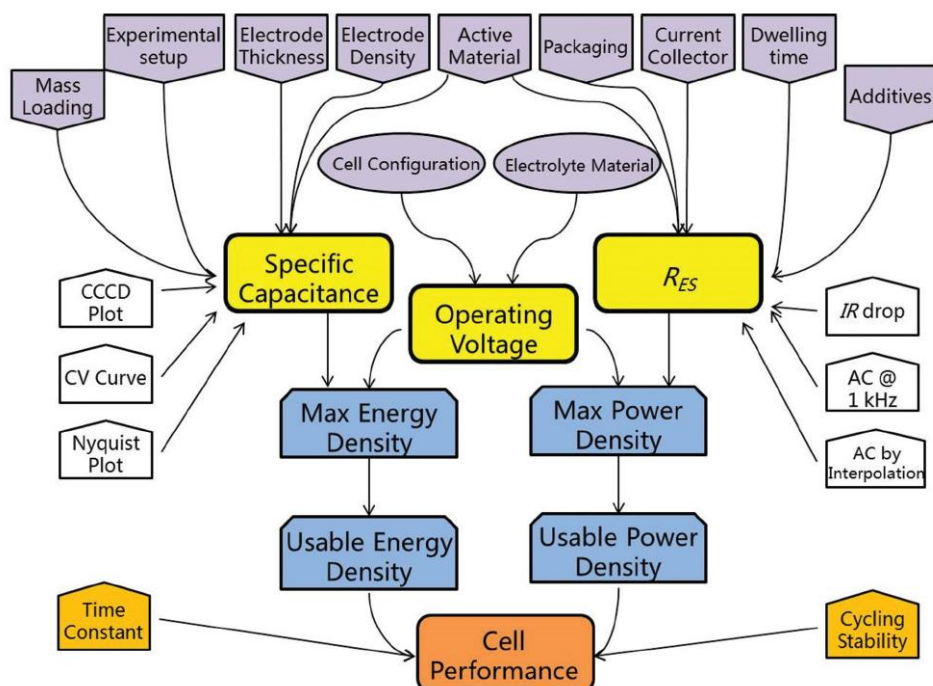


Figure 2.14 An illustration of key performance metrics, test methods, major affecting factors for the evaluation of supercapacitors [102].

Table 2.10 The nomenclature to identify different types of specific capacitance.

Specific capacitance	Normalized to	Equation	Unit
Gravimetric capacitance	Electrode's weight ( $m$ )	$C_g = \frac{C}{m}$	$F g^{-1}$
Areal capacitance	Electrode's apparent area ( $A$ )	$C_a = \frac{C}{A}$	$mF cm^{-2}$
Volumetric capacitance	Electrode's volume ( $Vol$ )	$C_v = \frac{C}{Vol}$	$F cm^{-3}$

The reporting methodology is not consistent among all authors as some use the CV as means to calculate the specific capacitance while others use the CCCD. While the US Department of Defense (DOD), the US Department of Energy (DOE), the International Electrochemical Commission (IEC), and the Society of automotive Engineers (SAE) have all tries to set performance evaluation standards, they all were application specific and target the industry as opposed to universal standards that could apply to industry and research [102].

It is also worth mentioning that comparisons among different supercapacitors' performances are not always valid as some are measured in the two-electrode configuration while others in the three-electrode configuration. If a single electrode is used, in the case of the three-electrode cell setup (where the other two are reference and counter electrodes), the specific capacitance calculations are straightforward. However, when two electrodes are used, the capacitance is halved and that is in the case where the two electrodes are identical. Calculating the specific capacitance can lead to even more discrepancies as, for example, the  $C_g$  of two identical electrodes is a quarter of that of a single electrode.

Electrode mass loading and thickness are also major factors that affect the measured specific capacitance, one specific electrode mass loading case is presented in chapter 6.

The lack of standardized testing and evaluation methodology can lead to inflated specific capacitance values that are only optimal in laboratories and are not functional commercially.

## CHAPTER 3: METHODOLOGY AND APPROACH FOR ELECTRODE MATERIAL DEPOSITION

### 3.1 Introduction

The fabrication of supercapacitor electrodes to match the design parameters discussed in chapter 2 is important to ensure proper performance of the electrodes. One of the main challenges in the supercapacitors' fabrication process is the adhesion of their electrode materials onto the substrates. Electrode deposition techniques vary from growing the material atop a silicon substrate to simply drop-casting or spin-coating a solution of the material onto a conductive substrate. Electrode materials may not always voluntarily adhere to the surface of the current collector and may require some additives to ensure complete attachment. Even when electrode materials seem to adhere properly to the substrates at first, the adhesion bond weakens over long cycles [5].

The techniques adopted for electrode materials deposition are mainly associated with binders. Binders like nafion [89-90], polytetrafluoroethylene (PTFE) [103-104], polyvinylidene fluoride (PVDF) [105], polyvinyl alcohol (PVA) [106], and polyvinylpyrrolidone (PVP) [107] are used to enhance the adhesion of the materials on the surface of the substrates. The biggest disadvantages of binders are their insulating nature so mixing them with the electrode materials can compromise the performance of supercapacitors, their reduction of the SSA of the electrode materials, and their addition of dead weight to the electrodes. However, using small weight percentages of the total electrodes' weight can have a small impact on the performance but can

also preserve the integrity electrode materials adhesion. Different binders, though not all, are compatible with all types of electrolytes [108].

This chapter covers the electrode preparation of commercially obtained graphene ( $G_c$ ) (purchased from Graphene-Supermarket) to examine the binder-assisted and binder-free deposition techniques and the electrochemical characterization of the supercapacitors in PVA- $H_3PO_4$  gel electrolyte in the two-electrode cell configuration.

### 3.2 Preparation of $G_c$ Supercapacitors

#### 3.2.1 $G_c$ /PVDF Electrodes

PVDF binder was prepared by heating its pellets in dimethylformamide (DMF) at  $100^\circ C$  under constant stirring until the PVDF pellets were completely dissolved. Once the solution cooled down to room temperature,  $G_c$  powder was added at an electrode weight percentage of 93%:7%  $G_c$ :PVDF. The slurry formed was drop-casted onto two graphite substrates of  $0.5\text{ cm}^2$  each. The gel electrolyte was sandwiched between the two electrodes as illustrated in Figure 3.1 and doctor blade, shown in Figure 3.2, was used to smooth the surfaces of the electrodes prior to applying the gel electrolyte to prevent the electrodes from short-circuiting. The thickness of each electrode, measured as a function of the apparent electrode area (also known as the electrode's mass loading), was  $2.2\text{ mg cm}^{-2}$ .

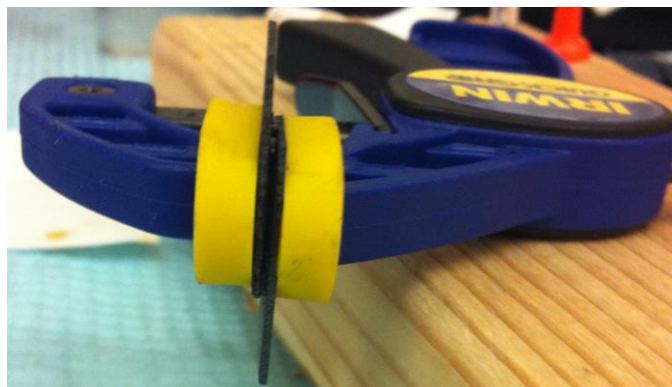


Figure 3.1 Two  $G_c$ :PVDF electrodes on graphite substrates with PVA- $H_3PO_4$  gel electrolyte sandwiched in the middle.

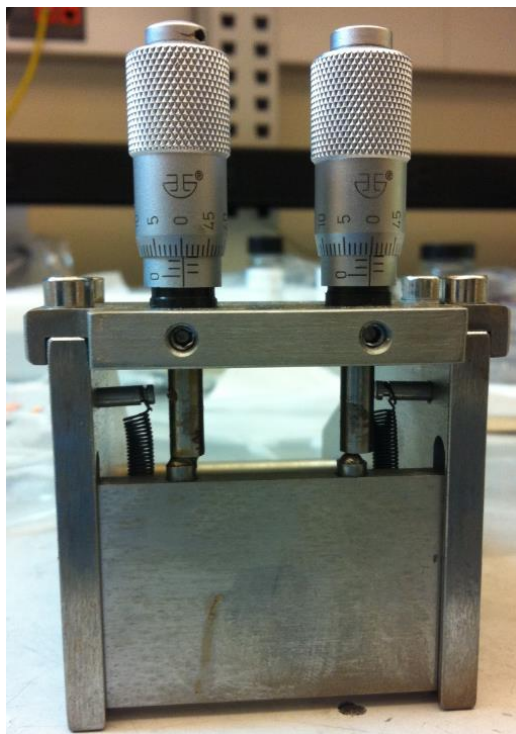


Figure 3.2 Doctor blade used to smooth the surface of the electrodes.

### 3.2.2 Binder-Free $G_c$ Electrodes

$G_c$  was deposited on the surface of diced ITO-coated glass substrates using a unique method called vacuum filtration deposition technique [32] that did not require any binding additives.  $G_c$  was dispersed in DMF at  $1 \text{ mg mL}^{-1}$  concentration and the solution was ultrasonicated for 30 minutes to ensure complete dispersion of  $G_c$  and to prevent any agglomeration prior to deposition. An alumina membrane of 47 mm diameter and 100 nm pore size (purchased from Fisher Scientific) was trapped at the bottom of a Buchner funnel with the same diameter and sealed to a Buchner flask. The  $G_c$ /DMF solution was then poured into the flask and vacuum was applied to drain the solution through the alumina membrane that trapped the  $G_c$  but allowed DMF to go through forming a uniform film whose thickness was depended on the amount of  $G_c$  dispersed in the DMF solution. The alumina membrane was moved to a furnace and dried for 10 minutes at  $50^\circ\text{C}$ . To remove the alumina membrane from the  $G_c$  film, it was placed in a 1M sodium hydroxide (NaOH) bath for about 20 minutes. The membrane detached and left a film

floating of  $G_c$  on the surface. The NaOH solution was removed with a syringe and the film was washed ten times. The film was finally deposited on top of an ITO-coated glass substrate and dried for 15 minutes at  $50^\circ\text{C}$ . The deposition stages are shown in Figure 3.3. The hydrophobic nature of graphite prevented it from being used as substrate in this deposition method. Since the area of the film is known (the same as the alumina membrane's) and the weight of  $G_c$  is also known (from the dispersion concentration of  $G_c$  in DMF), the electrode's mass loading was  $0.06 \text{ mg cm}^{-2}$ . The gel electrolyte was sandwiched between two electrodes and the supercapacitor device was made.

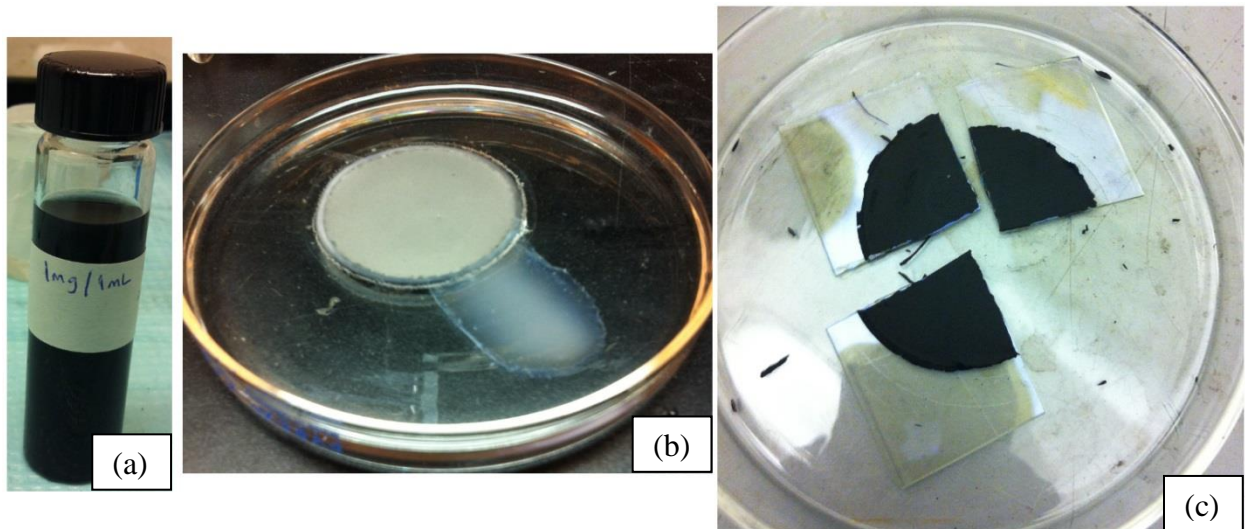


Figure 3.3 Deposition stages of binder-free  $G_c$  using an alumina membrane. (a)  $G_c$  dispersed in DMF, (b)  $G_c$  film on top of an alumina membrane that's detaching from the rim and dissolving in a bath of 1M NaOH, and (c)  $G_c$  film on ITO-coated glass substrate ready to be tested.

### 3.2.3 Gel Electrolyte

PVA (MW 89000-98000+%) was stirred and dissolved in deionized water and phosphoric acid ( $\text{H}_3\text{PO}_4$ ) was added, thoroughly stirred, and resulted in a viscous gel electrolyte. The supercapacitor electrodes were clamped with the gel in the middle and left for 24 hours prior to measuring their performance to ensure that the electrodes were completely adhered and cannot be easily separated.

### 3.3 Electrochemical Characterizations

The CV and EIS of the fabricated supercapacitors were measured and the results are shown in Figures 3.4 and 3.5 for  $G_c/PVDF$  and  $G_c$ , respectively. The CVs in both supercapacitors, as expected, do not show any current peaks due to the absence of Faradaic reactions in EDLC materials. The  $C_g$  and  $C_a$  of both deposition techniques were calculated using Equation 2.13 and the associated conversion equations in Table 2.10 and are listed in Table 3.1.

The measured EIS data were fitted using the BioLogic Science Instruments EC-Lab software according to the circuit model shown in Figure 3.4(d) and 3.5(d) where  $R_s$  represents the electrolyte's and contact resistance,  $R_p$  represents the leakage resistance of the supercapacitors,  $R_{CT}$  and  $Q_{CPE}$  represent the charge transfer resistance and non-ideal capacitance (constant phase element) of the porous electrodes. The values of each element of the equivalent circuits are given in Table 3.2.

Table 3.1 Specific capacitance values obtained from CV.

	Mass loading ( $\text{mg cm}^{-2}$ )	Scan rate ( $\text{mV s}^{-1}$ )	$C_g$ ( $\text{F g}^{-1}$ )	$C_a$ ( $\text{mF cm}^{-2}$ )
$G_c/PVDF$	2.2	5	13.3	29.8
		10	12.0	26.8
		20	11.4	25.5
		50	9.9	22.2
		100	8.8	19.6
$G_c$	0.06	5	19.9	2.3
		10	17.9	2.1
		20	17.5	2.0
		50	16.6	1.9
		100	15.6	1.8

Table 3.2 Circuit model parameters' values.

	$R_s$ ( $\Omega$ )	$R_p$ ( $M\Omega$ )	$R_{CT}$ ( $\Omega$ )	$Q_{CPE}$ ( $\text{F s}^{n-1}$ )	$n$	$C_{dl}$ ( $\text{mF}$ )
$G_c/PVDF$	31.1	11.1	46.1	0.00189	0.8	0.15
$G_c$	305.6	1.7	64.9	0.00064	0.9	0.33

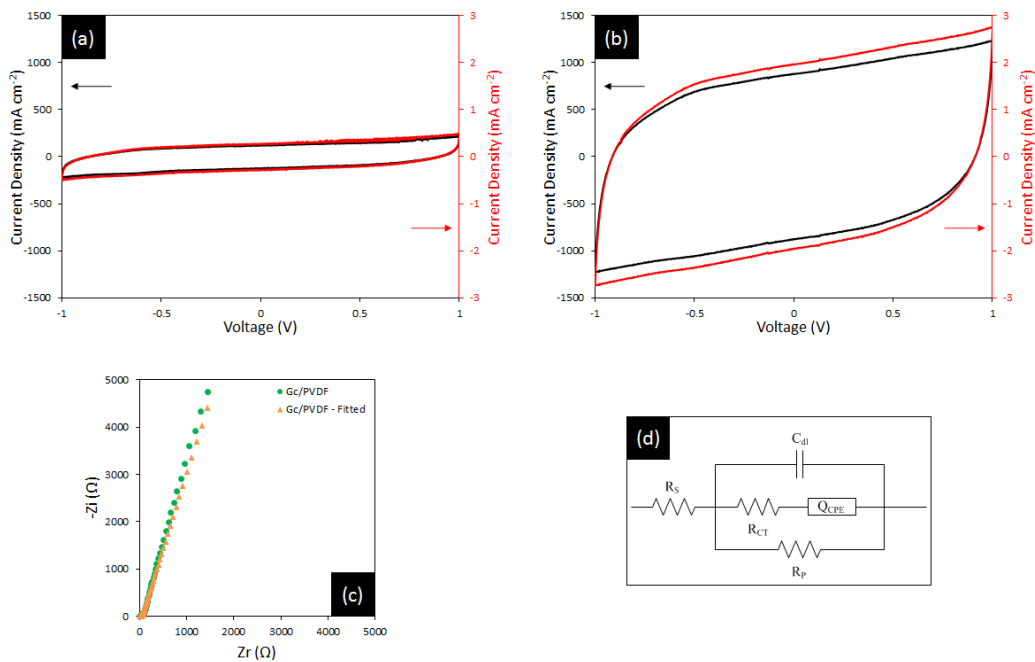


Figure 3.4 Electrochemical characterization of G<sub>c</sub>/PVDF. (a) gravimetric and area CV at 10 mV s<sup>-1</sup>, (b) gravimetric and area CV at 100 mV s<sup>-1</sup>, (c) measured and fitted EIS, (d) circuit model for EIS fitting.

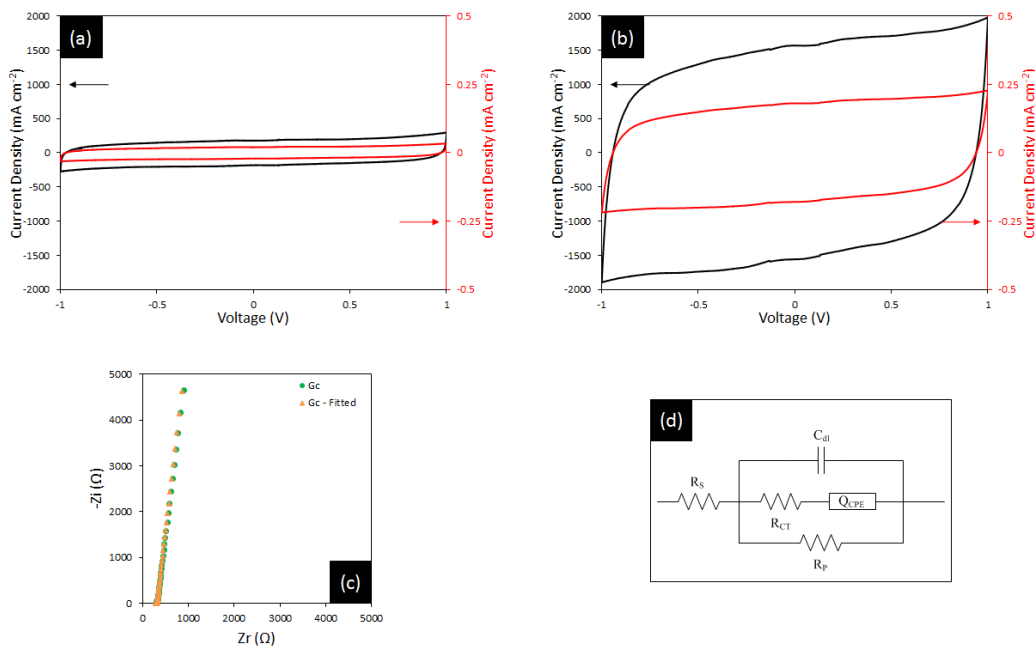


Figure 3.5 Electrochemical characterization of G<sub>c</sub>. (a) gravimetric and area CV at 10 mV s<sup>-1</sup>, (b) gravimetric and area CV at 100 mV s<sup>-1</sup>, (c) measured and fitted EIS, (d) circuit model for EIS fitting.



### 3.4 Discussion

The obtained values of  $n$  are an indication of the extent of the non-ideality of the supercapacitor electrodes for both deposition methods. The  $n$  values are close to unity (ideal capacitance) meaning that there was very little contribution from Faradaic reaction in the charge storage mechanism which is expected of graphene as it is an EDLC material. This is further supported by the CV measurement that do not show any peaks over the tested potential window.

While this was not intended to be a comparative study,  $R_s$  of both deposition techniques can be compared due to its independence from the electrode material and the electrode's thickness. The large  $R_s$  observed from  $G_c$  supercapacitor was due to the semiconducting ITO substrate, the electrolyte is constant for both supercapacitors.

Alumina membrane-assisted vacuum filtration deposition technique offers a great amount of control over the electrode's thickness and its overall performance due to the absence of the binding additives. However, this technique was ineffective when CPs and graphene-CPs were used instead of graphene alone as illustrated in Figure 3.6, as the supporting alumina membrane was dissolved from underneath, the films were completely destroyed. In addition, alumina membranes are much more costly compared to binders

Insulators such as PVDF decrease the overall performance of supercapacitors but their inclusion is important to ensure complete attachment of the electrode materials to the current collectors. It is, however, important not to excessively use binders and limit their weight to fewer than 10% of the total weight of the electrode. Electrodes' thicknesses cannot be reduced to the same amounts as with the vacuum filtration technique but this is not vital for supercapacitors.



Figure 3.6 Films of different graphene-CPs composites and CPs completely break before they can be deposited onto a substrate.

### 3.5 Conclusions

Commercial graphene was used as an electrode material to fabricate supercapacitors utilizing PVDF-bound and binder-free deposition techniques. Binder-free deposition yielded

higher gravimetric capacitance but its high cost and low scale production makes it unattractive for industrial production. PVDF-bound deposition, though PVDF is an insulator and adds dead weight to the supercapacitor electrodes, its ease of use and relative low cost makes it more likely to be widely used.

## **CHAPTER 4: BARIUM STRONTIUM TITANATE AS A HIGH DIELECTRIC BLOCKING LAYER TO REDUCE THE SUPERCAPACITOR SELF-DISCHARGE**

### **4.1 Introduction**

Supercapacitors have excellent energy storage capabilities; however, these devices have certain drawbacks that need to be addressed in order to make them comparable to and as widespread as batteries. While supercapacitors are trying to bridge the gap between conventional capacitors and batteries, their low energy density can be improved by either increasing their capacitance using different materials with high surface area or increasing their operating voltage. Increasing the operating voltage requires the use of alternative electrolytes such as organic or ionic liquid electrolytes.

Charged supercapacitors, similar to batteries, are in a state of higher Gibbs (free energy) and tend to be thermodynamically driven to lower states with time [109]. A self-discharge mechanism can arise as a result of: (i) polarization of the cell to overcharge potentials and thus reaching the thermodynamic decomposition voltages of the electrolyte solution, (ii) presence of impurities in the electrode material that can cause Faradaic reactions within the assigned voltage range, and (iii) cell short circuit between the anode and the cathode [110].

The scope of this chapter is to investigate the effects of barium strontium titanate's (BST) insulating particles' deposition on the self-discharge and specific capacitance of graphene electrodes. While this type of work has been carried out before [111] but with a different material, it showed that reduction of the leakage current but only by compromising the specific

capacitance. The theory is that by using BST one could solve the problem of reduction in specific capacitance because of BST's extremely high dielectric constant 12000-15000 as indicated in Equation 2.2 [112]. Electrochemical diagnostics in this work can prove whether adding BST can, in fact, reduce the self-discharge and at the same time maintain or increase the specific capacitance.

## 4.2 Preparation of Supercapacitor Electrodes

Three methods were adopted to fabricate the electrodes and deposit BST:

- i. D1: alumina membrane-assisted vacuum filtration deposition of commercial graphene ( $G_c$ ) (purchased from Graphene-Supermarket) then commercial barium strontium titanate ( $BST_c$ ) (purchased from TPL Inc. and its data sheet is provided in Appendix A) was deposited using the electrophoresis disposition technique
- ii. D2: drop-cast of commercial graphene ( $G_a$ ) (purchased from Angston Materials) and synthesized barium strontium titanate ( $BST_s$ ) where  $G_a$  was incorporated into the  $BST_s$  synthesis process to form a composite material.
- iii. D3: drop-cast of  $G_a/BST_c$  colloidal solution

D1 was the most important electrode as it allowed for accurate comparison of the same  $G_c$  electrode before and after  $BST_c$  deposition. D2 and D3 were merely exploratory electrodes to examine different deposition methods of  $BST_s$  and their effects of the overall performance of supercapacitors.

### 4.2.1 BST Electrophoresis Deposition

$G_c$  electrodes were deposited using the alumina membrane-assisted vacuum filtration on ITO-PET substrates. After the electrochemical measurements were performed on these electrodes,  $BST_c$  was deposited following the recipe for electrophoretic deposition of barium

titanate ( $\text{BaTiO}_3$ ) [113]: 5g of  $\text{BST}_c$  was added to 0.004g of iodine into 200mL of acetone, the solution was ultra-sonicated in a water bath for 5 minutes. For ceramic materials deposition, the electrode needed to be connected to the cathode while the anode was a platinum mesh. The applied voltage had to be at least 20V. The time of deposition varied depending on the desired amount of BST on the electrode.

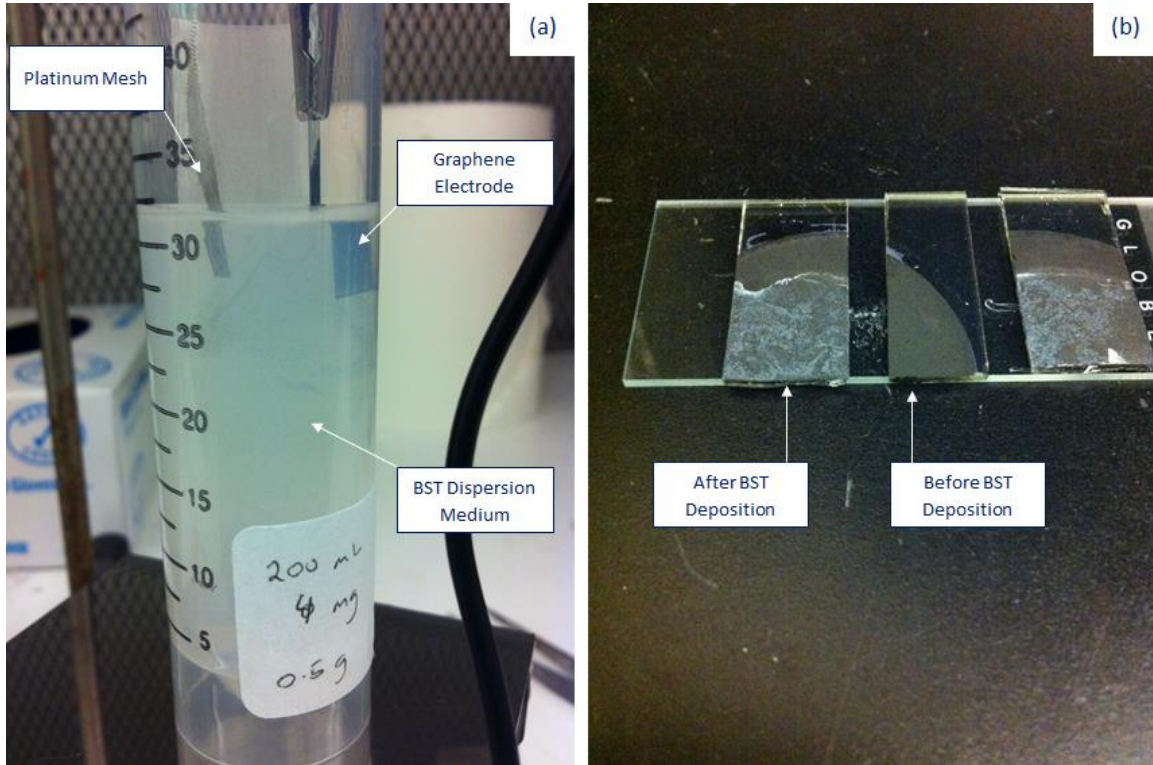


Figure 4.1  $\text{BST}_c$  deposition process on ITO-PET substrates. (a)  $G_c$  electrode dipped in  $\text{BST}_c$  dispersion medium, and (b)  $G_c$  electrode before and after  $\text{BST}_c$  electrophoretic deposition.

#### 4.2.2 BST Synthesis

BST was synthesized using the following precursors: barium acetate, strontium acetate, acetic acid, titanium (IV) isopropoxide and 2-propanol (all purchased from Sigma-Aldrich without any further modifications). 7.67 g of barium acetate was added to 40mL of acetic acid, separately 4.3 g of strontium acetate was added to 40 mL of acetic acid and both stirred until the acetates were completely dissolved. The two solutions were added together and refluxed at  $100^\circ\text{C}$  for five hours then left to cool down to room temperature. 12.66 mL of titanium

isopropoxide was added to 10 mL of 2-propanol and this mixture was added to the refluxed solution and refluxed at room temperature for 10 hours. The solution was refrigerated for at least 12 hours before use.  $Ba_{0.7}Sr_{0.3}TiO_3$  was formed, according to the molarity fraction used, and the synthesis procedure is shown in Figure 4.2 (the presence of graphene in the final step is to indicate the only difference between  $BST_s$  and  $G_a/BST_s$  synthesis). The decomposition temperature of  $BST_s$  was measured using the thermogravimetric analysis (TGA); though  $BST_s$  was never annealed to its decomposition temperature, shown in Figure 4.3, was measured for reference if necessary.

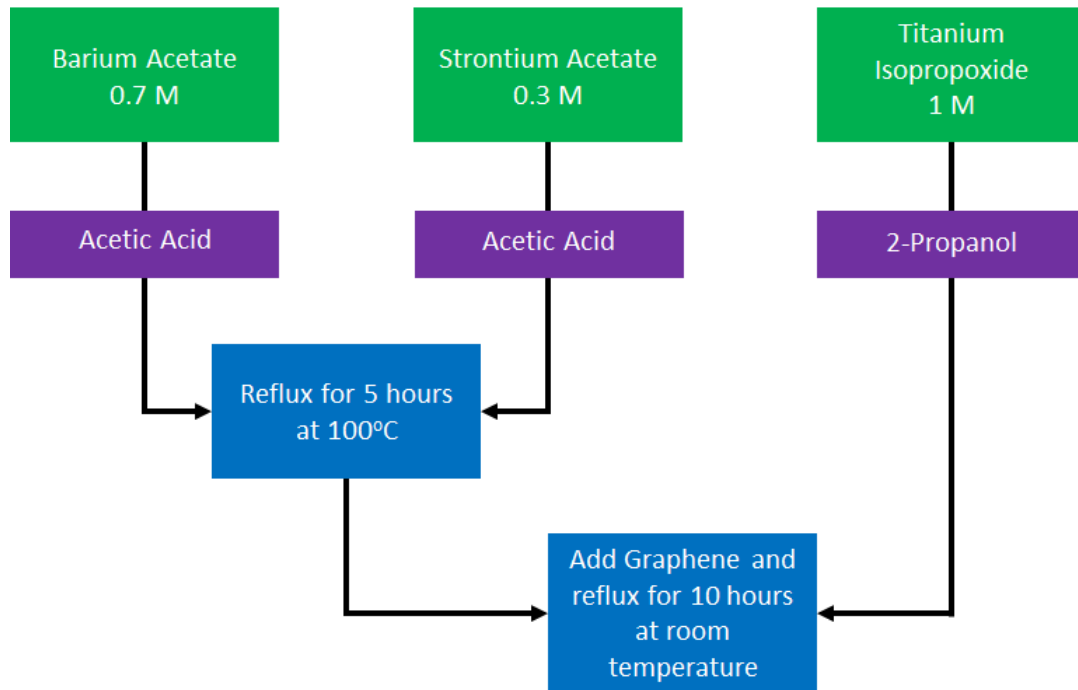


Figure 4.2  $BST_s$  sol-gel synthesis structure.

$G_a/BST_s$  was synthesized using the same process but  $G_a$  was added to the solution before the final refluxing at weight ratio of 1:1. The resulting powder was black instead of the normal white  $BST$  powder due to the presence of graphene.  $G_a/BST_s$  was deposited on graphite substrates and PVDF was used as a binder ( $G_a/BST_s$ :PVDF wt% 90%:10%).

Sample: BST\_pre\_ace\_100213  
Size: 3.6360 mg  
Method: Ramp  
Comment: Ba,Sr-acetate+Ti-propoxide in isopropanol

## DSC-TGA

File: P:\...Moe\TGA\BST\_PRE\_ACE\_100213  
Operator: TA\_MOE  
Run Date: 02-Oct-2013 11:57  
Instrument: SDT Q600 V8.3 Build 101

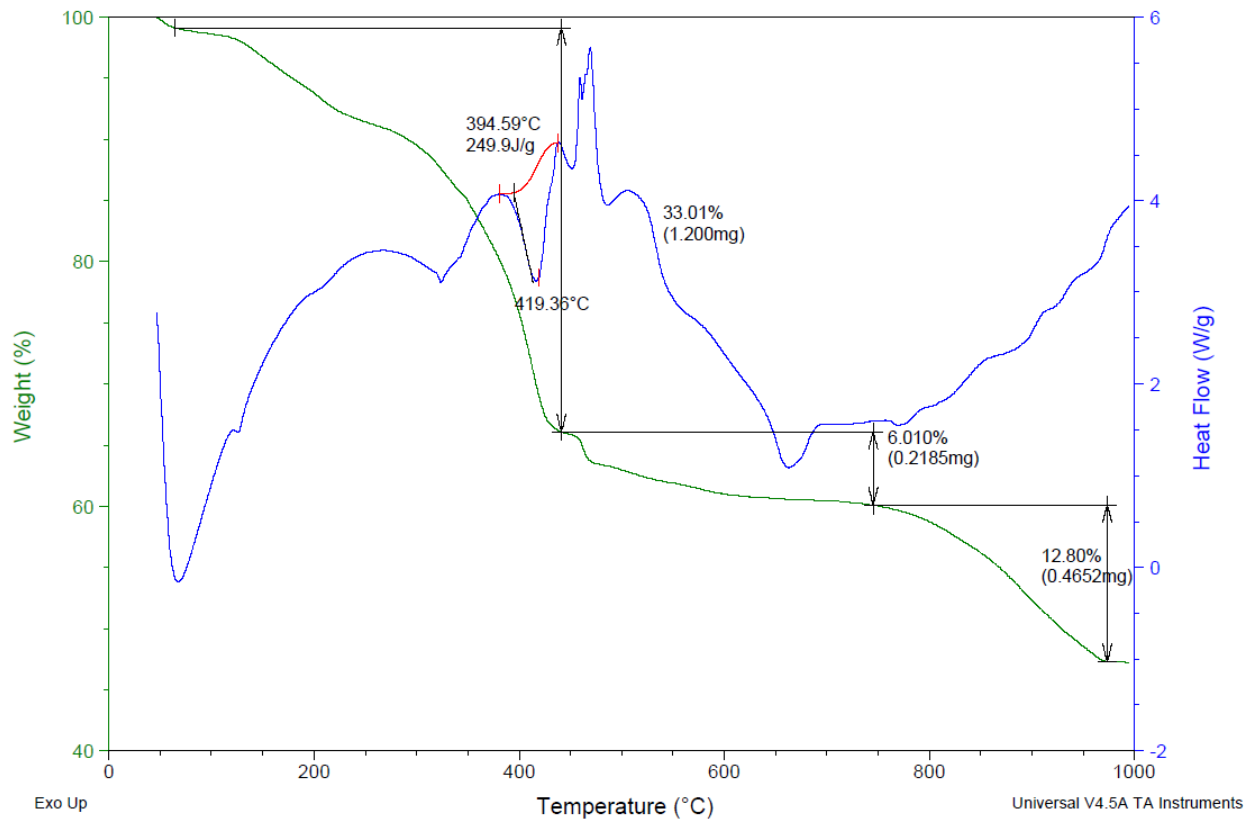


Figure 4.3 TGA of the sol-gel synthesized BST<sub>s</sub> powder.

### 4.3 Electrode Characterization

#### 4.3.1 Morphology

The SEM morphology images of D2 and D3 are shown in Figure 4.4. The top image shows the colloidal solution of G<sub>a</sub>/BST<sub>c</sub> deposited on a graphite substrate and bound by PVDF (G<sub>a</sub>/BST<sub>c</sub>:PVDF wt% 90%:10%), the apparent dispersed white dots are the BST<sub>c</sub> particles and show that they were not deposited as a single uniform layer. The bottom image shows the morphology of a G<sub>a</sub>/BST<sub>s</sub> electrode but in this instance the BST<sub>s</sub> particles are not visible due to the synthesis procedure.



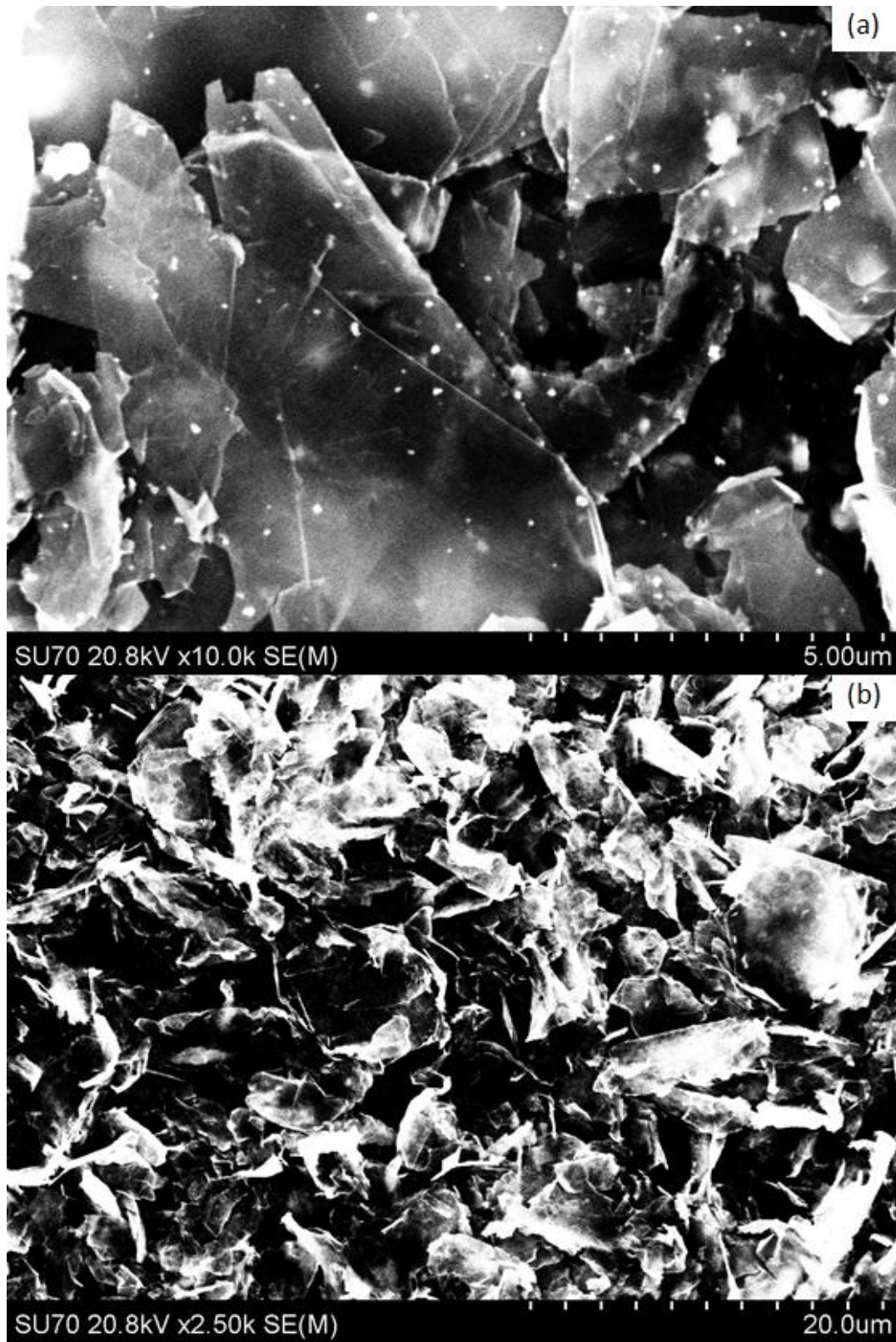


Figure 4.4 SEM images. (a) colloidal  $G_a/BST_c$  and (b)  $G_a/BST_s$  both bound by PVDF and deposited on graphite substrates.

### 4.3.2 Electrochemical Characterizations

D1, D2, and D3 were all measured in the two-electrode cell configuration but with different electrolytes. For D1, aqueous electrolytes persistently detached the deposited film from the current collector as shown in Figure 4.5 therefore 0.5 moles of lithium perchlorate ( $\text{LiClO}_4$ ) dissolved in propylene carbonate (PC) was used. PVA- $\text{H}_3\text{PO}_4$  gel electrolyte was used for D2 and D3.

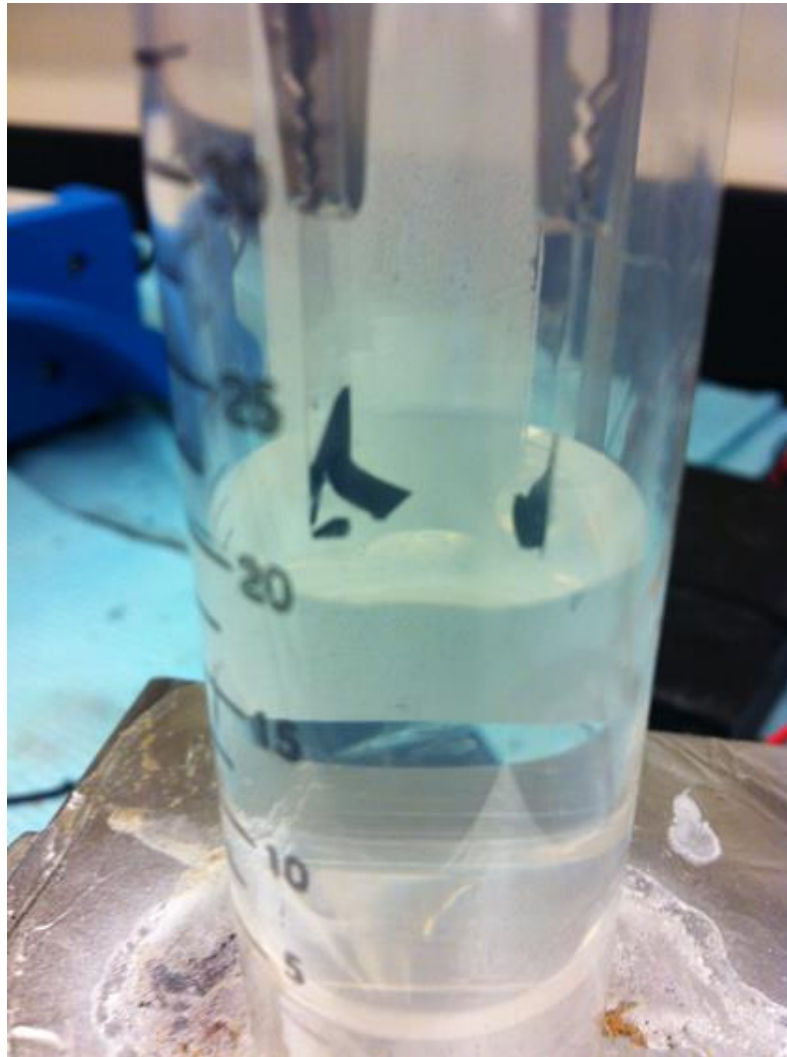


Figure 4.5 Aqueous electrolyte detaching the  $G_c$  film from the ITO-PET substrate.

The CVs of D1 at 4 minutes and 10 minutes of  $\text{BST}_c$  deposition time are shown in Figure 4.6(a-d).  $C_g$  and  $C_a$  of the graphene electrodes drop after the deposition of  $\text{BST}_c$  which is in

accordance with Equation 2.2 since the charge separation distance increased with the deposition of  $\text{BST}_c$ . However the percentage of the dropped capacitance is much lower than expected. The nominal particle size of  $\text{BST}_c$  is 50 nm that is much larger than the PC ion size which is only a few nanometers therefore the capacitance values were expected to drop by an order of magnitude but that was not the case as reported in Table 4.1.

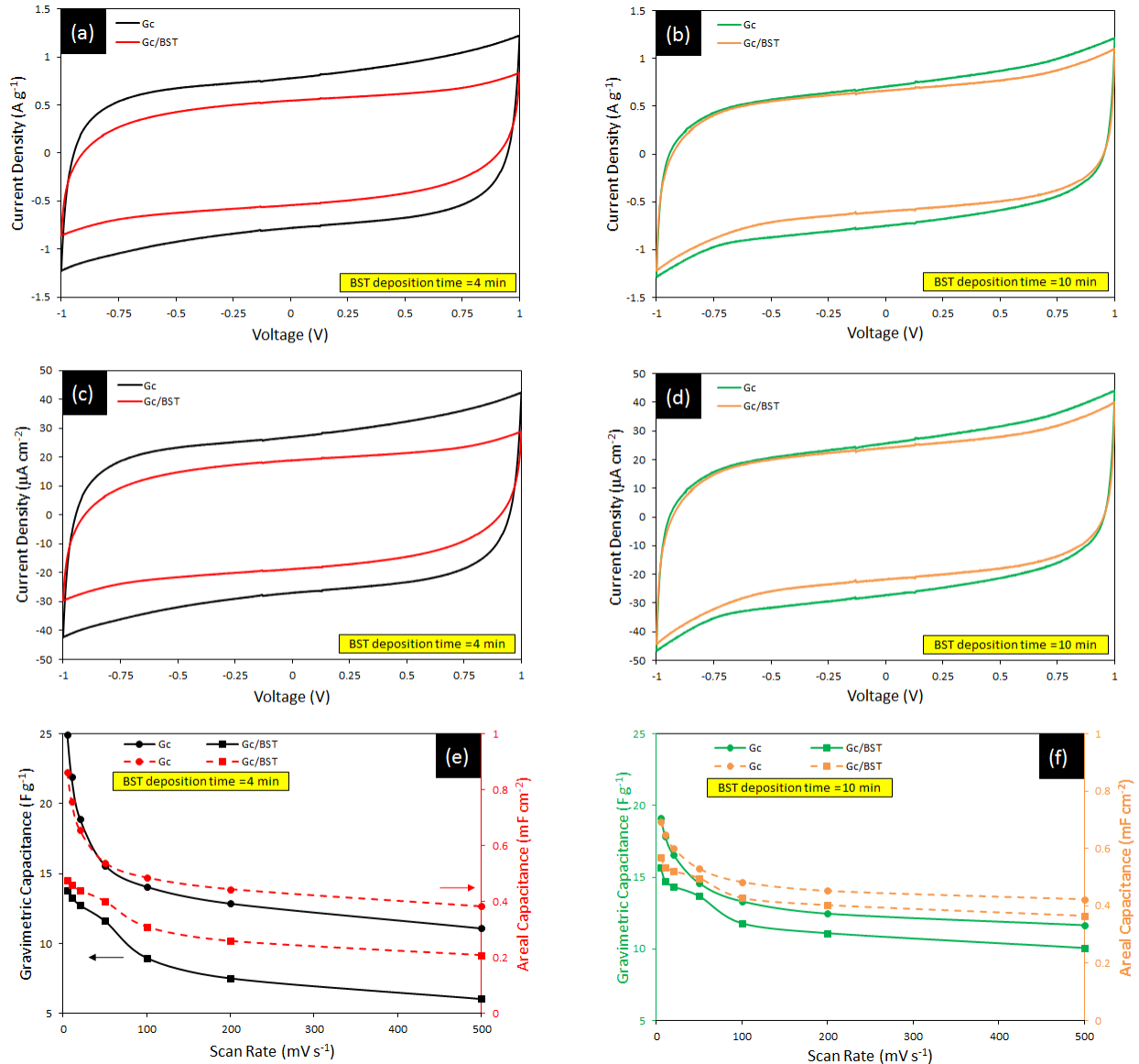


Figure 4.6 Gravimetric (a-b) and areal (c-d) CVs of  $\text{Gc}/\text{BST}_c$  at different deposition times at  $50 \text{ mV s}^{-1}$  scan rate. (e-f)  $C_g$  and  $C_a$  as a function of the scan rate.

Table 4.1  $C_g$ ,  $C_a$  and the percentage of drop in specific capacitance after  $BST_c$  deposition

	Mass loading ( $\mu\text{g cm}^{-2}$ )	Scan rate ( $\text{mV s}^{-1}$ )	$C_g$ ( $\text{F g}^{-1}$ )	$C_a$ ( $\text{mF cm}^{-2}$ )	C drop
$G_c$	34.6	5	24.9	0.86	
		10	21.9	0.76	
		20	18.9	0.65	
		50	15.6	0.54	
		100	14.1	0.49	
		200	12.9	0.44	
		500	11.1	0.38	
$G_c/BST_c$ 4 min	34.6	5	13.8	0.48	44.7%
		10	13.3	0.46	39.3%
		20	12.7	0.44	32.7%
		50	11.6	0.40	25.6%
		100	9.0	0.31	36.2%
		200	7.5	0.26	41.6%
		500	6.0	0.21	45.6%
$G_c$	36.3	5	19.1	0.69	
		10	17.9	0.65	
		20	16.5	0.60	
		50	14.6	0.53	
		100	13.3	0.48	
		200	12.5	0.45	
		500	11.7	0.42	
$G_c/BST_c$ 10 min	36.3	5	15.7	0.57	18.0%
		10	14.7	0.54	17.5%
		20	14.4	0.52	13.3%
		50	13.7	0.50	6.2%
		100	11.8	0.43	11.5%
		200	11.1	0.40	11.0%
		500	10.1	0.37	13.6%

Figure 4.6(e-f) shows the difference in the  $C_g$  and  $C_a$  as a function of the scan rate. The  $G_c$  electrodes exhibit a large drop as the slow scan rates increased (5, 10, and 20  $\text{mV s}^{-1}$ ) indicating a high porosity in the structure of the electrodes. However the same trend was not observed with the  $G_c/BST_c$  electrodes suggesting that the  $BST_c$  particles covered some of the pores preventing the electrolyte from penetrating deep into the electrodes' structure at slow scan rates as it did before the deposition  $BST_c$ . this trend was also confirmed with D2 and D3 supercapacitors as indicated in Figure 4.7.

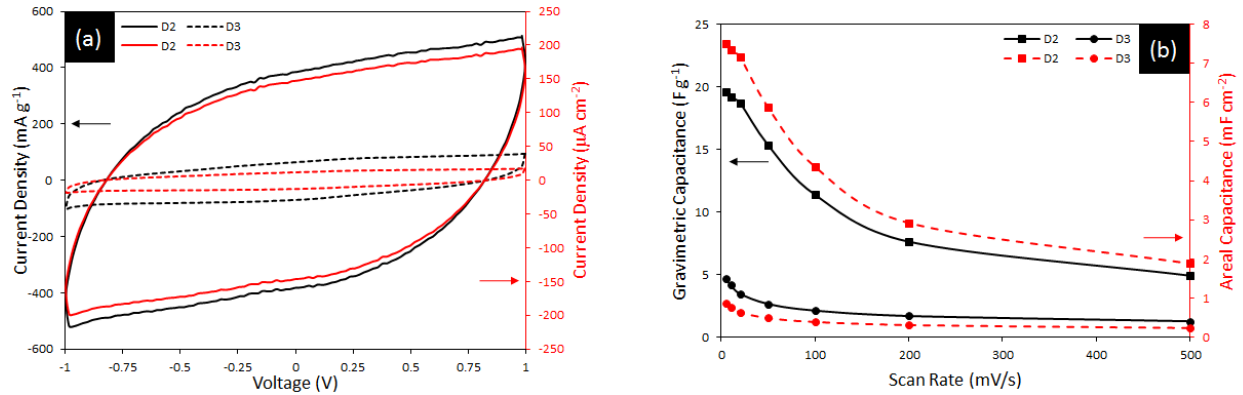


Figure 4.7 (a) gravimetric and areal CVs of D2 and D3 supercapacitors at  $50 \text{ mV s}^{-1}$  scan rate. (b)  $C_g$  and  $C_a$  as a function of the scan rate.

Reported studies on the deposition of a uniform layer with a low dielectric constant (polyphenylene oxide (PPO),  $\epsilon_r = 3.5$ ) and the effects the blocking layer thickness[111][114] on  $C_g$  show an exponential drop, for example, a 3 nm PPO layer reduced  $C_g$  by almost 72%. The  $\text{BST}_c$  particles are much larger yet their effect of  $C_g$  and  $C_a$  is not as large as what has been reported for the other material. Additionally, as the deposition time of  $\text{BST}_c$  increased, the drop in  $C_g$  and  $C_a$  decreased to as low as 6.2% only for  $\text{G}_c/\text{BST}_c$  at 10 minutes of deposition time tested at  $50 \text{ mV s}^{-1}$ .

The adopted model for the uniform blocking layer interface[111][114] is show in Figure 4.8(a) but this circuit cannot be used to model the intermittent particles disposition on the surface of the  $\text{G}_c$  electrodes. A suggested model is shown in Figure 4.8(b), where  $x$  is the  $\text{BST}_c$ -free area of the electrode and  $C_{bl}$  is the blocking layer capacitance, indicating that the blocking layer itself contributes to the overall capacitance.

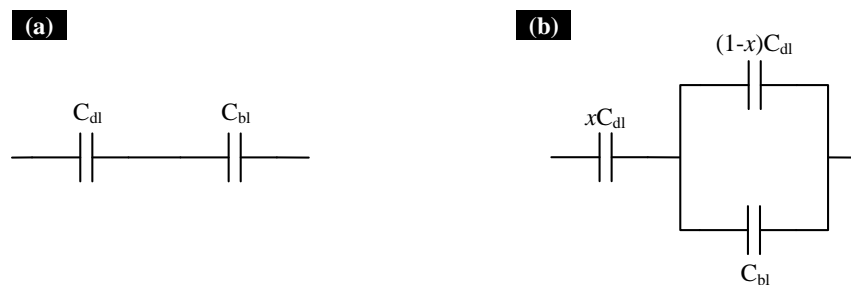


Figure 4.8 (a) uniform blocking layer model and (b)  $\text{G}_c/\text{BST}_c$  model.

The EIS measured and fitted data are shown in Figure 4.9 along with the fitting models using the BioLogic Science Instruments EC-Lab software. The presence of  $BST_c$  is modeled with the addition of a  $C_{bl}$  and a blocking layer resistance arising from  $BST_c$  ( $R_{bl}$ ). The circuit's components' values are listed in Table 4.2.

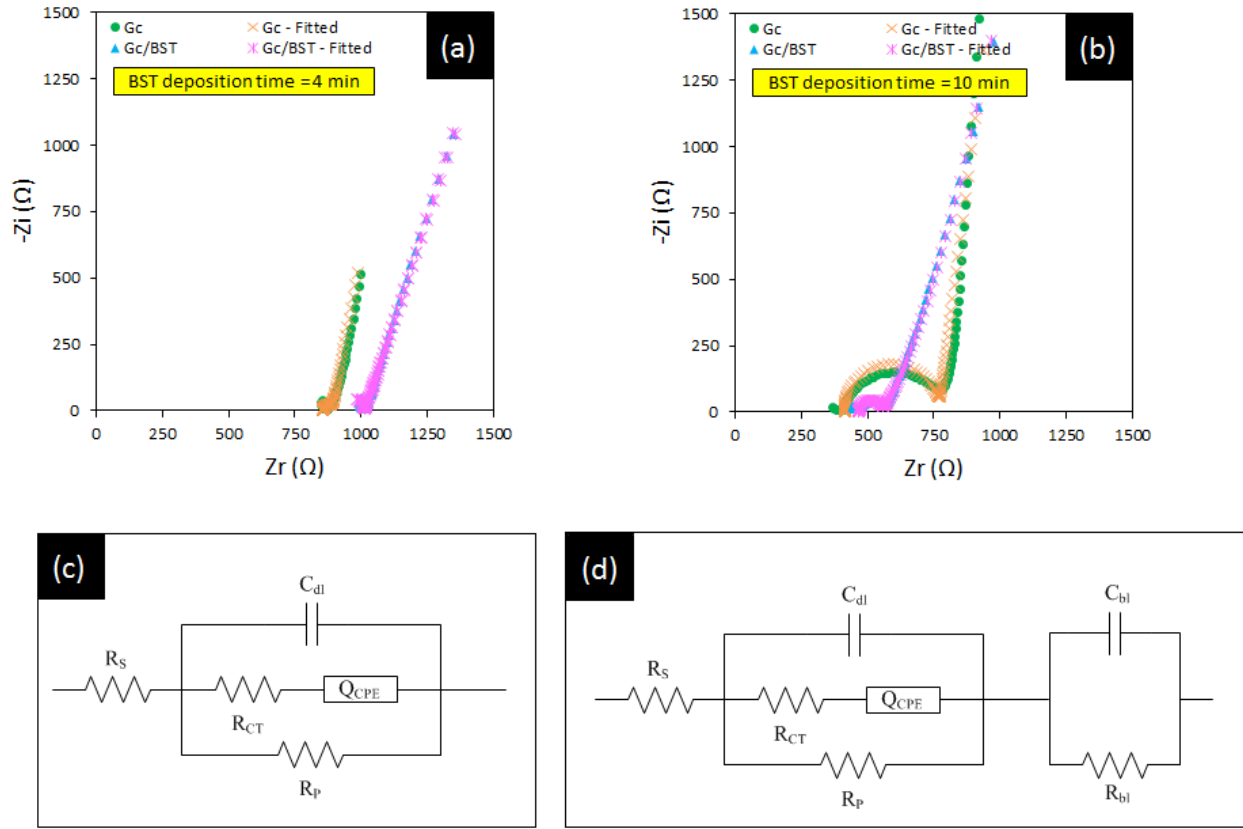


Figure 4.9 (a) and (b) measured and fitted EIS of  $G_c$  and  $G_c/BST_c$  at different deposition times. (c) circuit model used to fit  $G_c$ , and (d) circuit mode used to fit  $G_c/BST_c$ .

Table 4.2 EIS fitting parameters' values.

	$R_s$ (Ω)	$R_p$ (MΩ)	$R_{CT}$ (Ω)	$R_{bl}$ (kΩ)	$Q_{CPE}$ (mF s <sup>n-1</sup> )	n	$C_{dl}$ (μF)	$C_{bl}$ (mF)
$G_c$	856	23.9	42.9	-	0.35	0.87	23.9	-
$G_c/BST_c$ 4 min	916	0.245	95.7	44	0.22	0.79	0.011	3.8
$G_c$	413	395	359.7	-	0.28	0.92	1.2	-
$G_c/BST_c$ 10 min	468	0.004	87.2	206	0.72	0.58	0.6	0.3

$G_c/BST_c$  (4 min  $BST_c$  deposition time) supercapacitor was charge at 1 V for 12 hours then the open circuit potential was measured for 12 hours immediately after the charging was over. Figure 4.10 shows that the discharge rate for the  $G_c/BST_c$  was much faster than  $G_c$  alone indicating a larger leakage current in the  $G_c/BST_c$  supercapacitor which is confirmed by the large drop in  $R_p$  in the fitted model. It is suggested that the  $BST_c$  particles were charged effectively taking away the charges that the  $G_c$  pores could have stored and since  $BST_c$  is not a porous material it discharged much faster than  $G_c$ .

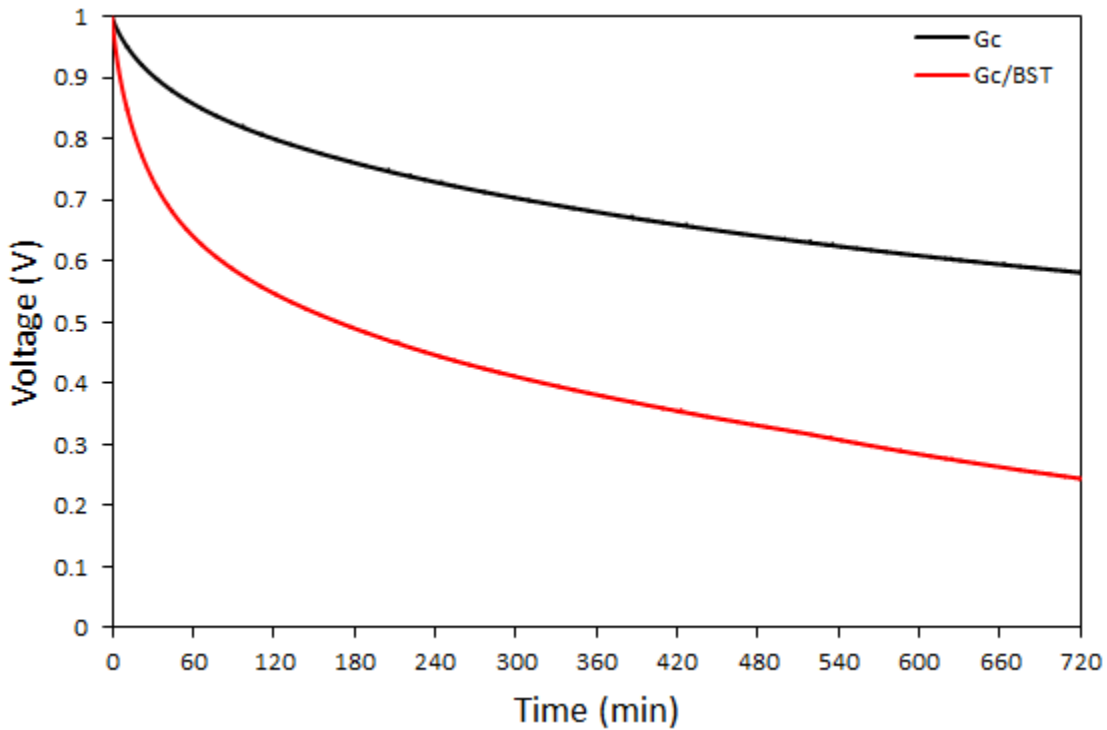


Figure 4.10 Open circuit potentials of  $G_c$  and  $G_c/BST_c$  (4 min) over a 12 hour period.

The role of  $BST$  was to reduce the self-discharge of graphene-based supercapacitors with a reduction of the specific capacitance was expected as a consequence of depositing  $BST$  particles. The other expectation was that with the increase of  $BST$  deposition time, the specific capacitance would decrease even further. However, those trends were not observed. A

comprehensive understanding of the role of BST on the self-discharge and specific capacitance is required in order to accurately describe the phenomena of this material.

#### 4.4 Conclusions

The electrophoresis deposition technique was used to deposit particles of  $BST_c$  on the surface of  $G_c$  electrodes. The high dielectric constant of  $BST_c$  contributed to a larger capacitance and prevented the specific capacitance from being substantially reduced, as compared to previous studies where a uniform blocking layer was used, with the capacitance dropping exponentially with an increase in the blocking layer thickness.

The  $BST_c$ , however, had a negative impact on the self-discharge and reduced the time constant of the  $G_c$  supercapacitor. The self-discharge increased even further with an increase in the thickness of the BST layer. While  $BST_c$  might not be the best material to reduce the supercapacitor self-discharge problem, it could potentially be used to enhance the capacitance. Further work is required to better understand these effects.



## CHAPTER 5: SOL-GEL SYNTHESIS OF RUTHENIUM OXIDE-GRAPHENE NANOCOMPOSITES AS ELECTRODE MATERIAL FOR SUPERCAPACITORS

### 5.1 Introduction

Ruthenium oxide ( $\text{RuO}_2$ ) is considered one of the most attractive materials for supercapacitor applications due to its exceptional charge storage properties. The two dominating energy storage mechanisms in supercapacitors are (i) the separation of charges in the electric double layer where the charges are accumulated at the electrode/electrolyte interface and (ii) the Faradiac reactions where the reduction and oxidation (redox) of the electrode material takes place which is also known as pseudocapitance.  $\text{RuO}_2$  storage mechanism is of the latter type however its relative low surface area, when compared to carbon materials, along with its toxicity and scarcity [115] prevents it from dominating supercapacitor electrodes.

To circumvent the disadvantages of  $\text{RuO}_2$  as a supercapacitor electrode material, nanocomposites of  $\text{RuO}_2$  and graphene were synthesized using the sol-gel synthesis process. Various nanocomposites of conducting polymers (CPs) and graphene (G) were synthesized previously by this group [90-92] and procedure was modified to use  $\text{RuO}_2$  instead of the polymers to fabricate electrodes.

### 5.2 Experimental

#### 5.2.1 Material Synthesis

$\text{RuO}_2$  powder was synthesized by dissolving 1g of  $\text{RuCl}_3 \cdot x\text{H}_2\text{O}$  in 100 mL of deionized water and, later, mixing the solution in 10 mL ammonium hydroxide ( $\text{NH}_4\text{OH}$  28%) and 90 mL

deionized water. The mixture was first heated to 80°C. 25 mL of hydrogen peroxide (H<sub>2</sub>O<sub>2</sub> 50%) was then dripped slowly into the solution for 4 hours at 80°C. The colloidal RuO<sub>2</sub> formed was allowed to react for 24 hours at room temperature. Further, the colloidal solution was centrifuged and any excess of hydrogen peroxide and ammonium hydroxide was removed. The precipitate was cleaned several times by the addition of water and subsequent centrifugation. It was then dried at 100°C and annealed at 400°C for 3 hours to yield RuO<sub>2</sub> nanoparticles. Similarly, RuO<sub>2</sub>-G nanocomposites were synthesized by employing the same process but with graphene added to RuCl<sub>3</sub>.xH<sub>2</sub>O in the first step of the reaction. The weight of graphene to RuCl<sub>3</sub>.xH<sub>2</sub>O was varied in order to obtain different ratios of RuO<sub>2</sub>-G nanocomposites.

The ruthenium chloride, ammonium hydroxide, hydrogen peroxide, nafion 117 and various electrolytes were purchased from Sigma-Aldrich. The chemicals RuCl<sub>3</sub>.xH<sub>2</sub>O and graphene were purchased from Angstrom Materials. All the purchased materials were used as purchased without any modification.

### **5.2.2 Characterization**

The X-ray diffraction (XRD) peaks were obtained using the Philips Panalytical Xpert Pro MRD with 2θ range from 20° to 60°. Surface morphology images of the electrodes were captured using the Hitachi S-800 scanning electron microscope (SEM) the same machine was used to obtain the peaks of the energy dispersive spectroscopy (EDS). TECNAI F20 transmission electron microscope (TEM) was also used.

### **5.2.3 Electrodes Preparation**

Powders produced by the sol-gel synthesis were used to fabricate the supercapacitor electrodes. To ensure thorough adhesion of electrode materials, nafion was used as a binder and

the resulting paste was drop-casted onto the graphite substrates of active area of approximately 1cm x 1cm.

#### 5.2.4 Electrochemical Measurements

All the electrochemical measurements were carried out in the two-electrode cell setup using 2M H<sub>2</sub>SO<sub>4</sub> aqueous electrolyte. The CV, CCCD, and EIS were all performed at room temperature.

#### 5.3 Results and Discussion

SEM and TEM images shown in Figure 5.1 of RuO<sub>2</sub> and RuO<sub>2</sub>-G nanocomposites, smaller sized particles are observed throughout the surface of the electrode. Upon the introduction of graphene into the RuO<sub>2</sub> synthesis procedure, an overlapping platelet-like structure is formed. The SEM images also confirm the formation of random big clusters of hydrous RuO<sub>2</sub> agglomeration in RuO<sub>2</sub>-G that increases with the higher ratio of RuO<sub>2</sub>[81].

The TEM images of RuO<sub>2</sub>-G 10:4 show that each graphene sheet is covered by RuO<sub>2</sub>. The RuO<sub>2</sub> results reveal a spacing of 3.16 Å corresponding to the 110 plane of the RuO<sub>2</sub> nanocomposite.

Figure 5.2 shows the EDS peaks of (a) synthesized RuO<sub>2</sub>, (b) RuO<sub>2</sub>-G 10:1, and (c) RuO<sub>2</sub>-G 1:1. The wt. % quantification was performed using EDS measurements of various synthesized nanomaterials. The synthesized RuO<sub>2</sub> showed a composition of Ru(L) 77.68% and O(K) 22.32%, whereas, for the RuO<sub>2</sub>-G 10:1 composition it showed Ru(L) 76.48% and C(K) 23.52%. The EDS study reveals a composition of Ru(L) 50.51% and C(K) 49.49% in the nanocomposite of RuO<sub>2</sub>-G with equal ratios. The percentage of each component indicates that the ratio of RuO<sub>2</sub> to carbon is close to what was calculated for this synthesis process.

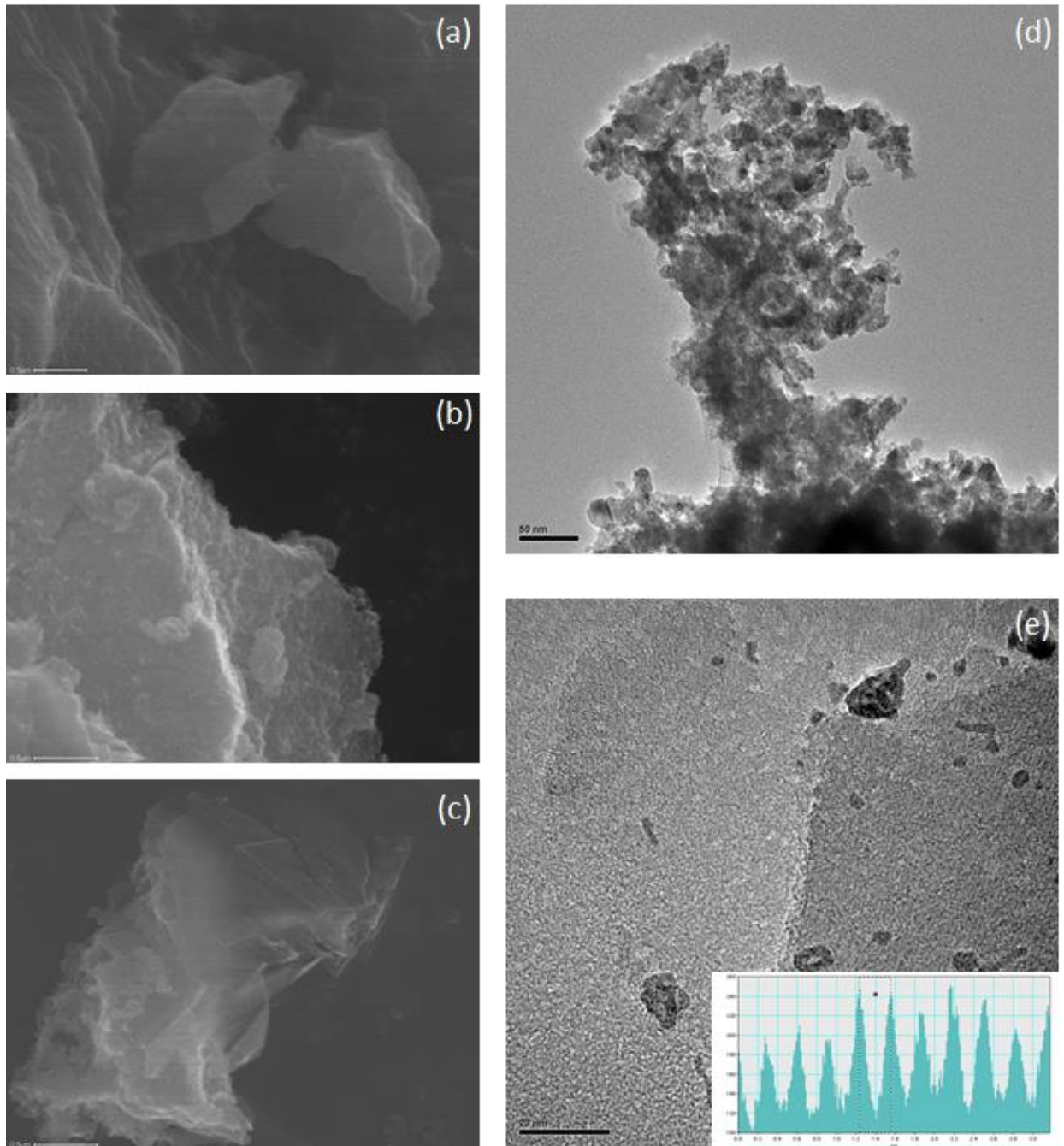


Figure 5.1 Morphology images of different synthesized powders. SEM : (a) synthesized  $\text{RuO}_2$ , (b)  $\text{RuO}_2\text{-G}$  at 10:1 ratio, and (c)  $\text{RuO}_2\text{-G}$  at 1:1 ratio. TEM: (d) and (e) both of  $\text{RuO}_2\text{-G}$  at 10:4 ratio.

The X-ray diffraction shown in Figure 5.3 of the  $\text{RuO}_2\text{-G}$  at 10:1 ratio reveals two peaks at  $26.5^\circ$  and  $54.5^\circ$  that correspond to the (002) and (004) planes of graphite, respectively. The presence of graphite planes indicate that restacking of graphene and the absence of the  $\text{RuO}_2$

peaks, with exception to the small peak in the middle, is attributed to the low annealing temperature used in the synthesis process [116-117].

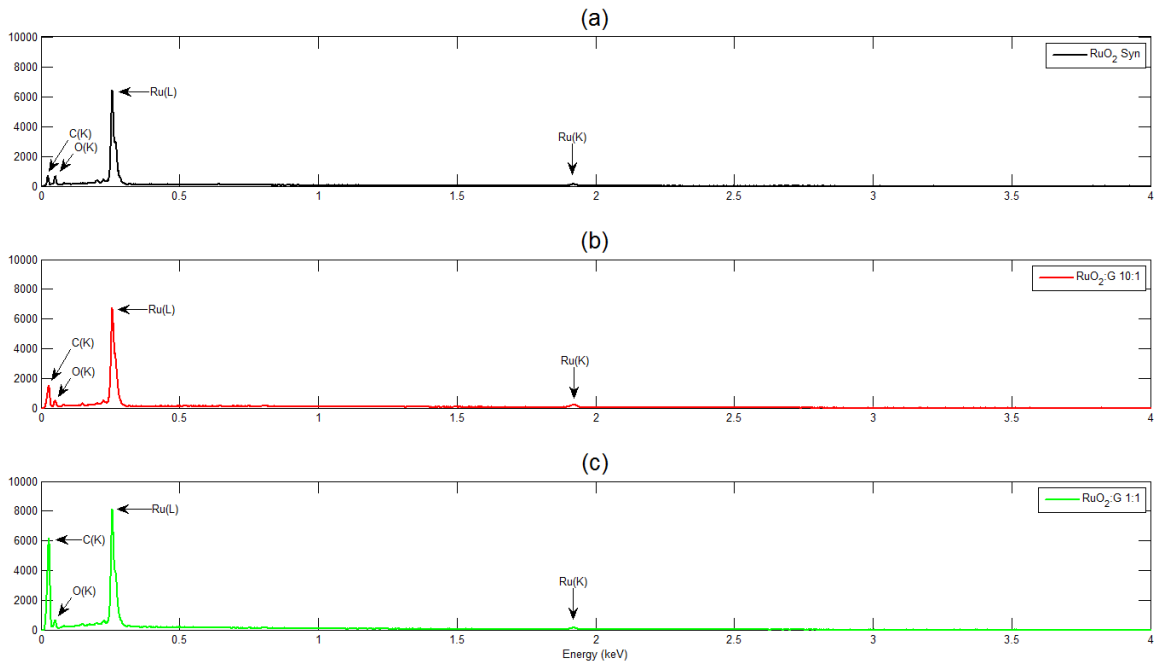


Figure 5.2 EDS peaks. (a) synthesized  $\text{RuO}_2$ , (b)  $\text{RuO}_2$ -G at a 10:1 ratio, and (c)  $\text{RuO}_2$ -G at a 1:1 ratio.

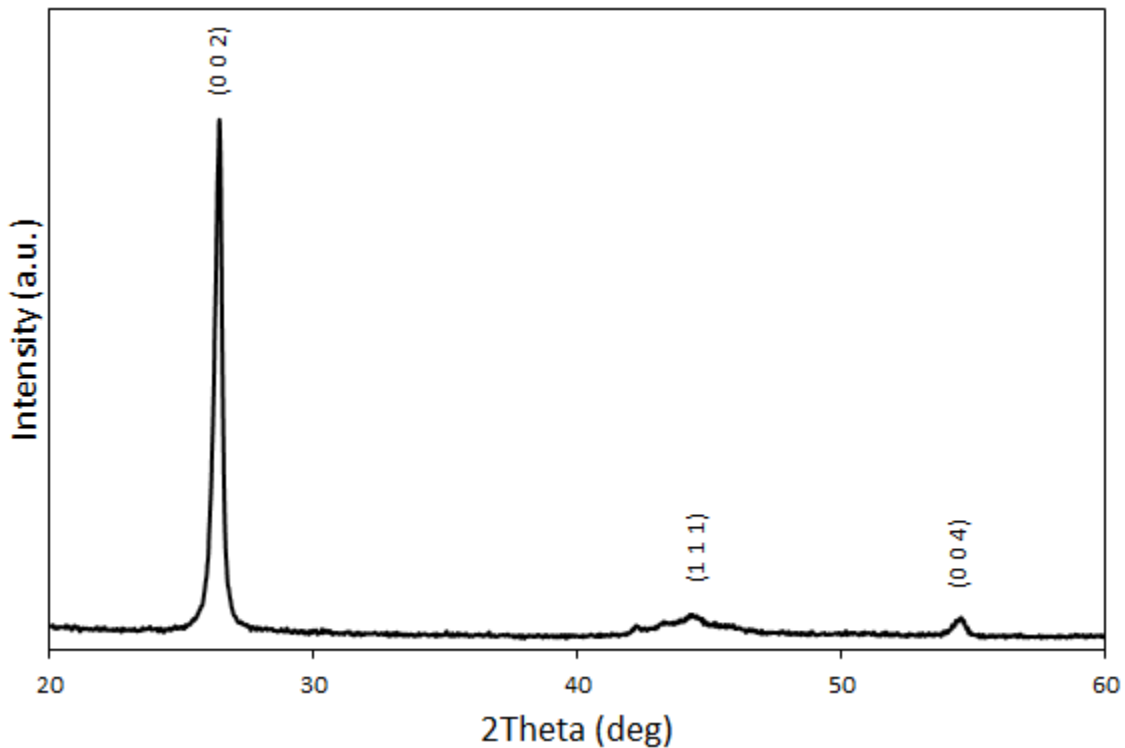


Figure 5.3 XRD diffraction peaks of  $\text{RuO}_2$ -G at a 10:1 ratio.

The CV curves shown in Figure 5.4(a) of the synthesized powders measured in a 2M H<sub>2</sub>SO<sub>4</sub> with the voltage range of -1 V to 1 V that is larger than expected for aqueous electrolytes but did not exhibit electrolyte breakdown. The observed current is higher for composite electrodes than that of RuO<sub>2</sub> only. The RuO<sub>2</sub> is present in the intercalated multilayers of G in the RuO<sub>2</sub>-G nanocomposites and this allows a larger number of ions to interact with electrode. The specific capacitance values are calculated using the equation:

$$C_{sc} = \frac{I}{Av} \quad (5.1)$$

where I is the average current, A is the area of the electrode, and  $v$  is the scan rate.

RuO<sub>2</sub>-G at the 10:1 ratio produced the highest areal capacitance indicating that the addition of graphene can improve the performance of the supercapacitor electrodes. The obtained areal capacitance of synthesized RuO<sub>2</sub> was 7.3 mF cm<sup>-2</sup> while the areal capacitance of RuO<sub>2</sub>-G at 10:1 and 1:1 ratios was 187.5 mF cm<sup>-2</sup> and 136.4 mF cm<sup>-2</sup>, respectively. These results of the areal capacitance are better than those of the synthesized hydrous RuO<sub>2</sub> (1.8 mF cm<sup>-2</sup>) [118] and RuO<sub>2</sub>-multiwire carbon nanotube composites (16.94 mF cm<sup>-2</sup>) [119]. The difference in the synthesis methods as well as the electrode thicknesses have been found to contribute to the variation in the values of the specific capacitance [120-121]. The comparison of areal capacitance with respect to the scan rate of the synthesized powders is shown in Figure 5.4(b). While the areal capacitance is higher for RuO<sub>2</sub>-G 1:10 at low scan rates, at high scan rates it deteriorates and becomes lower than that of RuO<sub>2</sub>-G 1:1. The reason behind the drop in areal capacitance at high scan rates is the content of RuO<sub>2</sub> particles. A higher surface area is exposed with RuO<sub>2</sub>-G 1:10 but agglomeration of the graphene sheets along with the fast voltage sweep prevents the electrolyte from utilizing the porous graphene structure. On the other hand, RuO<sub>2</sub>-G 1:1 includes more RuO<sub>2</sub> particles that act as spacers between the graphene sheets allowing

electrolyte ions to penetrate deeper at higher voltage sweeps resulting in more charge storage. The CCCD responses are shown in Figure 5.4(c) at a constant current of  $1 \text{ mA cm}^{-2}$  in a  $2\text{M H}_2\text{SO}_4$ . Following the same trend observed in the CV curves

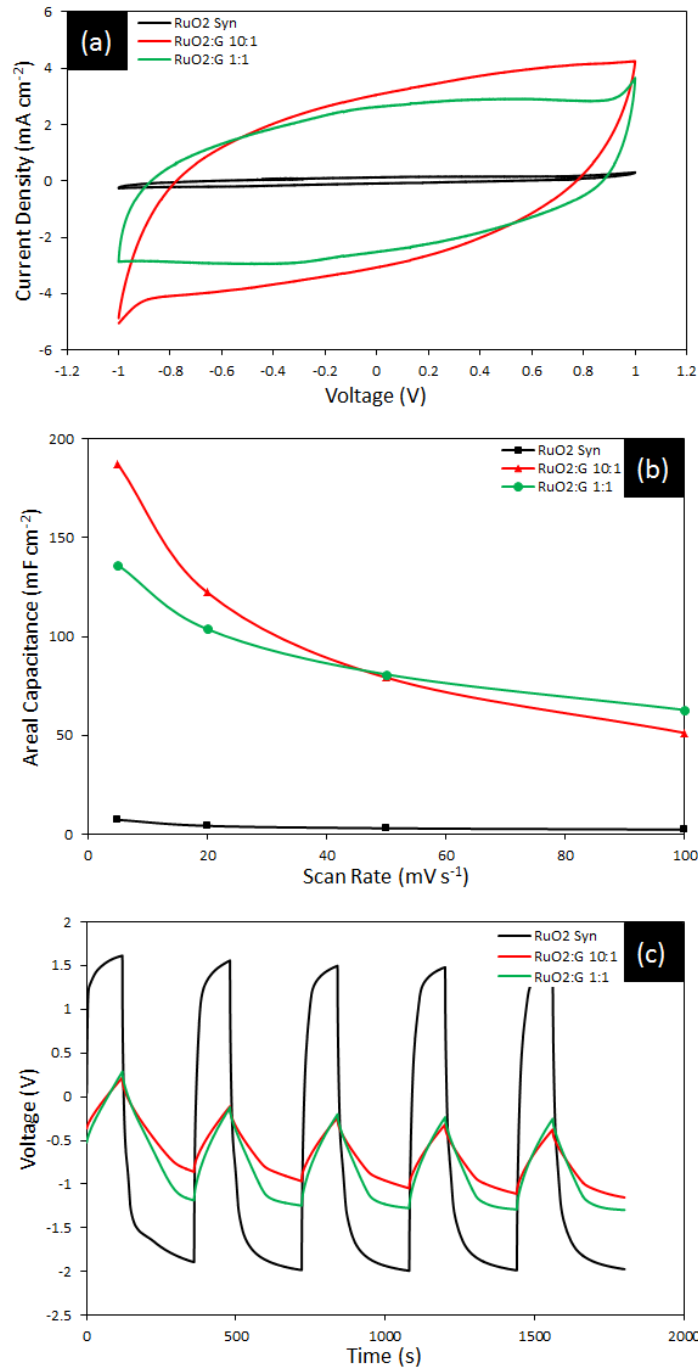


Figure 5.4 (a) CV of synthesized  $\text{RuO}_2$ ,  $\text{RuO}_2\text{-G 10:1}$  ratio, and  $\text{RuO}_2\text{-G 1:1}$  ratio in  $2\text{M H}_2\text{SO}_4$  at  $20 \text{ mV s}^{-1}$  scan rate. (b) specific capacitance as a function of scan rate. (c) CCCD of the synthesized powders at  $1 \text{ mA cm}^{-2}$  charge/discharge current in  $2\text{M H}_2\text{SO}_4$ .

EIS measurements, shown in Figure 5.5, were performed with a frequency sweep range of 100 kHz – 100 mHz and AC amplitude of 10mV in a 2M H<sub>2</sub>SO<sub>4</sub>. The Nyquist plots indicate a low equivalent series resistance for all the electrodes. Interestingly, RuO<sub>2</sub>-G 1:1 has a smaller resistance than RuO<sub>2</sub>-G 10:1 indicating once again that the graphene sheets agglomerate more with the lower content of RuO<sub>2</sub>. As for the charge transfer resistance, the Warburg impedance has been observed at the high frequency end of the Nyquist plot [122].

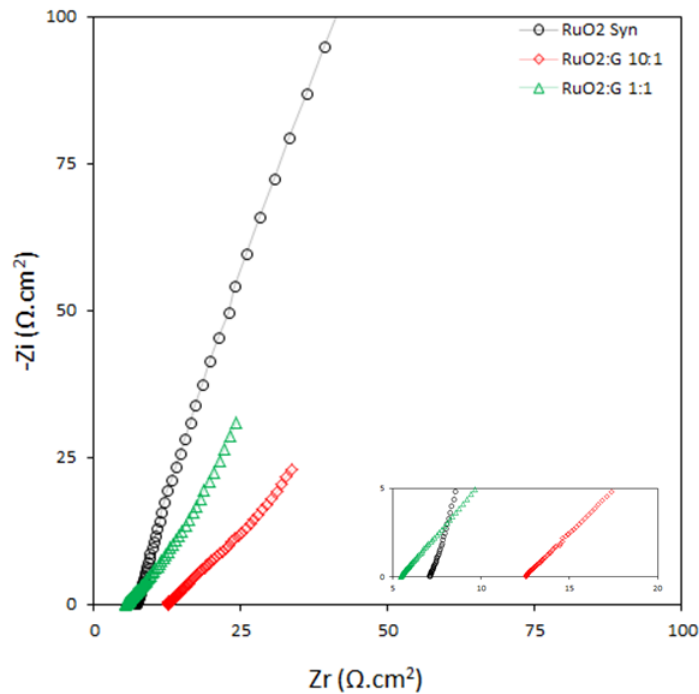


Figure 5.5 EIS of the synthesized RuO<sub>2</sub>, RuO<sub>2</sub>-G at the 10:1 ratio, and RuO<sub>2</sub>-G at the 1:1 ratio in 2M H<sub>2</sub>SO<sub>4</sub>.

#### 5.4 Conclusions

RuO<sub>2</sub>-G nanocomposites were synthesized using the sol-gel technique by optimizing the ratio of ruthenium oxide to graphene. The SEM studies performed on the synthesized RuO<sub>2</sub>-G nanocomposites have a distinct feature of a platelet of graphene covered with nanoparticles of RuO<sub>2</sub>. The EDS study has shown the ratio of RuO<sub>2</sub> to graphene to be very close to the one calculated. The TEM images of RuO<sub>2</sub>-G 10:4 show that each graphene sheet is covered by RuO<sub>2</sub> nanoparticles.



The two-electrode cell configuration was used to study the supercapacitor electrodes' properties. The best areal capacitance was obtained from the RuO<sub>2</sub>-G 10:1 electrodes. The areal capacitances of RuO<sub>2</sub>-G were higher than synthesized RuO<sub>2</sub>, 187.5 mF cm<sup>-2</sup> for RuO<sub>2</sub>-G 10:1 and 136.5 mF cm<sup>-2</sup> for RuO<sub>2</sub>-G 1:1 while synthesized RuO<sub>2</sub> produced only 7.3 mF cm<sup>-2</sup>. The Nyquist plot has shown that the presence of graphene in RuO<sub>2</sub>-G produces the lowest series resistance (R<sub>s</sub>).

## CHAPTER 6: THE EFFECTS OF VARYING THE MASS LOADING ON MoS<sub>2</sub>-PANI SUPERCAPACITOR ELECTRODES

### 6.1 Introduction

Molybdenum disulfide (MoS<sub>2</sub>), a two-dimensional layered transition metal chalcogenide, has generated a great deal of interest in semiconductor applications due to its outstanding electronic [123-124], optical [125], and high-mobility [126] properties. Strong covalent bonds hold the S-Mo-S layer in a prism like structure with the Mo plane centered between two S planes [127] forming monolayers of hexagonal honeycomb lattice [128]; those layers are stacked and bound by weak van der Waal forces [129]. MoS<sub>2</sub> has an indirect bandgap in its bulk form but transitions into a direct bandgap at the monolayer form [130] and it naturally exists in both n- and p- type crystals [131]. While MoS<sub>2</sub> monolayers are similar to graphene sheets, they have a more complicated geometrical structure at the molecular spacing level that differs depending on the synthesis process [132] yet the transition from indirect to direct bandgap as the bulk material thickness is decreased to monolayers makes it ideal for semiconducting devices especially when compared to the next generation graphene transistors that require bandgap engineering, since graphene is a zero bandgap material, which will negatively affect its superior electrical properties and increase the complexity of production [133].

Interest in MoS<sub>2</sub> is not only limited to electronics and optoelectronics but it is also used in photocatalysis [134], photovoltaics [135], and sensors [136]. Additionally, the layered structure of MoS<sub>2</sub> permits ions and molecules intercalation [131] making it beneficial for electrochemical

energy storage applications in the form of batteries [137-139] and electrochemical supercapacitors [140-149].

Though the structure of MoS<sub>2</sub> is similar to that of graphene, it does not exhibit similar conductivity; however, the MoS<sub>2</sub> layer spacing (0.615nm) is almost twice that of graphene (0.335nm) allowing for easier ion intercalation making it a viable candidate to replace graphite anodes in lithium ion batteries (LIBs) [150]; furthermore, the relative larger layer spacing allows diffused ions to penetrate in the MoS<sub>2</sub> structure without detrimental volume increase while damping the swelling effects from constant charging and discharging [151]. Also, composite of MoS<sub>2</sub> with graphene, carbon nanotubes (CNTs), and conducting polymers (CPs) have resulted in improved electrochemical behavior, conductivity, reversibility, and stability [28][152].

Conducting polymers, such as polyaniline (PANI), poly(o-anisidine) (POA), and polypyrrole (PPy), with their derivatives and composites have been widely studied as supercapacitor electrodes [90-92] showing constant improvement in charge storage and energy density while MoS<sub>2</sub>-CPs composites are gaining momentum and heading in the same direction. This study focuses on synthesized MoS<sub>2</sub>-PANI nanocomposites' electrode's mass loading and its effects on the gravimetric and areal capacitances. Although much attention has been given to the aforementioned thickness property of MoS<sub>2</sub>, where the bandgap is modified depending on whether bulk or monolayers of the material is used, the electrode's mass loading (mg cm<sup>-2</sup>) and thickness (µm or nm) have been largely neglected. Confidently, this study will shed some light on the matter and discuss the need for standardized supercapacitors' performance evaluation.

## 6.2 Experimental

### 6.2.1 Synthesis of MoS<sub>2</sub>-PANI

All the chemicals were purchased from Sigma-Aldrich without any modifications. To synthesize MoS<sub>2</sub>-PANI, 1g of MoS<sub>2</sub> (average particle size  $\leq 2\mu\text{m}$ ) and 0.5M aniline was added to 80mL of 2M HCl and stirred for 2 hours. 0.25M of ammonium persulfate (NH<sub>4</sub>)<sub>2</sub>S<sub>2</sub>O<sub>8</sub> (APS) was added to 20mL of 2M HCl and stirred until the APS was completely dissolved, the solution was then slowly dripped into the 80mL of 2M HCl containing MoS<sub>2</sub> and aniline and left stirring for 12 hours. Since the polyaniline synthesis is exothermic, it normally is placed in an ice bath. However, since MoS<sub>2</sub> is present, the energy released will be used to aid the in nanocomposite synthesis and the reaction can be left at room temperature. Using the vacuum filtration technique, the liquid waste was flushed out while trapping the MoS<sub>2</sub>-PANI composite powder. The powder was then washed with methanol, acetone, and deionized water, doped in 2M HCl, and later dried at 100°C for 24 hours.

### 6.2.2 Characterization

The X-ray diffraction (XRD) peaks were obtained using the Philips Panalytical Xpert Pro MRD with  $2\theta$  range from 5° to 65°. Images of the electrodes' surface morphology were taken with Hitachi SU70 scanning electron microscope (SEM) at accelerating voltage of 25kV. The Fourier transform infrared spectroscopy (FTIR) measurement was done using the Perkin Elmer Spectrum One FT-IR Spectrometer in the mid-infrared region from 4000cm<sup>-1</sup> to 400cm<sup>-1</sup>.

### 6.2.3 Electrode Preparation

The synthesized MoS<sub>2</sub>-PANI composite powder was ball milled for 30 minutes at 300rpm prior to being deposited onto the substrates. 0.1M of 10-camphorsulfonic acid (C<sub>10</sub>H<sub>16</sub>O<sub>4</sub>S) was dissolved in 3mL of 1-methyl-2-pyrrolidinone (C<sub>5</sub>H<sub>9</sub>NO) (NMP) and used as a

binder with 300mg of MoS<sub>2</sub>-PANI powder added after the camphorsulfonic acid completely dissolved in NMP. The resulting slur was stirred thoroughly before deposition. A micro-needle was used to dropcast the slur onto five graphite substrates with equal active area (1cm x 0.5cm) defined by kapton tape as shown in Figure 6.1, the edges and back of the substrates were insulated using an insulating polymer. The electrodes were labeled E<sub>1</sub> through E<sub>5</sub> with deposition volume increasing from E<sub>1</sub> to E<sub>5</sub> at 2.5μL intervals. To ensure complete adhesion, each electrode was dried at 60°C for 15 minutes before to applying the insulating polymer.

#### 6.2.4 Electrochemical Measurements

All the electrochemical measurements were conducted in a three-electrode cell setup with silver/silver chloride (Ag/AgCl) and platinum mesh as reference and counter electrodes, respectively. 1M H<sub>2</sub>SO<sub>4</sub> electrolyte was used at room temperature with cyclic voltammetry (CV) voltage range from -0.3V to 0.7V at 5, 10, 20, 50, and 100 mV s<sup>-1</sup> scan rates. 1, 2, 5, and 10 mA cm<sup>-2</sup> current densities were used for the constant current charge discharge (CCCD) measurements. Frequency range from 100kHz to 5mHz with AC amplitude of 5mV.

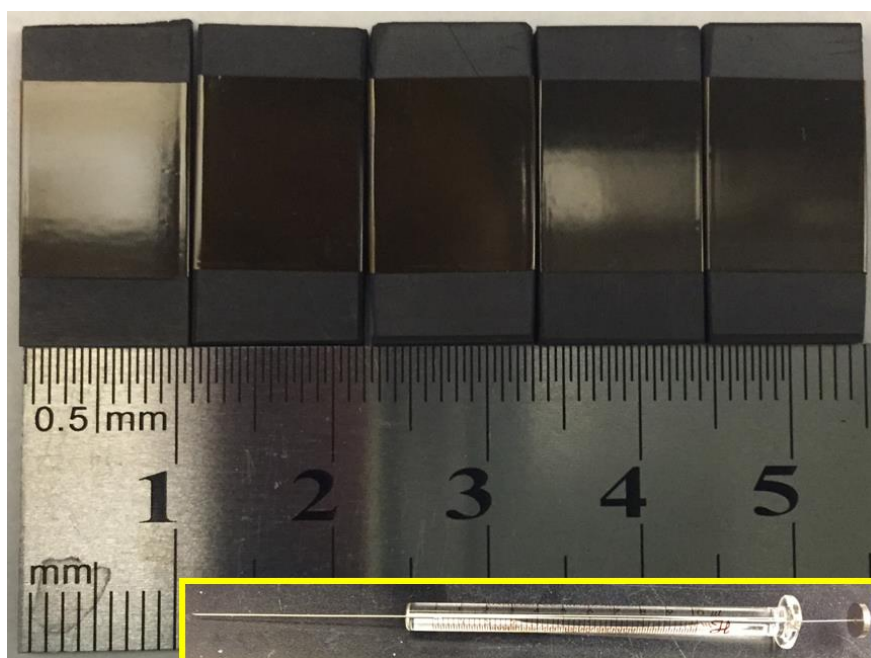


Figure 6.1 The graphite substrates and deposition micro-needle (inset).

### 6.3 Results and Discussion

Potassium bromide (KBr) pellets were made containing 1% MoS<sub>2</sub>-PANI powder for the FT-IR measurement. Figure 6.2(a) shows the FT-IR spectra of MoS<sub>2</sub>-PANI composite material. The peak at 3432cm<sup>-1</sup> corresponds to the stretching vibrations of the O-H bond, 1563cm<sup>-1</sup> is attributed to the stretching vibration of the quinonoid and 1478cm<sup>-1</sup> to that of the benzenoid [153]. The peaks at 1290cm<sup>-1</sup> and 1239cm<sup>-1</sup> correspond to the C-N bond stretching vibration while 1112cm<sup>-1</sup> corresponds to the in plane C-H bending vibration. The peaks at 878cm<sup>-1</sup> and 702cm<sup>-1</sup> are attributed to the out of plane bending vibrations of C-H[154]. However, the observed peaks at 590cm<sup>-1</sup>, 501cm<sup>-1</sup>, and 420cm<sup>-1</sup> are attributed to the Mo-S and the S=S bonds[155] in the MoS<sub>2</sub>-PANI composite structure.

The XRD pattern illustrated in Figure 6.2(b) shows 2θ peaks at 14.4°, 32.8°, 33.6°, 36.0°, 39.7°, 44.1°, 49.9°, 58.6°, and 60.6° which are assigned to (002), (100), (101), (102), (103), (006), (105), (110), and (112) planes, respectively, of MoS<sub>2</sub> and in accordance with the Joint Committee on Powder Diffraction Standards (JCPDS) reference pattern: 01-073-1508 (molybdenite). As for the 2θ peak at 26.4°, it is assigned to the (002) crystalline doped PANI [156].

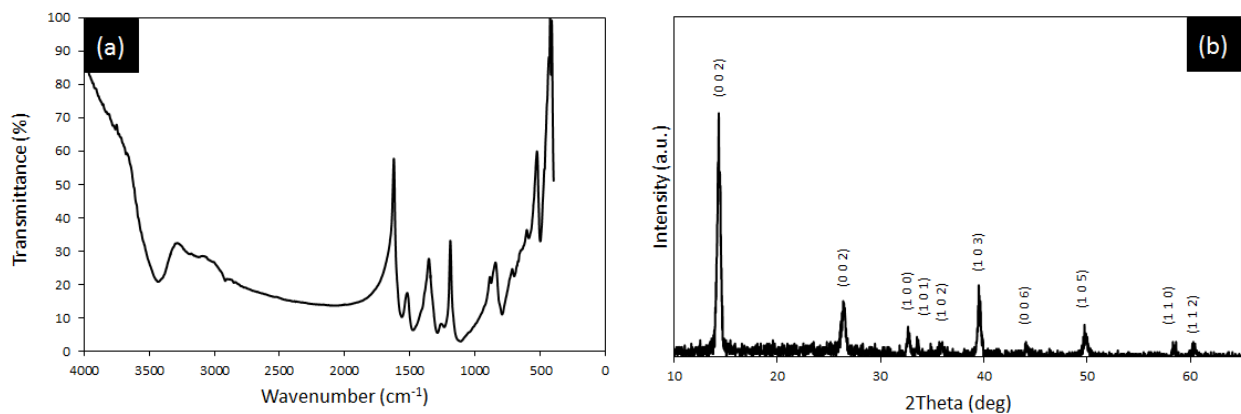


Figure 6.2 (a) FT-IR and (b) XRD peaks of synthesized MoS<sub>2</sub>-PANI.

SEM images of the MoS<sub>2</sub>-PANI electrodes are illustrated in Figure 6.3 at different magnifications. The images do not offer substantial information about the electrodes mass loading effects since the powder used in making the films was not modified on any of the substrates; however, the surface morphology of the electrodes show that PANI particles intercalation into the bulk MoS<sub>2</sub> layers.

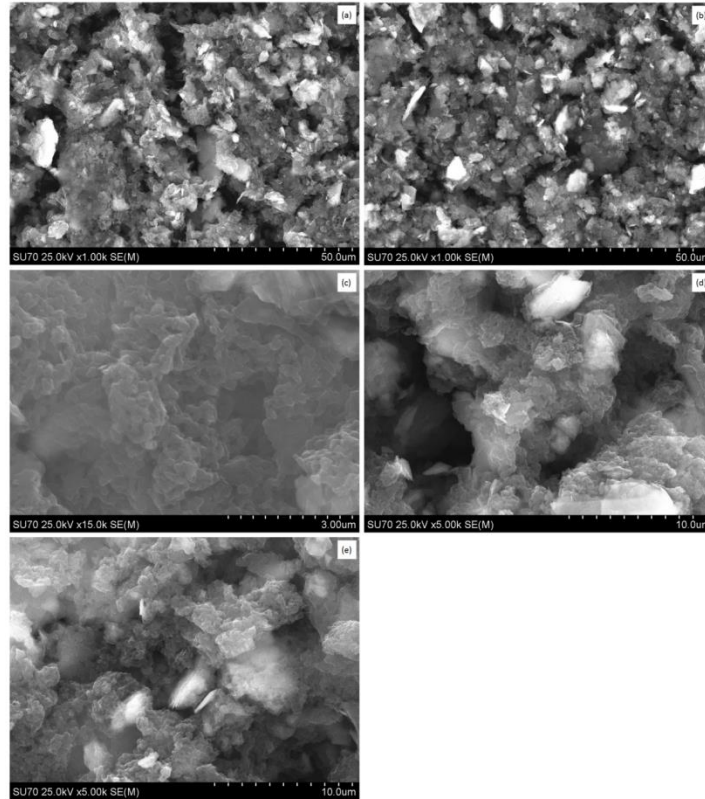


Figure 6.3 SEM images of MoS<sub>2</sub>-PANI electrodes. (a) E<sub>1</sub>, (b) E<sub>2</sub>, (c) E<sub>3</sub>, (d) E<sub>4</sub>, and (e) E<sub>5</sub>.

The electrochemical measurements were performed on the MoS<sub>2</sub>-PANI electrodes and the CVs are shown in Figure 6.4 at 10 mV s<sup>-1</sup>, the measured current is normalized individually to the different weights of the electrodes (A g<sup>-1</sup>) and to the constant area of all electrodes (mA cm<sup>-2</sup>). The peaks clearly indicate a dominating pseudocapacitive charge storage mechanism for all electrodes, as expected. The intensity of the gravimetric peaks decreases as the mass loading of the electrode increases but the exact opposite effect is observed with the areal peaks. Also, the peaks lose definition at higher electrodes' weight indicating that the material is not being fully

utilized. The specific capacitance,  $C_{sc}$ , was calculated from the CV results using the following equation:

$$C_{sc} = \frac{1}{xv} \sum_{n=1}^n \frac{i(n)}{n} \quad (6.1)$$

where  $x$  is either the mass of the electrode material or area of the electrode as the former yields the gravimetric capacitance while the latter yields the areal capacitance,  $v$  is the scan rate,  $n$  is the number of data point and  $i(n)$  is the current corresponding to the data point. The specific capacitance along with the electrodes' mass loading and the deposited volume are provided in Table 6.1.

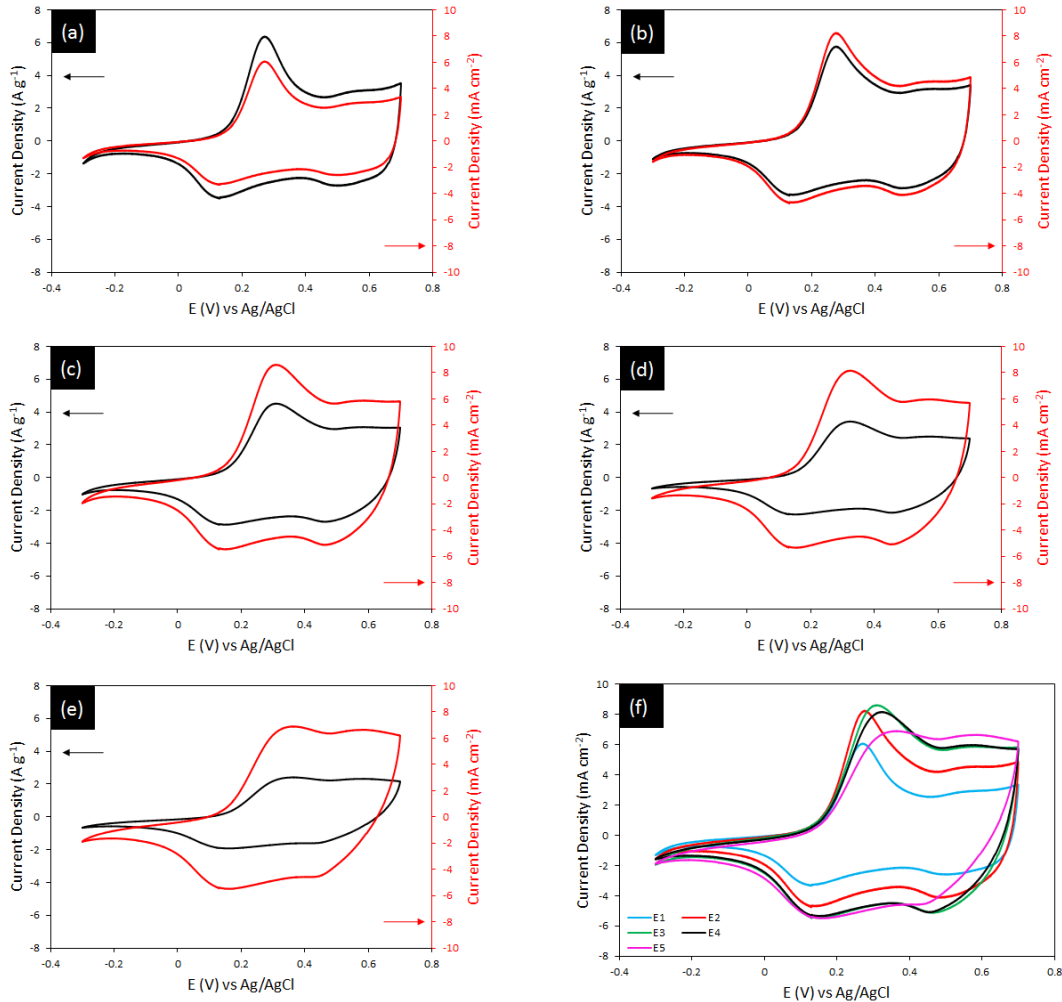


Figure 6.4 CV of MoS<sub>2</sub>-PANI electrodes. (a) E<sub>1</sub>, (b) E<sub>2</sub>, (c) E<sub>3</sub>, (d) E<sub>4</sub>, (e) E<sub>5</sub>, and (f) combined electrodes all measured at 10 mV s<sup>-1</sup> scan rate.



Table 6.1 Evaluation of MoS<sub>2</sub>-PANI electrodes with varying mass loading.

Electrode	Deposition volume (μL)	Mass loading (mg cm <sup>-2</sup> )	Scan Rate (mV s <sup>-1</sup> )	C <sub>g</sub> (F g <sup>-1</sup> )	C <sub>a</sub> (mF cm <sup>-2</sup> )
E <sub>1</sub>	5	0.95	5	203	194
			10	188	179
			20	172	164
			50	146	140
			100	120	114
E <sub>2</sub>	7.5	1.43	5	203	291
			10	187	267
			20	167	239
			50	136	194
			100	106	151
E <sub>3</sub>	10	1.90	5	187	356
			10	167	319
			20	143	273
			50	106	201
			100	74	141
E <sub>4</sub>	12.5	2.38	5	148	352
			10	130	309
			20	109	260
			50	78	186
			100	53	127
E <sub>5</sub>	15	2.86	5	125	358
			10	103	293
			20	79	226
			50	51	145
			100	33	95

The CCCD characteristics performed in the same voltage range as that in CV (-0.3V to 0.7V) are shown in Figure 6.5 at different current densities. The nonlinearity of the responses indicates a pseudocapacitive effect reaffirming what was observed in the CV measurements. With increasing current density, the time it takes for the voltage to reach its preset limits decreases tremendously preventing E<sub>5</sub>, the electrode with the most mass load, from utilizing all the deposited electrode material. E<sub>5</sub> was not the only electrode with deteriorating performance but it was the worst. This is much similar to what was observed in the gravimetric peaks of the CV measurements.

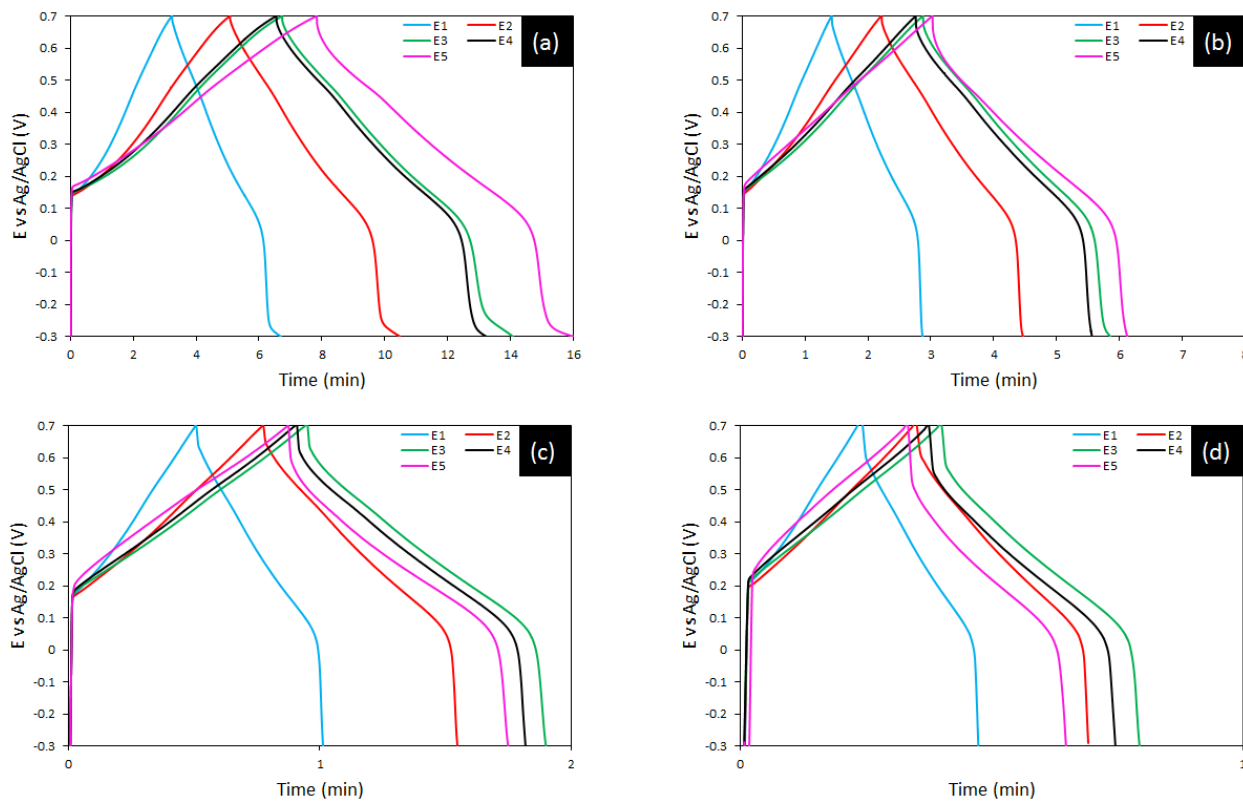


Figure 6.5 CCCD of MoS<sub>2</sub>-PANI electrodes. (a) 1 mA cm<sup>-2</sup>, (b) 2 mA cm<sup>-2</sup>, (c) 5 mA cm<sup>-2</sup>, and (d) 10 mA cm<sup>-2</sup>.

MoS<sub>2</sub>-PANI electrodes showed high stability at 100 cycles where the capacitance was unchanged from the first cycle to the last as indicated in the CV measured at 100 mV s<sup>-1</sup> in Figure 6.6.

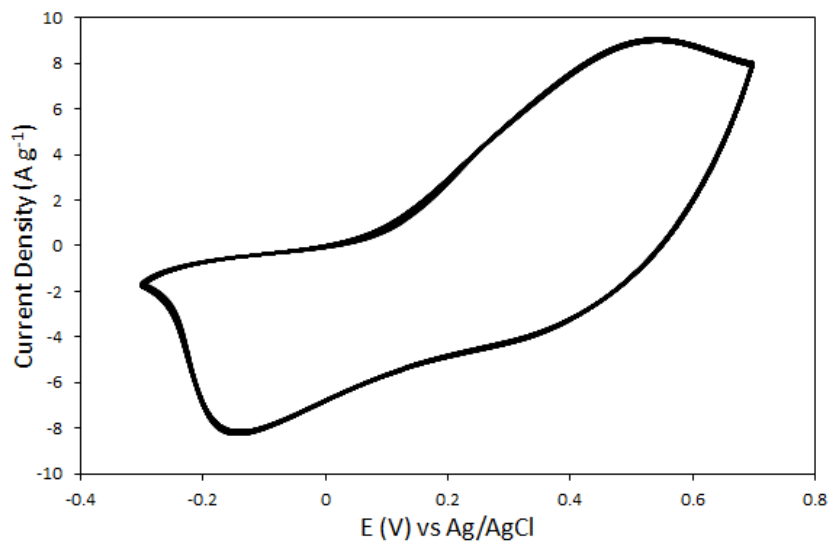


Figure 6.6 The stability of MoS<sub>2</sub>-PANI over 100 cycles at 100 mV s<sup>-1</sup> scan rate.

The EIS responses of the MoS<sub>2</sub>-PANI electrodes are shown in Figure 6.7 illustrating an increase in the series resistance as the mass load of each electrode increases except for E<sub>1</sub> yet the difference among the electrodes is approximately only 1.2 Ω.cm<sup>2</sup>. Increasing the electrodes' mass loading leads to an increase in the ion/electron transport distance which in turn increase the resistance of the electrodes [157].

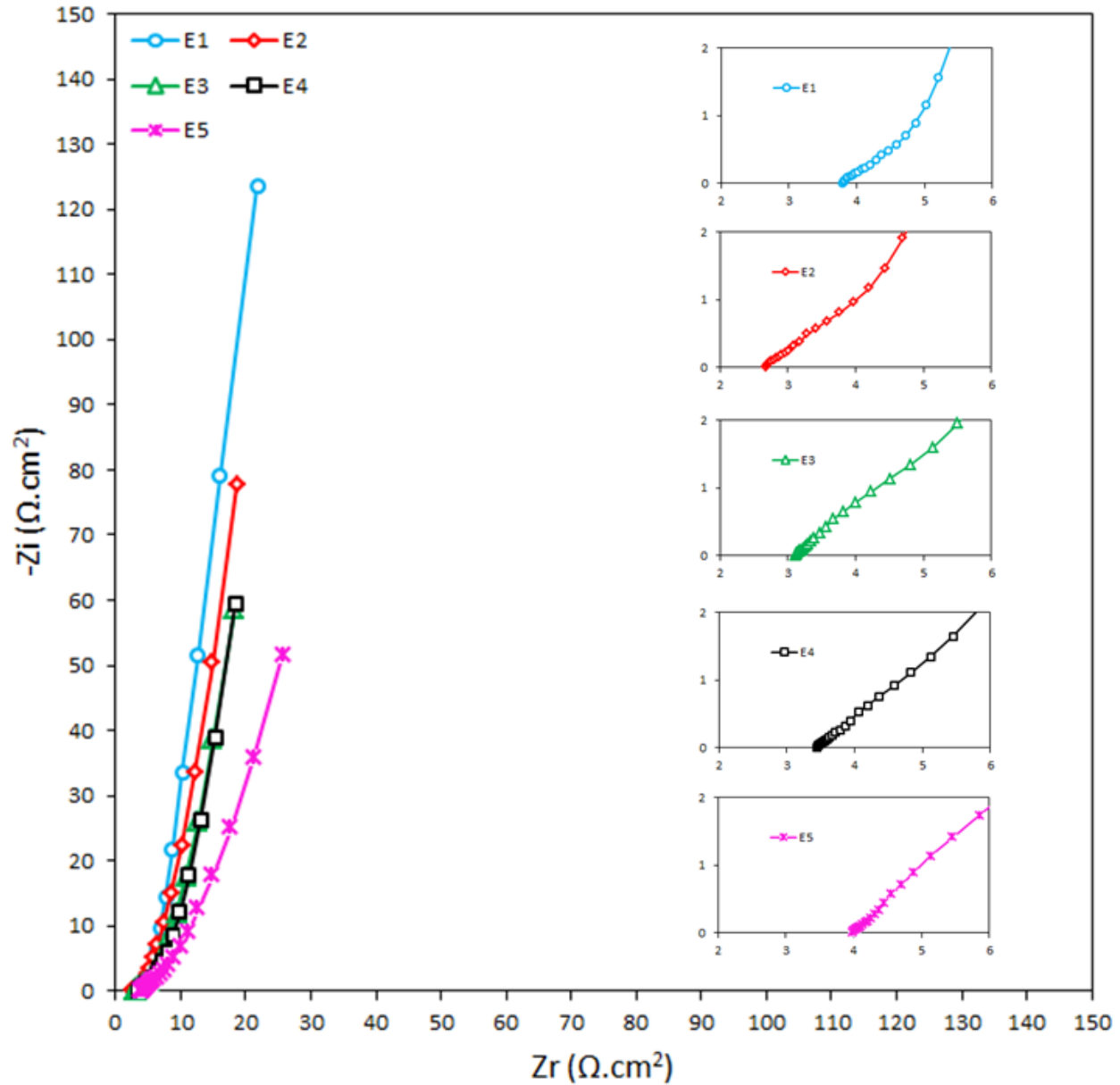


Figure 6.7 EIS of MoS<sub>2</sub>-PANI electrodes. (a) E<sub>1</sub>, (b) E<sub>2</sub>, (c) E<sub>3</sub>, (d) E<sub>4</sub>, and (e) E<sub>5</sub>.

Electrode mass loading has a significant impact on the performance of supercapacitors. Thickness of porous electrode materials can be difficult to obtain, it is sufficient to use electrode mass loading. Owing to the fact that the area of the electrodes was maintained constant, the mass loading of the electrodes is essentially treated as the thickness of the electrode material and therefore can be referred to as such henceforth. Figure 6.8 shows the gravimetric and areal capacitances as a function of electrodes' mass loading or thickness, each plot is a result of a different scan rate: 5, 10, 20, 50, 100  $\text{mV s}^{-1}$ , in order. At 5  $\text{mV s}^{-1}$ , the gravimetric capacitance decreases while the areal capacitance increases as the electrode thickness increases, as expected [32][45]. However, as the scan rate starts to increase, the areal capacitance loses its trend and thick electrodes start to similarly to thin electrodes. At 100  $\text{mV s}^{-1}$  the areal capacitance of thickest electrode drops below that of the thinnest one. Gravimetric capacitance does not follow suit yet at high scan rates,  $E_2$  is no longer comparable to  $E_1$  and yields lower values. The specific capacitance variation proves that the electrodes' performance is dependent of their thicknesses. If the electrolyte does not have sufficient time to diffuse deep into the porous electrode material at high scan rates or charge/discharge times, it renders the material that is not being utilized useless and therefore wasted. The drop in gravimetric capacitance was observed in ruthenium oxide ( $\text{RuO}_2$ ) electrodes from  $788 \text{ F g}^{-1}$  to  $300 \text{ F g}^{-1}$  as the thickness increased from  $1.4 \text{ mg cm}^{-2}$  to  $2.3 \text{ mg cm}^{-2}$  and it was attributed to the reduction in electrode porosity when the inner layers are compact closely in thick electrodes [121]. Similar trends are observed in wrinkled and flat graphene sheets [157] as their morphology was studied for scalability of supercapacitors, chemically converted graphene [158] as variations of its density was studied for compact capacitive energy storage, and carbide-derived carbon [159] studied for micros-supercapacitors applications in aqueous and organic electrolytes. The anisotropic nature of  $\text{MoS}_2$  increases its

resistance if its sheets are aligned perpendicularly to the electron transport plane [160] so increasing the thickness of MoS<sub>2</sub>-PANI electrodes leads to higher resistance, more compact inner layers making it harder for the ions of the electrolyte to diffuse deeply, and porosity reduction of the surface area can all lead to a drop in the electrochemical storage capabilities MoS<sub>2</sub>-PANI based supercapacitors.

With careful consideration, electrode thickness can be selected that would best fit the electrolyte's ion size with the electrode materials' pore distributions for the desired application whether it is for small scale portable electronics, electric vehicles, or large scale electrochemical storage in sustainable energy power plants.

The lack of standardized supercapacitors' performance evaluation methodology makes it difficult to compare electrochemical storage capabilities [102] of emerging materials such as MoS<sub>2</sub> and MoS<sub>2</sub>-composites. Table 6.2 lists the work that has been done on the supercapacitive behavior of MoS<sub>2</sub> and MoS<sub>2</sub>-composites by different research group. Though tremendous strides have taken place in synthesizing bulk materials that can well be used as supercapacitor electrodes, evaluations of the performances are not consistent. Failure to report electrode thicknesses, with only the first and last references in Table 6.2 doing so at 1 mg cm<sup>-2</sup> and 0.45 μm, respectively, along with using different charge/discharge currents and/or CV scan rates to calculate the specific capacitances makes any comparisons impractical. Moreover, using extremely thin electrodes to produce misleadingly large specific capacitances is of disservice to supercapacitors as they are touted to be supplement batteries or replace them altogether.

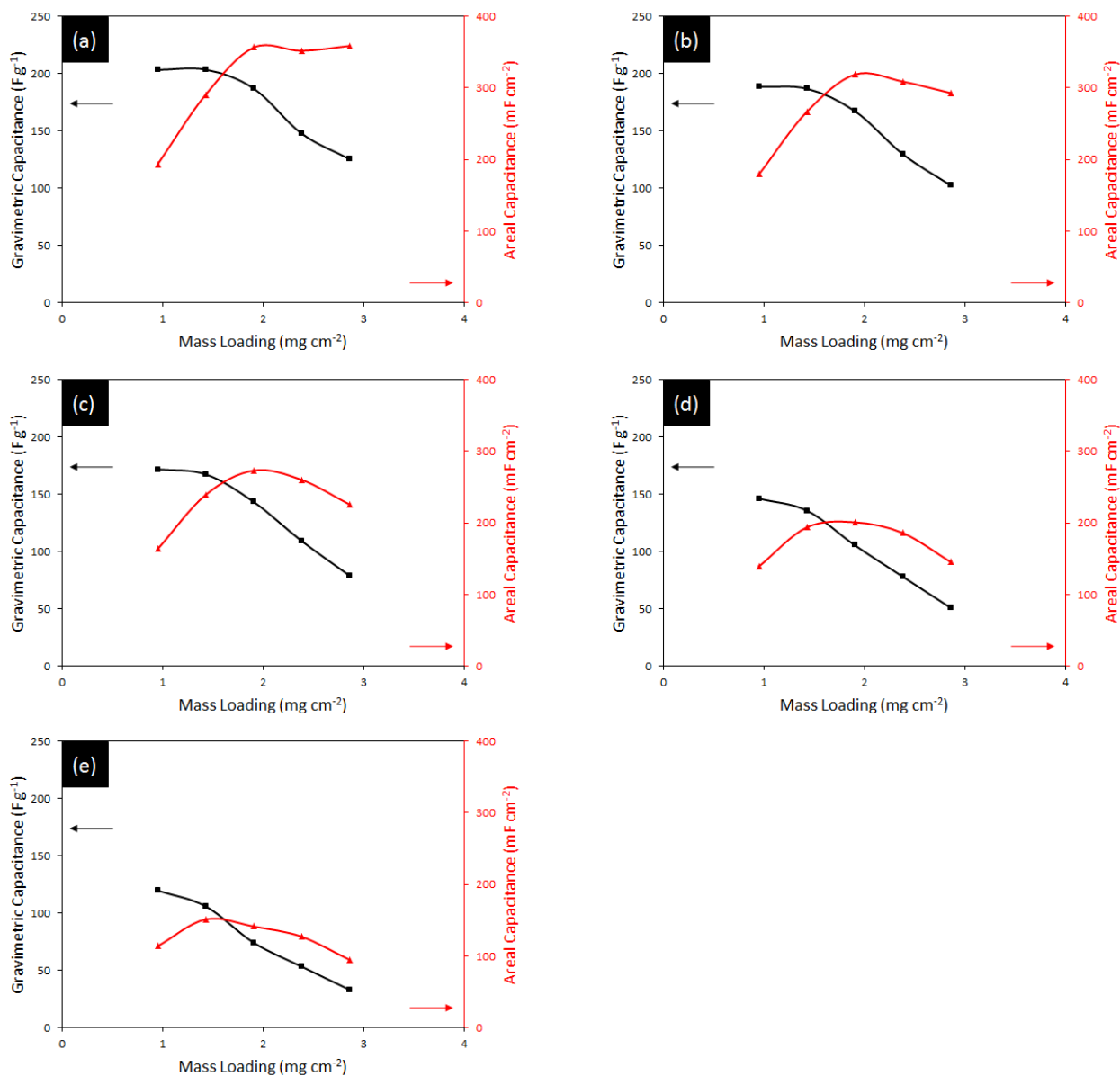


Figure 6.8 MoS<sub>2</sub>-PANI electrodes' specific capacitance as a function the mass loading. (a) 5 mV s<sup>-1</sup>, (b) 10 mV s<sup>-1</sup>, (c) 20 mV s<sup>-1</sup>, (d) 50 mV s<sup>-1</sup>, and (e) 100 mV s<sup>-1</sup>.

Table 6.2 List of MoS<sub>2</sub> and MoS<sub>2</sub>-composites as electrode materials for supercapacitors.

Electrode material	Binder	Electrolyte	Specific capacitance	Ref
MoS <sub>2</sub> spheres	PVDF <sup>a</sup>	1M Na <sub>2</sub> SO <sub>4</sub> <sup>*</sup>	106 F g <sup>-1</sup> at 5mV s <sup>-1</sup>	[141]
MoS <sub>2</sub> -graphene	PTFE <sup>b</sup>	1M Na <sub>2</sub> SO <sub>4</sub> <sup>*</sup>	243 F g <sup>-1</sup> at 1 A g <sup>-1</sup>	[142]
MoS <sub>2</sub> /PANI-38		1M H <sub>2</sub> SO <sub>4</sub> <sup>*</sup>	390 F g <sup>-1</sup> at 0.8 A g <sup>-1</sup>	[143]
MoS <sub>2</sub> /MWCNT <sup>c</sup>	PTFE <sup>b</sup>	1M Na <sub>2</sub> SO <sub>4</sub> <sup>*</sup>	452.7 F g <sup>-1</sup> at 1 A g <sup>-1</sup>	[144]

Table 6.2 (Continued)

Electrode material	Binder	Electrolyte	Specific capacitance	Ref
PPy/MoS <sub>2</sub>	PTFE <sup>b</sup>	1M KCl <sup>*</sup>	553.7 F g <sup>-1</sup> at 1 A g <sup>-1</sup>	[145]
MoS <sub>2</sub> -PANI(1:1) MoS <sub>2</sub> -PANI(1:6)	Nafion	2M KCl <sup>*</sup>	417 F g <sup>-1</sup> at 0.2 A g <sup>-1</sup> 567 F g <sup>-1</sup> at 0.5 A g <sup>-1</sup>	[146]
PANI/MoS <sub>2</sub>	PTFE <sup>b</sup>	1M H <sub>2</sub> SO <sub>4</sub> <sup>*</sup>	575 F g <sup>-1</sup> at 1 A g <sup>-1</sup>	[147]
MoS <sub>2</sub> bulk MoS <sub>2</sub> monolayers MoS <sub>2</sub> monolayers MoS <sub>2</sub> monolayers		6M KOH <sup>**</sup> 6M KOH <sup>**</sup> 1M Et <sub>4</sub> NBF <sub>4</sub> in PC <sup>d**</sup> BMIM-PF <sub>6</sub> <sup>e**</sup>	0.5 mF cm <sup>-2</sup> at 10mV s <sup>-1</sup> 2 mF cm <sup>-2</sup> at 10mV s <sup>-1</sup> 2.25 mF cm <sup>-2</sup> at 10mV s <sup>-1</sup> 2.4 mF cm <sup>-2</sup> at 10mV s <sup>-1</sup>	[148]
MoS <sub>2</sub> laser-patterned		1M NaOH <sup>**</sup>	8 mF cm <sup>-2</sup> 178 F cm <sup>-3</sup> at 10mV s <sup>-1</sup>	[149]

<sup>a</sup> PVDF: polyvinylidene fluoride

<sup>b</sup> PTFE: poly(tetrafluoroethylene)

<sup>c</sup> MWCNT: multi-walled carbon nanotube

<sup>d</sup> Tetraethylammonium tetrafluoroborate in propylene carbonate

<sup>e</sup> 1-butyl-3-methylimidazolium hexafluorophosphate

<sup>\*</sup> Three-electrode cell configuration

<sup>\*\*</sup> Two-electrode cell configuration

## 6.4 Conclusions

This study has focused on the effect of electrode mass loading, the amount of material deposited on the substrate active surface area, on the performance of supercapacitors using MoS<sub>2</sub>-PANI as the active electrode material. At low scan rates the gravimetric and areal capacitances behaved as expected. That is, the former decreased while the latter increased with increasing electrode thickness. The occurred because at high scan rates the areal capacitance started to decrease as the electrode thickness increased, because the electrolyte ions were not able to diffuse into the electrode pores in the limited amount time thus preventing the utilization

of the entire electrode surface area. Lack of standards and inconsistencies in evaluating supercapacitors can lead to confusion regarding the actual electrochemical storage capabilities and the amount of energy and power densities they can provide. Reporting electrodes' mass loading and/or thicknesses as well as gravimetric ( $F g^{-1}$ ), and areal ( $mF cm^{-2}$ ) capacitances could pave the way to start standardizing evaluation methods.



## CHAPTER 7: CONCLUSIONS AND RECOMMENDATIONS FOR FUTURE WORK

### 7.1 Conclusions

The work presented in this dissertation has focused on material synthesis and electrochemical characterization of supercapacitor electrodes and the effects of mass loading on the supercapacitor performance. The proper reporting of the effect of electrode mass loading on the supercapacitor performance is very significant for the objective comparison of different electrode materials in the absence of standardized reporting methods. Also, a short study was carried out on the use of BST to increase the capacitance and reduce the supercapacitor self-discharge.

Even though the use of a three electrode cell configuration provides information about the electrochemical characteristics of electrode materials, it does not provide sufficient information on the performance of supercapacitor devices made of such materials. This can compromise the reported energy and power densities. A careful analysis of the electrode material thickness is needed to determine the optimum electrode thickness. Some materials might appear promising for supercapacitor applications at the monolayer level; however, this does not mean the material will perform well as its thickness increases. Commercial supercapacitors use bulk electrode materials in a two electrode configuration with the presence of separators and packaging which has consequences on the overall performance.

The three major conclusions of this work are:

- i. Barium strontium titanate's (BST) deposition did not reduce the self-discharge of supercapacitors but its high dielectric constant had a positive impact on the overall capacitance.
- ii. The addition of graphene on ruthenium oxide enhanced the performance of the supercapacitor electrodes.
- iii. Increase in the thickness of molybdenum sulfide-polyaniline electrode mass loading resulted in significant changes in the specific capacitance. Therefore, it is important to consider this factor in the optimization of supercapacitor performances.

## 7.2 Recommendations for Future Work

This work has evolved from initially studying the electrochemical behavior of commercial graphene for supercapacitor applications to synthesizing conducting polymers (from their monomers) and synthesizing composites of conducting polymers with graphene, metal oxides with graphene, and finally to layered transition chalcogenides with conducting polymers. It is only natural for the work to continue and grow in the same direction while learning from the old synthesis and fabrication processes and improving on them.

Testing each material in the three electrode configuration is crucial but should not be the final step. Testing of a two electrode configuration in the form of a device structure and evaluation of its specific capacitance, multiple (>1000) cycle stability, and energy and power densities can present a more accurate picture of the supercapacitive materials. A breakdown of a coin cell is shown in Figure 7.1(a) is one way of making supercapacitor devices, however packaging (to avoid electrolyte leak), type of separator, and pressure applied to seal the coin can

be detrimental factors affecting the response of the supercapacitor. Another, simpler, method of making devices is sandwiching a gel electrolyte between two electrodes, as shown in Figure 7.1(b), eliminating the need for a separator and cell packaging; this method might not be of industrial value but it provides an easy way to realistically test laboratory fabricated supercapacitors.

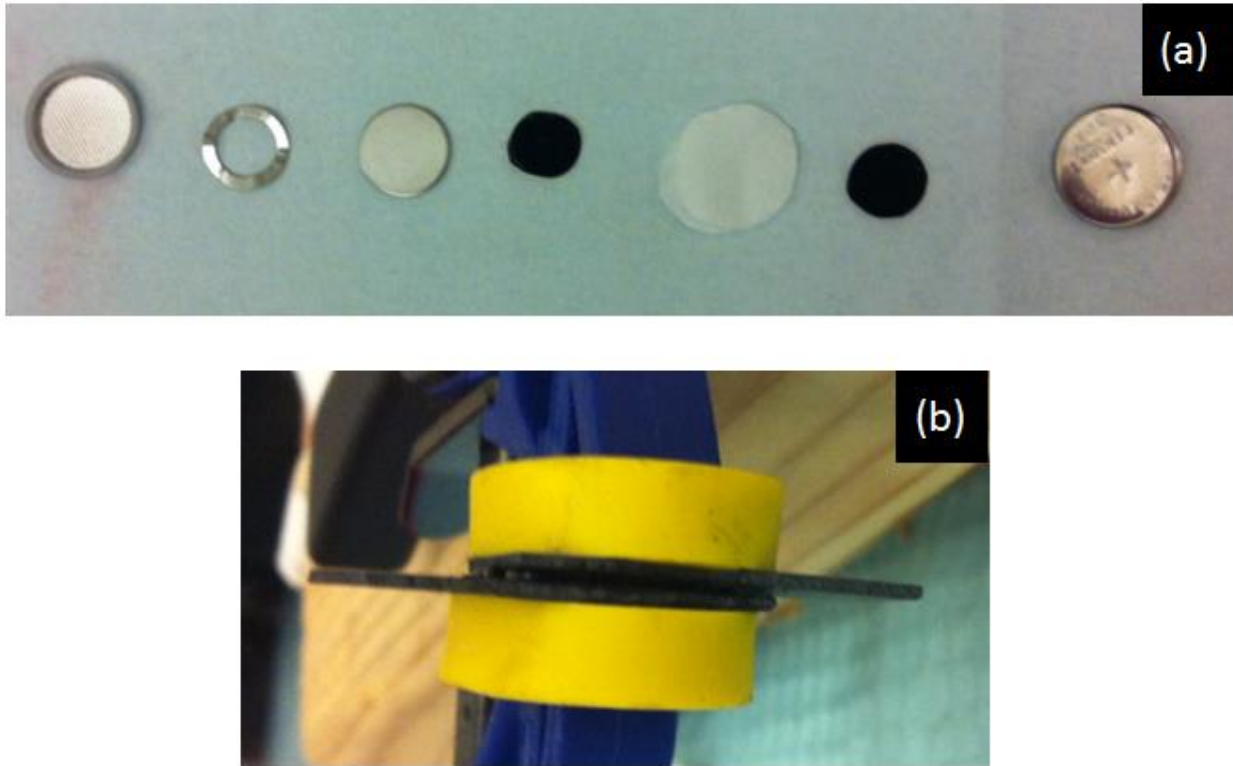


Figure 7.1 Supercapacitor devices. (a) A breakdown of the components of a coin cell and (b) gel electrolyte sandwiched between two electrodes deposited on graphite substrates.

Measuring the specific surface area of the electrodes using the Brunauer-Emmett-Teller (BET) apparatus and selecting an electrolyte whose ion size matches the electrode surface pore size could yield more effective results. Measuring the electrode volume as well as the mass loading provides the best way to evaluate the performance of supercapacitors; that is, report the gravimetric ( $F g^{-1}$ ), areal ( $F cm^{-2}$ ), and volumetric ( $F cm^{-3}$ ) capacitance, thus removing all doubt about the integrity and the performance of the electrodes.

Lastly, studying, and possibly synthesizing, new electrolytes could be the most effective way in increasing the energy density. The ratio of energy to power is directly proportional to the time constant which in turn is directly proportional to the stored capacitance and series resistance (in the simplest model of the equivalent resistance of supercapacitors) so by increasing the capacitance the response time of the supercapacitor decreases. Yet increasing the electrolyte decomposition potential (voltage range) would raise the energy without affecting the time constant. Currently, aqueous electrolytes operate at 1V range and 2.7-3V for organic electrolytes. The operating voltage is higher for ionic liquids but their dependence on temperature is a hindrance that is yet to be overcome. Providing a new generation of electrolytes with a large operating voltage range could go a long way in improving the performance of supercapacitors.

## REFERENCES

- [1] M. Mikkelsen, M. Jørgensen, and F. C. Krebs, “The teraton challenge. A review of fixation and transformation of carbon dioxide,” *Energy Environ. Sci.*, vol. 3, no. 1, pp. 43–81, 2010.
- [2] P. Simon and Y. Gogotsi, “Materials for electrochemical capacitors,” *Nat. Mater.*, vol. 7, no. 11, pp. 845–54, Nov. 2008.
- [3] P. Sharma and T. S. Bhatti, “A review on electrochemical double-layer capacitors,” *Energy Convers. Manag.*, vol. 51, no. 12, pp. 2901–2912, Dec. 2010.
- [4] B. E. Conway, *Electrochemical Supercapacitors: Scientific Fundamentals and Technological Applications*. New York: Kluwer Academic / Plenum Publishers, 1999.
- [5] A. Yu, V. Chabot, and J. Zhang, *Electrochemical Supercapacitors for Energy Storage and Delivery: Fundamentals and Applications*, 1st ed. Boca Raton: CRC Press Taylor & Francis Group, 2013.
- [6] H. Helmholtz, “Ueber einige Gesetze der Vertheilung elektrischer Ströme in körperlichen Leitern mit Anwendung auf die thierisch-elektrischen Versuche,” *Ann. der Phys. und Chemie*, vol. 165, no. 6, pp. 211–233, 1853.
- [7] M. Gouy, “Sur la constitution de la charge électrique à la surface d’un électrolyte,” *J. Phys. Théorique Appliquée*, vol. 9, no. 1, pp. 457–468, 1910.
- [8] D. L. Chapman, “LI. A contribution to the theory of electrocapillarity,” *Philos. Mag. Ser. 6*, vol. 25, no. 148, pp. 475–481, Apr. 1913.
- [9] O. Stern, “ZUR THEORIE DER ELEKTROLYTISCHEN DOPPELSCHICHT,” *Zeitschrift für Elektrochemie und Angew. Phys. Chemie*, vol. 30, no. 21–22, pp. 508–516, Nov. 1924.
- [10] D. C. Grahame, “The Electrical Double Layer and the Theory of Electrocapillarity,” *Chem. Rev.*, vol. 41, no. 3, pp. 441–501, Dec. 1947.
- [11] H. I. Becker and V. Ferry, “Low voltage electrolytic capacitor,” 28006161957.

- [12] B. E. Conway, "Transition from 'Supercapacitor' to 'Battery' Behavior in Electrochemical Energy Storage," *J. Electrochem. Soc.*, vol. 138, no. 6, p. 1539, Jun. 1991.
- [13] B. E. Conway, V. Birss, and J. Wojtowicz, "The role and utilization of pseudocapacitance for energy storage by supercapacitors," *J. Power Sources*, vol. 66, no. 1–2, pp. 1–14, 1997.
- [14] B. E. Conway and W. G. Pell, "Double-layer and pseudocapacitance types of electrochemical capacitors and their applications to the development of hybrid devices," *J. Solid State Electrochem.*, vol. 7, no. 9, pp. 637–644, Sep. 2003.
- [15] A. Davies and A. Yu, "Material advancements in supercapacitors: From activated carbon to carbon nanotube and graphene," *Can. J. Chem. Eng.*, vol. 89, no. 6, pp. 1342–1357, Dec. 2011.
- [16] N. Lang and W. Kohn, "Theory of Metal Surfaces: Charge Density and Surface Energy," *Phys. Rev. B*, vol. 1, no. 12, pp. 4555–4568, Jun. 1970.
- [17] L. L. Zhang and X. S. Zhao, "Carbon-based materials as supercapacitor electrodes," *Chem. Soc. Rev.*, vol. 38, no. 9, pp. 2520–31, Sep. 2009.
- [18] Y. Zhang, H. Feng, X. Wu, L. Wang, A. Zhang, T. Xia, H. Dong, X. Li, and L. Zhang, "Progress of electrochemical capacitor electrode materials: A review," *Int. J. Hydrogen Energy*, vol. 34, no. 11, pp. 4889–4899, Jun. 2009.
- [19] I. I. Grigorchak, "Redox Processes and Pseudocapacitance of Capacitors in Light of Intercalation Nanotechnologies," *Russ. J. Electrochem.*, vol. 39, no. 6, pp. 695–698, Jun. 2003.
- [20] A. T. Hubbard and F. C. Anson, "Linear Potential Sweep Voltammetry in Thin Layers of Solution," *Anal. Chem.*, vol. 38, no. 1, pp. 58–61, Jan. 1966.
- [21] S. L. Candelaria, Y. Shao, W. Zhou, X. Li, J. Xiao, J.-G. Zhang, Y. Wang, J. Liu, J. Li, and G. Cao, "Nanostructured carbon for energy storage and conversion," *Nano Energy*, vol. 1, no. 2, pp. 195–220, Mar. 2012.
- [22] M. Nawa, T. Nogami, and H. Mikawa, "Application of Activated Carbon Fiber Fabrics to Electrodes of Rechargeable Battery and Organic Electrolyte Capacitor," *J. Electrochem. Soc.*, vol. 131, no. 6, p. 1457, Jun. 1984.
- [23] R. Xue, J. Yan, X. Liu, Y. Tian, and B. Yi, "Effect of activation on the carbon fibers from phenol–formaldehyde resins for electrochemical supercapacitors," *J. Appl. Electrochem.*, vol. 41, no. 11, pp. 1357–1366, Oct. 2011.

- [24] P.-L. Taberna, G. Chevallier, P. Simon, D. Plée, and T. Aubert, “Activated carbon–carbon nanotube composite porous film for supercapacitor applications,” *Mater. Res. Bull.*, vol. 41, no. 3, pp. 478–484, Mar. 2006.
- [25] V. V. N. Obreja, “On the performance of supercapacitors with electrodes based on carbon nanotubes and carbon activated material—A review,” *Phys. E Low-dimensional Syst. Nanostructures*, vol. 40, no. 7, pp. 2596–2605, May 2008.
- [26] R. W. Pekala, J. C. Farmer, C. T. Alviso, T. D. Tran, S. T. Mayer, J. M. Miller, and B. Dunn, “Carbon aerogels for electrochemical applications,” *J. Non. Cryst. Solids*, vol. 225, no. 1–3, pp. 74–80, 1998.
- [27] Y. Zhu, H. Hu, W.-C. Li, and X. Zhang, “Cresol–formaldehyde based carbon aerogel as electrode material for electrochemical capacitor,” *J. Power Sources*, vol. 162, no. 1, pp. 738–742, Nov. 2006.
- [28] S. Ding, J. S. Chen, and X. W. D. Lou, “Glucose-assisted growth of MoS<sub>2</sub> nanosheets on CNT backbone for improved lithium storage properties.,” *Chemistry*, vol. 17, no. 47, pp. 13142–5, Nov. 2011.
- [29] M. Kaempgen, C. K. Chan, J. Ma, Y. Cui, and G. Gruner, “Printable thin film supercapacitors using single-walled carbon nanotubes,” *Nano Lett.*, vol. 9, no. 5, pp. 1872–6, May 2009.
- [30] K. Ku, B. Kim, H. Chung, and W. Kim, “Characterization of graphene-based supercapacitors fabricated on Al foils using Au or Pd thin films as interlayers,” *Synth. Met.*, vol. 160, no. 23–24, pp. 2613–2617, Dec. 2010.
- [31] Y. Zhu, S. Murali, M. D. Stoller, K. J. Ganesh, W. Cai, P. J. Ferreira, A. Pirkle, R. M. Wallace, K. A. Cyhosh, M. Thommes, D. Su, E. A. Stach, and R. S. Ruoff, “Carbon-based supercapacitors produced by activation of graphene.,” *Science*, vol. 332, no. 6037, pp. 1537–41, Jun. 2011.
- [32] J. Liu, M. Notarianni, G. Will, V. T. Tiong, H. Wang, and N. Motta, “Electrochemically exfoliated graphene for electrode films: effect of graphene flake thickness on the sheet resistance and capacitive properties.,” *Langmuir*, vol. 29, no. 43, pp. 13307–14, Oct. 2013.
- [33] Y. Zhu, S. Murali, W. Cai, X. Li, J. W. Suk, J. R. Potts, and R. S. Ruoff, “Graphene and graphene oxide: synthesis, properties, and applications.,” *Adv. Mater.*, vol. 22, no. 35, pp. 3906–24, Sep. 2010.
- [34] Z.-S. Wu, G. Zhou, L.-C. Yin, W. Ren, F. Li, and H.-M. Cheng, “Graphene/metal oxide composite electrode materials for energy storage,” *Nano Energy*, vol. 1, no. 1, pp. 107–131, Jan. 2012.

- [35] M. D. Stoller, S. Park, Y. Zhu, J. An, and R. S. Ruoff, "Graphene-based ultracapacitors.," *Nano Lett.*, vol. 8, no. 10, pp. 3498–502, Oct. 2008.
- [36] Y. Tao, X. Xie, W. Lv, D.-M. Tang, D. Kong, Z. Huang, H. Nishihara, T. Ishii, B. Li, D. Golberg, F. Kang, T. Kyotani, and Q.-H. Yang, "Towards ultrahigh volumetric capacitance: graphene derived highly dense but porous carbons for supercapacitors.," *Sci. Rep.*, vol. 3, p. 2975, Jan. 2013.
- [37] S. Iijima, "Helical microtubules of graphitic carbon," *Nature*, vol. 354, no. 6348, pp. 56–58, 1991.
- [38] S. Iijima and T. Ichihashi, "Single-shell carbon nanotubes of 1-nm diameter," *Nature*, vol. 363, no. 6430, pp. 603–605, 1993.
- [39] J. Wei, H. Zhu, B. Jiang, L. Ci, and D. Wu, "Electronic properties of double-walled carbon nanotube films," *Carbon N. Y.*, vol. 41, no. 13, pp. 2495–2500, Jan. 2003.
- [40] R. H. Baughman, A. A. Zakhidov, and W. A. de Heer, "Carbon nanotubes--the route toward applications.," *Science*, vol. 297, no. 5582, pp. 787–92, Aug. 2002.
- [41] K. Hata, D. N. Futaba, K. Mizuno, T. Namai, M. Yumura, and S. Iijima, "Water-assisted highly efficient synthesis of impurity-free single-walled carbon nanotubes.," *Science*, vol. 306, no. 5700, pp. 1362–4, Nov. 2004.
- [42] O. Tanaike, D. N. Futaba, K. Hata, and H. Hatori, "Supercapacitors using Pure Single-walled Carbon Nanotubes," *Carbon Letters*, 2009. [Online]. Available: [http://carbonlett.org/PublishedPaper/year\\_abstract.asp?idx=253](http://carbonlett.org/PublishedPaper/year_abstract.asp?idx=253). [Accessed: 24-Jun-2015].
- [43] T. Hiraoka, A. Izadi-Najafabadi, T. Yamada, D. N. Futaba, S. Yasuda, O. Tanaike, H. Hatori, M. Yumura, S. Iijima, and K. Hata, "Compact and Light Supercapacitor Electrodes from a Surface-Only Solid by Opened Carbon Nanotubes with 2 200 m<sup>2</sup> g<sup>-1</sup> Surface Area," *Adv. Funct. Mater.*, vol. 20, no. 3, pp. 422–428, Feb. 2010.
- [44] M. Inagaki, H. Konno, and O. Tanaike, "Carbon materials for electrochemical capacitors," *J. Power Sources*, vol. 195, no. 24, pp. 7880–7903, Dec. 2010.
- [45] M. Notarianni, J. Liu, F. Mirri, M. Pasquali, and N. Motta, "Graphene-based supercapacitor with carbon nanotube film as highly efficient current collector.," *Nanotechnology*, vol. 25, no. 43, p. 435405, Oct. 2014.
- [46] K. S. Novoselov, A. K. Geim, S. V Morozov, D. Jiang, Y. Zhang, S. V Dubonos, I. V Grigorieva, and A. A. Firsov, "Electric field effect in atomically thin carbon films.," *Science*, vol. 306, no. 5696, pp. 666–9, Oct. 2004.



- [47] A. Taheri Najafabadi, "Emerging applications of graphene and its derivatives in carbon capture and conversion: Current status and future prospects," *Renew. Sustain. Energy Rev.*, vol. 41, pp. 1515–1545, Jan. 2015.
- [48] K. I. Bolotin, K. J. Sikes, Z. Jiang, M. Klima, G. Fudenberg, J. Hone, P. Kim, and H. L. Stormer, "Ultrahigh electron mobility in suspended graphene," *Solid State Commun.*, vol. 146, no. 9–10, pp. 351–355, Jun. 2008.
- [49] A. A. Balandin, S. Ghosh, W. Bao, I. Calizo, D. Teweldebrhan, F. Miao, and C. N. Lau, "Superior thermal conductivity of single-layer graphene," *Nano Lett.*, vol. 8, no. 3, pp. 902–7, Mar. 2008.
- [50] C. Lee, X. Wei, J. W. Kysar, and J. Hone, "Measurement of the elastic properties and intrinsic strength of monolayer graphene," *Science*, vol. 321, no. 5887, pp. 385–8, Jul. 2008.
- [51] M. F. El-Kady, V. Strong, S. Dubin, and R. B. Kaner, "Laser scribing of high-performance and flexible graphene-based electrochemical capacitors," *Science*, vol. 335, no. 6074, pp. 1326–30, Mar. 2012.
- [52] Z. Weng, Y. Su, D.-W. Wang, F. Li, J. Du, and H.-M. Cheng, "Graphene-Cellulose Paper Flexible Supercapacitors," *Adv. Energy Mater.*, vol. 1, no. 5, pp. 917–922, Oct. 2011.
- [53] C.-C. Hu, M.-J. Liu, and K.-H. Chang, "Anodic deposition of hydrous ruthenium oxide for supercapacitors," *J. Power Sources*, vol. 163, no. 2, pp. 1126–1131, Jan. 2007.
- [54] Y.-Z. Zheng, H.-Y. Ding, and M.-L. Zhang, "Hydrous-ruthenium-oxide thin film electrodes prepared by cathodic electrodeposition for supercapacitors," *Thin Solid Films*, vol. 516, no. 21, pp. 7381–7385, Sep. 2008.
- [55] I.-H. Kim and K.-B. Kim, "Ruthenium Oxide Thin Film Electrodes for Supercapacitors," *Electrochem. Solid-State Lett.*, vol. 4, no. 5, p. A62, 2001.
- [56] T. P. Gujar, V. R. Shinde, C. D. Lokhande, W.-Y. Kim, K.-D. Jung, and O.-S. Joo, "Spray deposited amorphous RuO<sub>2</sub> for an effective use in electrochemical supercapacitor," *Electrochem. commun.*, vol. 9, no. 3, pp. 504–510, Mar. 2007.
- [57] W. Lee, R. S. Mane, V. V. Todkar, S. Lee, O. Egorova, W.-S. Chae, and S.-H. Han, "Implication of Liquid-Phase Deposited Amorphous RuO<sub>2</sub> Electrode for Electrochemical Supercapacitor," *Electrochem. Solid-State Lett.*, vol. 10, no. 9, p. A225, 2007.
- [58] C.-C. Hu, C.-C. Wang, and K.-H. Chang, "A comparison study of the capacitive behavior for sol-gel-derived and co-annealed ruthenium-tin oxide composites," *Electrochim. Acta*, vol. 52, no. 7, pp. 2691–2700, Feb. 2007.

- [59] J. H. Park and O. O. Park, "Morphology and electrochemical behaviour of ruthenium oxide thin film deposited on carbon paper," *J. Power Sources*, vol. 109, no. 1, pp. 121–126, Jun. 2002.
- [60] S.-L. Kuo and N.-L. Wu, "Investigation of Pseudocapacitive Charge-Storage Reaction of  $\text{MnO}_2 \cdot n\text{H}_2\text{O}$  Supercapacitors in Aqueous Electrolytes," *J. Electrochem. Soc.*, vol. 153, no. 7, p. A1317, 2006.
- [61] C.-C. Hu and C.-C. Wang, "Nanostructures and Capacitive Characteristics of Hydrous Manganese Oxide Prepared by Electrochemical Deposition," *J. Electrochem. Soc.*, vol. 150, no. 8, p. A1079, 2003.
- [62] X. Zhang, W. Yang, and D. G. Evans, "Layer-by-layer self-assembly of manganese oxide nanosheets/polyethylenimine multilayer films as electrodes for supercapacitors," *J. Power Sources*, vol. 184, no. 2, pp. 695–700, Oct. 2008.
- [63] S.-C. Pang, M. A. Anderson, and T. W. Chapman, "Novel Electrode Materials for Thin-Film Ultracapacitors: Comparison of Electrochemical Properties of Sol-Gel-Derived and Electrodeposited Manganese Dioxide," *J. Electrochem. Soc.*, vol. 147, no. 2, p. 444, 2000.
- [64] T. Cottineau, M. Toupin, T. Delahaye, T. Brousse, and D. Bélanger, "Nanostructured transition metal oxides for aqueous hybrid electrochemical supercapacitors," *Appl. Phys. A*, vol. 82, no. 4, pp. 599–606, Nov. 2005.
- [65] H. Shirakawa, E. J. Louis, A. G. MacDiarmid, C. K. Chiang, and A. J. Heeger, "Synthesis of electrically conducting organic polymers: halogen derivatives of polyacetylene,  $(\text{CH})_x$ ," *J. Chem. Soc. Chem. Commun.*, no. 16, p. 578, 1977.
- [66] R. B. Kaner and A. G. MacDiarmid, "Electrochemistry of polyacetylene,  $(\text{CH})_x$ . Characteristics of the reduced polyacetylene electrode," *J. Chem. Soc. Faraday Trans. 1 Phys. Chem. Condens. Phases*, vol. 80, no. 8, p. 2109, 1984.
- [67] J. Caja, R. B. Kaner, and A. G. MacDiarmid, "RECHARGEABLE BATTERY EMPLOYING A REDUCED POLYACETYLENE ANODE AND A TITANIUM DISULFIDE CATHODE," *J. Electrochem. Soc.*, vol. 131, no. 12, pp. 2744–2750, 1984.
- [68] R. J. Mammone and A. G. MacDiarmid, "The aqueous chemistry and electrochemistry of polyacetylene,  $(\text{CH})_x$ ," *Synth. Met.*, vol. 9, no. 2, pp. 143–154, Apr. 1984.
- [69] R. B. Kaner and A. G. Macdiarmid, "Reversible electrochemical reduction of polyacetylene,  $(\text{CH})_x$ ," *Synth. Met.*, vol. 14, no. 1–2, pp. 3–12, Mar. 1986.
- [70] E. Llorens, E. Armelin, M. del Mar Pérez-Madrigal, L. del Valle, C. Alemán, and J. Puiggali, "Nanomembranes and Nanofibers from Biodegradable Conducting Polymers," *Polymers (Basel)*, vol. 5, no. 3, pp. 1115–1157, Sep. 2013.

- [71] R. Liu, S. Il Cho, and S. B. Lee, "Poly(3,4-ethylenedioxythiophene) nanotubes as electrode materials for a high-powered supercapacitor.," *Nanotechnology*, vol. 19, no. 21, p. 215710, May 2008.
- [72] R. K. Sharma, A. C. Rastogi, and S. B. Desu, "Pulse polymerized polypyrrole electrodes for high energy density electrochemical supercapacitor.," *Electrochem. commun.*, vol. 10, no. 2, pp. 268–272, Feb. 2008.
- [73] A. Subramania and S. L. Devi, "Polyaniline nanofibers by surfactant-assisted dilute polymerization for supercapacitor applications.," *Polym. Adv. Technol.*, vol. 19, no. 7, pp. 725–727, Jul. 2008.
- [74] C. Meng, C. Liu, L. Chen, C. Hu, and S. Fan, "Highly flexible and all-solid-state paperlike polymer supercapacitors.," *Nano Lett.*, vol. 10, no. 10, pp. 4025–31, Oct. 2010.
- [75] K. Wang, J. Huang, and Z. Wei, "Conducting Polyaniline Nanowire Arrays for High Performance Supercapacitors.," *J. Phys. Chem. C*, vol. 114, no. 17, pp. 8062–8067, May 2010.
- [76] V. S. Jamadade, D. S. Dhawale, and C. D. Lokhande, "Studies on electrosynthesized leucoemeraldine, emeraldine and pernigraniline forms of polyaniline films and their supercapacitive behavior.," *Synth. Met.*, vol. 160, no. 9–10, pp. 955–960, May 2010.
- [77] H. Letheby, "XXIX. - On the production of a blue substance by the electrolysis of sulphate of aniline.," *J. Chem. Soc.*, vol. 15, p. 161, Jan. 1862.
- [78] E. T. Kang, K. G. Neoh, and K. L. Tan, "Polyaniline: A polymer with many interesting intrinsic redox states.," *Prog. Polym. Sci.*, vol. 23, no. 2, pp. 277–324, 1998.
- [79] K. Hu, D. D. Kulkarni, I. Choi, and V. V. Tsukruk, "Graphene-polymer nanocomposites for structural and functional applications.," *Prog. Polym. Sci.*, vol. 39, no. 11, pp. 1934–1972, Nov. 2014.
- [80] W. Wang, S. Guo, I. Lee, K. Ahmed, J. Zhong, Z. Favors, F. Zaera, M. Ozkan, and C. S. Ozkan, "Hydrous ruthenium oxide nanoparticles anchored to graphene and carbon nanotube hybrid foam for supercapacitors.," *Sci. Rep.*, vol. 4, p. 4452, Jan. 2014.
- [81] Z.-S. Wu, D.-W. Wang, W. Ren, J. Zhao, G. Zhou, F. Li, and H.-M. Cheng, "Anchoring Hydrous RuO<sub>2</sub> on Graphene Sheets for High-Performance Electrochemical Capacitors.," *Adv. Funct. Mater.*, vol. 20, no. 20, pp. 3595–3602, Oct. 2010.
- [82] G. Xiong, K. P. S. S. Hembram, R. G. Reifenberger, and T. S. Fisher, "MnO<sub>2</sub>-coated graphitic petals for supercapacitor electrodes.," *J. Power Sources*, vol. 227, pp. 254–259, Apr. 2013.

- [83] Y. Qian, S. Lu, and F. Gao, "Preparation of MnO<sub>2</sub>/graphene composite as electrode material for supercapacitors," *J. Mater. Sci.*, vol. 46, no. 10, pp. 3517–3522, Jan. 2011.
- [84] B. Wang, J. Park, C. Wang, H. Ahn, and G. Wang, "Mn<sub>3</sub>O<sub>4</sub> nanoparticles embedded into graphene nanosheets: Preparation, characterization, and electrochemical properties for supercapacitors," *Electrochim. Acta*, vol. 55, no. 22, pp. 6812–6817, Sep. 2010.
- [85] S.-J. Kim, G.-J. Park, B. C. Kim, J.-K. Chung, G. G. Wallace, and S.-Y. Park, "Investigations into the electrochemical characteristics of nickel oxide hydroxide/multi-walled carbon nanotube nanocomposites for use as supercapacitor electrodes," *Synth. Met.*, vol. 161, no. 23–24, pp. 2641–2646, Jan. 2012.
- [86] C. Xiang, M. Li, M. Zhi, A. Manivannan, and N. Wu, "A reduced graphene oxide/Co<sub>3</sub>O<sub>4</sub> composite for supercapacitor electrode," *J. Power Sources*, vol. 226, pp. 65–70, Mar. 2013.
- [87] A. K. Mishra and S. Ramaprabhu, "Functionalized Graphene-Based Nanocomposites for Supercapacitor Application," *J. Phys. Chem. C*, vol. 115, no. 29, pp. 14006–14013, Jul. 2011.
- [88] J. Wang, Z. Gao, Z. Li, B. Wang, Y. Yan, Q. Liu, T. Mann, M. Zhang, and Z. Jiang, "Green synthesis of graphene nanosheets/ZnO composites and electrochemical properties," *J. Solid State Chem.*, vol. 184, no. 6, pp. 1421–1427, Jun. 2011.
- [89] F. Alvi, M. K. Ram, P. A. Basnayaka, E. Stefanakos, Y. Goswami, and A. Kumar, "Graphene–polyethylenedioxythiophene conducting polymer nanocomposite based supercapacitor," *Electrochim. Acta*, vol. 56, no. 25, pp. 9406–9412, Oct. 2011.
- [90] P. A. Basnayaka, M. K. Ram, L. Stefanakos, and A. Kumar, "Graphene/Polypyrrole Nanocomposite as Electrochemical Supercapacitor Electrode: Electrochemical Impedance Studies," *Graphene*, vol. 02, no. 02, pp. 81–87, Apr. 2013.
- [91] P. A. Basnayaka, M. K. Ram, L. Stefanakos, and A. Kumar, "High performance graphene-poly (o-anisidine) nanocomposite for supercapacitor applications," *Mater. Chem. Phys.*, vol. 141, no. 1, pp. 263–271, Aug. 2013.
- [92] P. A. Basnayaka, M. K. Ram, E. K. Stefanakos, and A. Kumar, "Supercapacitors based on graphene–polyaniline derivative nanocomposite electrode materials," *Electrochim. Acta*, vol. 92, pp. 376–382, Mar. 2013.
- [93] H. Wang, Q. Hao, X. Yang, L. Lu, and X. Wang, "A nanostructured graphene/polyaniline hybrid material for supercapacitors," *Nanoscale*, vol. 2, no. 10, pp. 2164–70, Oct. 2010.
- [94] R. K. Sharma, A. C. Rastogi, and S. B. Desu, "Manganese oxide embedded polypyrrole nanocomposites for electrochemical supercapacitor," *Electrochim. Acta*, vol. 53, no. 26, pp. 7690–7695, Nov. 2008.

- [95] A. G. Pandolfo and A. F. Hollenkamp, "Carbon properties and their role in supercapacitors," *J. Power Sources*, vol. 157, no. 1, pp. 11–27, Jun. 2006.
- [96] M. D. Stoller and R. S. Ruoff, "Best practice methods for determining an electrode material's performance for ultracapacitors," *Energy Environ. Sci.*, vol. 3, no. 9, p. 1294, 2010.
- [97] A. Lewandowski and M. Galinski, "Practical and theoretical limits for electrochemical double-layer capacitors," *J. Power Sources*, vol. 173, no. 2, pp. 822–828, Nov. 2007.
- [98] A. Lewandowski, A. Olejniczak, M. Galinski, and I. Stepniak, "Performance of carbon–carbon supercapacitors based on organic, aqueous and ionic liquid electrolytes," *J. Power Sources*, vol. 195, no. 17, pp. 5814–5819, Sep. 2010.
- [99] M. Galiński, A. Lewandowski, and I. Stepniak, "Ionic liquids as electrolytes," *Electrochim. Acta*, vol. 51, no. 26, pp. 5567–5580, Aug. 2006.
- [100] J. Liu, F. Mirri, M. Notarianni, M. Pasquali, and N. Motta, "High performance all-carbon thin film supercapacitors," *J. Power Sources*, vol. 274, pp. 823–830, Oct. 2014.
- [101] P. T. Kissinger and W. R. Heineman, "Cyclic voltammetry," *Journal of Chemical Education*, vol. 60, no. 9, pp. 702–706, 1983.
- [102] S. Zhang and N. Pan, "Supercapacitors Performance Evaluation," *Adv. Energy Mater.*, vol. 5, no. 6, p. n/a–n/a, Dec. 2014.
- [103] C. Portet, P. Taberna, P. Simon, and C. Laberty-Robert, "Modification of Al current collector surface by sol–gel deposit for carbon–carbon supercapacitor applications," *Electrochim. Acta*, vol. 49, no. 6, pp. 905–912, Mar. 2004.
- [104] B. Fang and L. Binder, "A novel carbon electrode material for highly improved EDLC performance," *J. Phys. Chem. B*, vol. 110, no. 15, pp. 7877–82, Apr. 2006.
- [105] W. Lu, R. Hartman, L. Qu, and L. Dai, "Nanocomposite Electrodes for High-Performance Supercapacitors," *J. Phys. Chem. Lett.*, vol. 2, no. 6, pp. 655–660, Mar. 2011.
- [106] Z. Dai, C. Peng, J. H. Chae, K. C. Ng, and G. Z. Chen, "Cell voltage versus electrode potential range in aqueous supercapacitors," *Sci. Rep.*, vol. 5, p. 9854, Apr. 2015.
- [107] M. Aslan, D. Weingarh, N. Jäckel, J. S. Atchison, I. Grobelsek, and V. Presser, "Polyvinylpyrrolidone as binder for castable supercapacitor electrodes with high electrochemical performance in organic electrolytes," *J. Power Sources*, vol. 266, pp. 374–383, Nov. 2014.

- [108] N. Böckenfeld, S. S. Jeong, M. Winter, S. Passerini, and A. Balducci, "Natural, cheap and environmentally friendly binder for supercapacitors," *J. Power Sources*, vol. 221, pp. 14–20, Jan. 2013.
- [109] B. E. Conway, W. G. Pell, and T. C. Liu, "Diagnostic analyses for mechanisms of self-discharge of electrochemical capacitors and batteries," *J. Power Sources*, vol. 65, no. 1–2, pp. 53–59, 1997.
- [110] J. Niu, B. E. Conway, and W. G. Pell, "Comparative studies of self-discharge by potential decay and float-current measurements at C double-layer capacitor and battery electrodes," *J. Power Sources*, vol. 135, no. 1–2, pp. 332–343, Sep. 2004.
- [111] T. Tevi, H. Yaghoubi, J. Wang, and A. Takshi, "Application of poly (p-phenylene oxide) as blocking layer to reduce self-discharge in supercapacitors," *J. Power Sources*, vol. 241, pp. 589–596, Nov. 2013.
- [112] E. G. Bakhoun, "New mega-Farad ultracapacitors.," *IEEE Trans. Ultrason. Ferroelectr. Freq. Control*, vol. 56, no. 1, pp. 14–21, Jan. 2009.
- [113] S. Okamura, T. Tsukamoto, and N. Koura, "Fabrication of ferroelectric BaTiO<sub>3</sub> films by electrophoretic deposition," *Japanese J. Appl. Physics, Part 1 Regul. Pap. Short Notes Rev. Pap.*, vol. 32, no. 9 B, pp. 4182–4185, 1993.
- [114] T. Tevi and A. Takshi, "Modeling and simulation study of the self-discharge in supercapacitors in presence of a blocking layer," *J. Power Sources*, vol. 273, pp. 857–862, Jan. 2015.
- [115] H. Kim and B. N. Popov, "Characterization of hydrous ruthenium oxide/carbon nanocomposite supercapacitors prepared by a colloidal method," *J. Power Sources*, vol. 104, no. 1, pp. 52–61, Jan. 2002.
- [116] I.-H. Kim and K.-B. Kim, "Ruthenium Oxide Thin Film Electrodes Prepared by Electrostatic Spray Deposition and Their Charge Storage Mechanism," *J. Electrochem. Soc.*, vol. 151, no. 1, p. E7, 2004.
- [117] V. Subramanian, S. C. Hall, P. H. Smith, and B. Rambabu, "Mesoporous anhydrous RuO<sub>2</sub> as a supercapacitor electrode material," *Solid State Ionics*, vol. 175, no. 1–4, pp. 511–515, Nov. 2004.
- [118] U. M. Patil, S. B. Kulkarni, V. S. Jamadade, and C. D. Lokhande, "Chemically synthesized hydrous RuO<sub>2</sub> thin films for supercapacitor application," *J. Alloys Compd.*, vol. 509, no. 5, pp. 1677–1682, Feb. 2011.
- [119] J.-S. Ye, H. F. Cui, X. Liu, T. M. Lim, W.-D. Zhang, and F.-S. Sheu, "Preparation and characterization of aligned carbon nanotube-ruthenium oxide nanocomposites for supercapacitors.," *Small*, vol. 1, no. 5, pp. 560–5, May 2005.

- [120] B. J. Lee, S. R. Sivakkumar, J. M. Ko, J. H. Kim, S. M. Jo, and D. Y. Kim, “Carbon nanofibre/hydrous RuO<sub>2</sub> nanocomposite electrodes for supercapacitors,” *J. Power Sources*, vol. 168, no. 2, pp. 546–552, Jun. 2007.
- [121] B.-O. Park, C. . Lokhande, H.-S. Park, K.-D. Jung, and O.-S. Joo, “Performance of supercapacitor with electrodeposited ruthenium oxide film electrodes—effect of film thickness,” *J. Power Sources*, vol. 134, no. 1, pp. 148–152, Jul. 2004.
- [122] W. Sugimoto, H. Iwata, K. Yokoshima, Y. Murakami, and Y. Takasu, “Proton and electron conductivity in hydrous ruthenium oxides evaluated by electrochemical impedance spectroscopy: the origin of large capacitance.,” *J. Phys. Chem. B*, vol. 109, no. 15, pp. 7330–8, Apr. 2005.
- [123] H. Wang, L. Yu, Y.-H. Lee, Y. Shi, A. Hsu, M. L. Chin, L.-J. Li, M. Dubey, J. Kong, and T. Palacios, “Integrated circuits based on bilayer MoS<sub>2</sub> transistors,” *Nano Lett.*, vol. 12, no. 9, pp. 4674–80, Sep. 2012.
- [124] Y. Yoon, K. Ganapathi, and S. Salahuddin, “How good can monolayer MoS<sub>2</sub> transistors be?,” *Nano Lett.*, vol. 11, no. 9, pp. 3768–73, Sep. 2011.
- [125] T. Korn, S. Heydrich, M. Hirmer, J. Schmutzler, and C. Schüller, “Low-temperature photocarrier dynamics in monolayer MoS<sub>2</sub>,” *Appl. Phys. Lett.*, vol. 99, no. 10, p. 102109, 2011.
- [126] V. Podzorov, M. E. Gershenson, C. Kloc, R. Zeis, and E. Bucher, “High-mobility field-effect transistors based on transition metal dichalcogenides,” *Appl. Phys. Lett.*, vol. 84, no. 17, p. 3301, 2004.
- [127] K. F. Mak, C. Lee, J. Hone, J. Shan, and T. F. Heinz, “Atomically Thin MoS<sub>2</sub>: A New Direct-Gap Semiconductor,” *Phys. Rev. Lett.*, vol. 105, no. 13, p. 136805, Sep. 2010.
- [128] K. Behnia, “Condensed-matter physics: Polarized light boosts valleytronics.,” *Nat. Nanotechnol.*, vol. 7, no. 8, pp. 488–9, Aug. 2012.
- [129] Y.-C. Lin, D. O. Dumcenco, Y.-S. Huang, and K. Suenaga, “Atomic mechanism of the semiconducting-to-metallic phase transition in single-layered MoS<sub>2</sub>.,” *Nat. Nanotechnol.*, vol. 9, no. 5, pp. 391–6, May 2014.
- [130] A. Splendiani, L. Sun, Y. Zhang, T. Li, J. Kim, C.-Y. Chim, G. Galli, and F. Wang, “Emerging photoluminescence in monolayer MoS<sub>2</sub>.,” *Nano Lett.*, vol. 10, no. 4, pp. 1271–5, Apr. 2010.
- [131] K. Lee, H.-Y. Kim, M. Lotya, J. N. Coleman, G.-T. Kim, and G. S. Duesberg, “Electrical characteristics of molybdenum disulfide flakes produced by liquid exfoliation.,” *Adv. Mater.*, vol. 23, no. 36, pp. 4178–82, Sep. 2011.

- [132] M. Kan, J. Y. Wang, X. W. Li, S. H. Zhang, Y. W. Li, Y. Kawazoe, Q. Sun, and P. Jena, "Structures and Phase Transition of a MoS<sub>2</sub> Monolayer," *J. Phys. Chem. C*, vol. 118, no. 3, pp. 1515–1522, Jan. 2014.
- [133] B. Radisavljevic, A. Radenovic, J. Brivio, V. Giacometti, and A. Kis, "Single-layer MoS<sub>2</sub> transistors," *Nat. Nanotechnol.*, vol. 6, no. 3, pp. 147–50, Mar. 2011.
- [134] W. Ho, J. C. Yu, J. Lin, J. Yu, and P. Li, "Preparation and Photocatalytic Behavior of MoS<sub>2</sub> and WS<sub>2</sub> Nanocluster Sensitized TiO<sub>2</sub>," *Langmuir*, vol. 20, no. 14, pp. 5865–5869, Jul. 2004.
- [135] E. Gourmelon, O. Lignier, H. Hadouda, G. Couturier, J. C. Bernède, J. Tedd, J. Pouzet, and J. Salardenne, "MS<sub>2</sub> (M = W, Mo) photosensitive thin films for solar cells," *Sol. Energy Mater. Sol. Cells*, vol. 46, no. 2, pp. 115–121, 1997.
- [136] D. Wang, K. Zhou, M. Sun, Z. Fang, X. Liu, and X. Sun, "Room temperature elemental mercury sensor using MoS<sub>2</sub>-PANI nano-sheet-flowers composite," *Anal. Methods*, vol. 5, no. 23, p. 6576, 2013.
- [137] D. Chen, W. Chen, L. Ma, G. Ji, K. Chang, and J. Y. Lee, "Graphene-like layered metal dichalcogenide/graphene composites: synthesis and applications in energy storage and conversion," *Mater. Today*, vol. 17, no. 4, pp. 184–193, May 2014.
- [138] L. Yang, S. Wang, J. Mao, J. Deng, Q. Gao, Y. Tang, and O. G. Schmidt, "Hierarchical MoS<sub>2</sub> /Polyaniline Nanowires with Excellent Electrochemical Performance for Lithium-Ion Batteries," *Adv. Mater.*, vol. 25, no. 8, pp. 1180–1184, Feb. 2013.
- [139] C. Feng, J. Ma, H. Li, R. Zeng, Z. Guo, and H. Liu, "Synthesis of molybdenum disulfide (MoS<sub>2</sub>) for lithium ion battery applications," *Mater. Res. Bull.*, vol. 44, no. 9, pp. 1811–1815, Sep. 2009.
- [140] J. M. Soon and K. P. Loh, "Electrochemical Double-Layer Capacitance of MoS<sub>2</sub> Nanowall Films," *Electrochem. Solid-State Lett.*, vol. 10, no. 11, p. A250, 2007.
- [141] K. Krishnamoorthy, G. K. Veerasubramani, S. Radhakrishnan, and S. J. Kim, "Supercapacitive properties of hydrothermally synthesized sphere like MoS<sub>2</sub> nanostructures," *Mater. Res. Bull.*, vol. 50, pp. 499–502, Feb. 2014.
- [142] K.-J. Huang, L. Wang, Y.-J. Liu, Y.-M. Liu, H.-B. Wang, T. Gan, and L.-L. Wang, "Layered MoS<sub>2</sub>-graphene composites for supercapacitor applications with enhanced capacitive performance," *Int. J. Hydrogen Energy*, vol. 38, no. 32, pp. 14027–14034, Oct. 2013.
- [143] J. Wang, Z. Wu, K. Hu, X. Chen, and H. Yin, "High conductivity graphene-like MoS<sub>2</sub>/polyaniline nanocomposites and its application in supercapacitor," *J. Alloys Compd.*, vol. 619, pp. 38–43, Jan. 2015.



- [144] K.-J. Huang, L. Wang, J.-Z. Zhang, L.-L. Wang, and Y.-P. Mo, "One-step preparation of layered molybdenum disulfide/multi-walled carbon nanotube composites for enhanced performance supercapacitor," *Energy*, vol. 67, pp. 234–240, Apr. 2014.
- [145] G. Ma, H. Peng, J. Mu, H. Huang, X. Zhou, and Z. Lei, "In situ intercalative polymerization of pyrrole in graphene analogue of MoS<sub>2</sub> as advanced electrode material in supercapacitor," *J. Power Sources*, vol. 229, pp. 72–78, May 2013.
- [146] K. Gopalakrishnan, S. Sultan, A. Govindaraj, and C. N. R. Rao, "Supercapacitors based on composites of PANI with nanosheets of nitrogen-doped RGO, BC1.5N, MoS<sub>2</sub> and WS<sub>2</sub>," *Nano Energy*, vol. 12, pp. 52–58, Mar. 2015.
- [147] K.-J. Huang, L. Wang, Y.-J. Liu, H.-B. Wang, Y.-M. Liu, and L.-L. Wang, "Synthesis of polyaniline/2-dimensional graphene analog MoS<sub>2</sub> composites for high-performance supercapacitor," *Electrochim. Acta*, vol. 109, pp. 587–594, Oct. 2013.
- [148] A. Winchester, S. Ghosh, S. Feng, A. L. Elias, T. Mallouk, M. Terrones, and S. Talapatra, "Electrochemical characterization of liquid phase exfoliated two-dimensional layers of molybdenum disulfide.," *ACS Appl. Mater. Interfaces*, vol. 6, no. 3, pp. 2125–30, Feb. 2014.
- [149] L. Cao, S. Yang, W. Gao, Z. Liu, Y. Gong, L. Ma, G. Shi, S. Lei, Y. Zhang, S. Zhang, R. Vajtai, and P. M. Ajayan, "Direct laser-patterned micro-supercapacitors from paintable MoS<sub>2</sub> films.," *Small*, vol. 9, no. 17, pp. 2905–10, Sep. 2013.
- [150] L. Hu, Y. Ren, H. Yang, and Q. Xu, "Fabrication of 3D hierarchical MoS<sub>2</sub>/polyaniline and MoS<sub>2</sub>/C architectures for lithium-ion battery applications.," *ACS Appl. Mater. Interfaces*, vol. 6, no. 16, pp. 14644–52, Aug. 2014.
- [151] J. Xiao, D. Choi, L. Cosimbescu, P. Koech, J. Liu, and J. P. Lemmon, "Exfoliated MoS<sub>2</sub> Nanocomposite as an Anode Material for Lithium Ion Batteries," *Chem. Mater.*, vol. 22, no. 16, pp. 4522–4524, Aug. 2010.
- [152] Y. Shi, Y. Wang, J. I. Wong, A. Y. S. Tan, C.-L. Hsu, L.-J. Li, Y.-C. Lu, and H. Y. Yang, "Self-assembly of hierarchical MoS<sub>x</sub>/CNT nanocomposites (2<x<3): towards high performance anode materials for lithium ion batteries.," *Sci. Rep.*, vol. 3, p. 2169, Jan. 2013.
- [153] Q. Gao, S. Wang, Y. Tang, and C. Giordano, "Preparation of organic-inorganic hybrid Fe-MoO(x)/polyaniline nanorods as efficient catalysts for alkene epoxidation.," *Chem. Commun. (Camb.)*, vol. 48, no. 2, pp. 260–2, Jan. 2012.
- [154] Z.-A. Hu, Y.-L. Xie, Y.-X. Wang, L.-P. Mo, Y.-Y. Yang, and Z.-Y. Zhang, "Polyaniline/SnO<sub>2</sub> nanocomposite for supercapacitor applications," *Mater. Chem. Phys.*, vol. 114, no. 2–3, pp. 990–995, Apr. 2009.

- [155] S. Liu, X. Zhang, H. Shao, J. Xu, F. Chen, and Y. Feng, "Preparation of MoS<sub>2</sub> nanofibers by electrospinning," *Mater. Lett.*, vol. 73, pp. 223–225, Apr. 2012.
- [156] H. K. Chaudhari and D. S. Kelkar, "X-ray diffraction study of doped polyaniline," *J. Appl. Polym. Sci.*, vol. 62, no. 1, pp. 15–18, 1996.
- [157] J. Luo, H. D. Jang, and J. Huang, "Effect of sheet morphology on the scalability of graphene-based ultracapacitors.," *ACS Nano*, vol. 7, no. 2, pp. 1464–71, Feb. 2013.
- [158] X. Yang, C. Cheng, Y. Wang, L. Qiu, and D. Li, "Liquid-mediated dense integration of graphene materials for compact capacitive energy storage.," *Science*, vol. 341, no. 6145, pp. 534–7, Aug. 2013.
- [159] J. Chmiola, C. Largeot, P.-L. Taberna, P. Simon, and Y. Gogotsi, "Monolithic carbide-derived carbon films for micro-supercapacitors.," *Science*, vol. 328, no. 5977, pp. 480–3, Apr. 2010.
- [160] E. Benavente, "Intercalation chemistry of molybdenum disulfide," *Coord. Chem. Rev.*, vol. 224, no. 1–2, pp. 87–109, Jan. 2002.

## APPENDIX A: COMMERCIAL BARIUM STRONTIUM TITANATE DATASHEET

HPB-1000

Technical Bulletin



Technologies to Products...On the Leading Edge

### NanOxide™ HPB-1000 <100 nm Barium Titanate

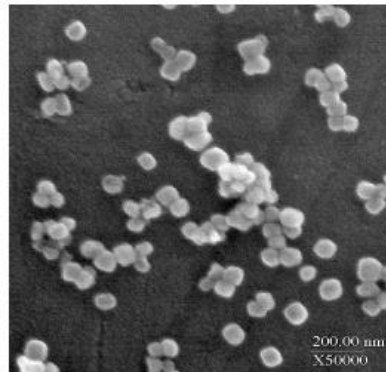
TPL's NanOxide™ is a chemically precipitated high purity barium titanate designed to meet a variety of demanding electronics applications. HPB-1000 has an extremely tight particle size distribution and is the smallest commercially available barium titanate on the market.

It is recommended for dielectric applications in the form of ceramic tapes, monolithic capacitors, and composites.

### Typical Properties

HPB-1000 is a crystallographically cubic, phase pure barium titanate.

Specific Surface Area	15-18 m <sup>2</sup> /g
Nominal Size	50 nm (BET)
Loss On Ignition	<1.5%
pH (ASTM - D1208)	9.0-11.0
Chemical Analysis	
Ba:Ti (XRF)	0.995-1.010
SrO (ICP)	<0.1%
CaO (ICP)	<10 ppm
MgO (ICP)	<10 ppm
SiO <sub>2</sub> (ICP)	<200 ppm
Al <sub>2</sub> O <sub>3</sub> (ICP)	<100 ppm
Fe <sub>2</sub> O <sub>3</sub> (ICP)	<10 ppm
BaTiO <sub>3</sub>	>99.5%



© TPL 2005 HPB-1000 (Rev. 1)

Figure A1 BST datasheet

## APPENDIX B: COPYRIGHT PERMISSIONS FOR FIGURES AND TABLES

Copyright permission for the reuse of content from the accepted manuscript and the modified work is presented as chapter 5 of this dissertation.

[02GRAPH02-1044] Reuse Permission Inbox x 📧 🖨️ 📧

**Mohamad Khawaja** <mkhawaja@mail.usf.edu> May 29 ☆ ↶  
to Ramaprabhu, angpub, aspsupport ▾

Prof. Ramaprabhu,

I am contacting you to requests reuse permission for [02GRAPH02-1044] article that was accepted by your journal. As a first author on the accepted submission, I would like to use the submitted paper as a chapter in my dissertation and will properly reference it under the guidelines of my university.

I have already sent you the signed (by my major professor) copyright transfer agreement and I am now requesting your permission to use the text and figures in my dissertation.

Thank you,  
Mohamad

---

**Ramaprabhu S** Jun 1 (13 days ago) ☆ ↶  
to me, angpub, aspsupport ▾

Dear Author  
You can use your own results, published in GRAPHENE, in your thesis. The figures published may be used with the modified version of the text (do not cut and paste the text of the manuscript).  
Best wishes  
Ramaprabhu S

From: Mohamad Khawaja [mkhawaja@mail.usf.edu]  
Sent: Friday, May 29, 2015 9:45 PM  
To: Ramaprabhu S  
Cc: angpub@covad.net; aspsupport@covad.net  
Subject: [02GRAPH02-1044] Reuse Permission  
...

Copyright permission for the use and reprint of Figure 1.1 is below.



RightsLink®

My Orders > Orders > All Orders

## License Details


This is a License Agreement between Mohamad Khawaja ("You") and Nature Publishing Group ("Nature Publishing Group"). The license consists of your order details, the terms and conditions provided by Nature Publishing Group, and the [payment terms and conditions](#).

[Get the printable license.](#)

License Number	3637871432263
License date	May 28, 2015
Order Content Publisher	Nature Publishing Group
Order Content Publication	Nature Materials
Order Content Title	Materials for electrochemical capacitors
Order Content Author	Patrice Simon and Yury Gogotsi
Order Content Date	Nov 1, 2008
Type of Use	reuse in a dissertation / thesis
Volume number	7
Issue number	11
Requestor type	academic/educational
Format	print and electronic
Portion	figures/tables/illustrations
Number of figures/tables/illustrations	1
High-res required	no
Figures	Figure 1
Author of this NPG article	no
Your reference number	None
Title of your thesis / dissertation	Synthesis and Fabrication of Graphene/Conducting Polymers/Metal Oxides Nanocomposite Materials for Supercapacitor Applications
Expected completion date	Jun 2015
Estimated size (number of pages)	100
<b>Total</b>	<b>0.00 USD</b>

Copyright permission for the use and reprint of Figure 2.1 and Table 2.8 is below.

Webpage Screenshot



# RightsLink®

Account Info

Help

Live Chat

**Title:** Electrochemical supercapacitors for energy storage and delivery : fundamentals and applications

**Article ID:** To be determined

**Publication:** Publication1

**Publisher:** CCC Reproduction

**Date:** Jan 1, 2013

Copyright © 2013, CCC Reproduction

Logged in as:  
Mohamad Khavaja  
Account #: 3000923579

[LOGOUT](#)

**Order Completed**

Thank you for your order.

This Agreement between Mohamad Khavaja ("You") and Taylor and Francis Group LLC Books ("Taylor and Francis Group LLC Books") consists of your order details and the terms and conditions provided by Taylor and Francis Group LLC Books and Copyright Clearance Center.

License number	Reference confirmation email for license number
License date	May 29, 2015
Licensed content publisher	Taylor and Francis Group LLC Books
Licensed content title	Electrochemical supercapacitors for energy storage and delivery : fundamentals and applications
Licensed content date	Jan 1, 2013
Type of use	Thesis/Dissertation
Requestor type	Academic institution
Format	Print, Electronic
Portion	image/photo
Number of images/photos requested	2
Title or numeric reference of the portion(s)	Chapter 1, Figure 1.1. Chapter 4, Table 4.7.
Title of the article or chapter the portion is from	Figure 1.1: Fundamental of Electric Capacitors. Table 4.7: Components and Materials for Electrochemical Supercapacitors.
Editor of portion(s)	N/A
Author of portion(s)	N/A
Volume of serial or monograph	N/A
Issue, if republishing an article from a serial	N/A
Page range of portion	Figure 1.1: page 2. Table 4.7: page 181.
Publication date of portion	2013
Rights for	Main product
Duration of use	Life of current edition
Creation of copies for the disabled	no
With minor editing privileges	yes
For distribution to	Worldwide
In the following language(s)	Original language of publication
With incidental promotional use	no
Lifetime unit quantity of new product	Up to 999
Made available in the following markets	University
The requesting person/organization	Mohamad Khavaja / University of South Florida
Order reference number	None
Author/Editor	Mohamad Khavaja
The standard identifier	NA
Title	Synthesis and Fabrication of Graphene/Conducting Polymers/Metal Oxides Nanocomposite Materials for Supercapacitor Applications
Publisher	University of South Florida
Expected publication date	Jun 2015
Estimated size (pages)	100
Billing Type	Invoice
Billing address	Mohamad Khavaja 4202 E Fowler Ave. ENB 118  TAMPA, FL 33620 United States Attn: Mohamad Khavaja
Total (may include CCC user fee)	0.00 USD

CLOSE WINDOW

Copyright © 2015 Copyright Clearance Center, Inc. All Rights Reserved. [Privacy statement](#). [Terms and Conditions](#). Comments? We would like to hear from you. E-mail us at [customercare@copyright.com](mailto:customercare@copyright.com)

<https://s100.copyright.com/AppDispatchServlet> Wed Jun 03 2015 12:20:36 GMT-0400 (Eastern Daylight Time)

Copyright permission for the use and reprint of Figure 2.3 is below.



RightsLink®

[My Orders](#)

[My Library](#)

[My Profile](#)

Welcome mkhawaja@mail.usf.edu

[Log out](#) | [Help](#)

[My Orders](#) > [Orders](#) > [All Orders](#)

## License Details

This Agreement between Mohamad Khawaja ("You") and John Wiley and Sons ("John Wiley and Sons") consists of your license details and the terms and conditions provided by John Wiley and Sons and Copyright Clearance Center.

[Get the printable license.](#)

License Number	3637861216131
License date	May 28, 2015
Licensed Content Publisher	John Wiley and Sons
Licensed Content Publication	Canadian Journal of Chemical Engineering
Licensed Content Title	Material advancements in supercapacitors: From activated carbon to carbon nanotube and graphene
Licensed Content Author	Aaron Davies, Aiping Yu
Licensed Content Date	Jun 21, 2011
Licensed Content Pages	16
Type of use	Dissertation/Thesis
Requestor type	University/Academic
Format	Print and electronic
Portion	Figure/table
Number of figures/tables	1
Original Wiley figure/table number(s)	Figure 2
Will you be translating?	No
Title of your thesis / dissertation	Synthesis and Fabrication of Graphene/Conducting Polymers/Metal Oxides Nanocomposite Materials for Supercapacitor Applications
Expected completion date	Jun 2015
Expected size (number of pages)	100
Requestor Location	Mohamad Khawaja 4202 E Fowler Ave. ENB 118 None TAMPA, FL 33620 United States Attn: Mohamad Khawaja
Billing Type	Invoice
Billing address	Mohamad Khawaja 4202 E Fowler Ave. ENB 118 None TAMPA, FL 33620 United States Attn: Mohamad Khawaja
<b>Total</b>	<b>0.00 USD</b>

Copyright permission for the use and reprint of Figure 2.4 and Table 2.3 is below.



RightsLink®

[My Orders](#)

[My Library](#)

[My Profile](#)

Welcome mkhawaja@mail.usf.edu

[Log out](#) | [Help](#)

[My Orders](#) > [Orders](#) > [All Orders](#)

## License Details

This is a License Agreement between Mohamad Khawaja ("You") and Royal Society of Chemistry ("Royal Society of Chemistry"). The license consists of your order details, the terms and conditions provided by Royal Society of Chemistry, and the [payment terms and conditions](#).

[Get the printable license.](#)

License Number	3637871020295
License date	May 28, 2015
Order Content Publisher	Royal Society of Chemistry
Order Content Publication	Chemical Society Reviews
Order Content Title	Carbon-based materials as supercapacitor electrodes
Order Content Author	Li Li Zhang,X. S. Zhao
Order Content Date	Jun 12, 2009
Volume number	38
Issue number	9
Type of Use	Thesis/Dissertation
Requestor type	academic/educational
Portion	figures/tables/images
Number of figures/tables/images	2
Distribution quantity	10
Format	print and electronic
Will you be translating?	no
Order reference number	None
Title of the thesis/dissertation	Synthesis and Fabrication of Graphene/Conducting Polymers/Metal Oxides Nanocomposite Materials for Supercapacitor Applications
Expected completion date	Jun 2015
Estimated size	100
<b>Total</b>	<b>0.00 USD</b>



Copyright permission for the use and reprint of Figure 2.6 is below.



RightsLink®

My Orders > Orders > All Orders

## License Details

Thank you very much for your order.

This is a License Agreement between Mohamad Khawaja ("You") and Elsevier ("Elsevier"). The license consists of your order details, the terms and conditions provided by Elsevier, and the [payment terms and conditions](#).

[Get the printable license.](#)

License Number	3637880726172
License date	May 28, 2015
Order Content Publisher	Elsevier
Order Content Publication	Renewable and Sustainable Energy Reviews
Order Content Title	Emerging applications of graphene and its derivatives in carbon capture and conversion: Current status and future prospects
Order Content Author	Amin Taheri Najafabadi
Order Content Date	January 2015
Licensed content volume number	41
Licensed content issue number	n/a
Number of pages	31
Type of Use	reuse in a thesis/dissertation
Portion	figures/tables/illustrations
Number of figures/tables/illustrations	1
Format	both print and electronic
Are you the author of this Elsevier article?	No
Will you be translating?	No
Original figure numbers	Figure 1
Title of your thesis/dissertation	Synthesis and Fabrication of Graphene/Conducting Polymers/Metal Oxides Nanocomposite Materials for Supercapacitor Applications
Expected completion date	Jun 2015
Estimated size (number of pages)	100
Elsevier VAT number	GB 494 6272 12
Price	0.00 USD
VAT/Local Sales Tax	0.00 USD / 0.00 GBP
Total	<b>0.00 USD</b>

Copyright permission for the use and reprint of Figure 2.8 is below.



RightsLink®

[My Orders](#)

[My Library](#)

[My Profile](#)

Welcome mkhawaja@mail.usf.edu [Log out](#) | [Help](#)

[My Orders](#) > [Orders](#) > [All Orders](#)

## License Details

Thank you very much for your order.

This is a License Agreement between Mohamad Khawaja ("You") and Elsevier ("Elsevier"). The license consists of your order details, the terms and conditions provided by Elsevier, and the [payment terms and conditions](#).

[Get the printable license.](#)

License Number	3658210415905
License date	Jun 28, 2015
Licensed Content Publisher	Elsevier
Licensed Content Publication	Synthetic Metals
Licensed Content Title	Studies on electrosynthesized leucoemeraldine, emeraldine and pernigraniline forms of polyaniline films and their supercapacitive behavior
Licensed Content Author	V.S. Jamadade,D.S. Dhawale,C.D. Lokhande
Licensed Content Date	May 2010
Licensed content volume number	160
Licensed content issue number	9-10
Number of pages	6
Type of Use	reuse in a thesis/dissertation
Portion	figures/tables/illustrations
Number of figures/tables/illustrations	1
Format	both print and electronic
Are you the author of this Elsevier article?	No
Will you be translating?	No
Original figure numbers	Figure 1
Title of your thesis/dissertation	Synthesis and Fabrication of Graphene/Conducting Polymers/Metal Oxides Nanocomposite Materials for Supercapacitor Applications
Expected completion date	Jun 2015
Elsevier VAT number	GB 494 6272 12
Price	0.00 USD
VAT/Local Sales Tax	0.00 USD / 0.00 GBP
Total	<b>0.00 USD</b>

Copyright permission for the use and reprint of Figure 2.9(a) is below.



RightsLink®

Home

Account  
Info

Help



ACS Publications  
Most Trusted. Most Cited. Most Read.

**Title:** Graphene-Based Ultracapacitors  
**Author:** Meryl D. Stoller, Sungjin Park,  
Yanwu Zhu, et al

**Publication:** Nano Letters

**Publisher:** American Chemical Society

**Date:** Oct 1, 2008

Copyright © 2008, American Chemical Society

Logged in as:  
Mohamad Khawaja

LOGOUT

### PERMISSION/LICENSE IS GRANTED FOR YOUR ORDER AT NO CHARGE

This type of permission/license, instead of the standard Terms & Conditions, is sent to you because no fee is being charged for your order. Please note the following:

- Permission is granted for your request in both print and electronic formats, and translations.
- If figures and/or tables were requested, they may be adapted or used in part.
- Please print this page for your records and send a copy of it to your publisher/graduate school.
- Appropriate credit for the requested material should be given as follows: "Reprinted (adapted) with permission from (COMPLETE REFERENCE CITATION). Copyright (YEAR) American Chemical Society." Insert appropriate information in place of the capitalized words.
- One-time permission is granted only for the use specified in your request. No additional uses are granted (such as derivative works or other editions). For any other uses, please submit a new request.

If credit is given to another source for the material you requested, permission must be obtained from that source.

Copyright permission for the use and reprint of Figure 2.11 is below.



RightsLink®

Home

Account  
Info

Help



ACS Publications  
Most Trusted. Most Cited. Most Read.

**Title:** Cyclic voltammetry  
**Author:** Peter T. Kissinger, William R. Heineman

**Publication:** Journal of Chemical Education

**Publisher:** American Chemical Society

**Date:** Sep 1, 1983

Copyright © 1983, American Chemical Society

Logged in as:  
Mohamad Khawaja

LOGOUT

### PERMISSION/LICENSE IS GRANTED FOR YOUR ORDER AT NO CHARGE

This type of permission/license, instead of the standard Terms & Conditions, is sent to you because no fee is being charged for your order. Please note the following:

- Permission is granted for your request in both print and electronic formats, and translations.
- If figures and/or tables were requested, they may be adapted or used in part.
- Please print this page for your records and send a copy of it to your publisher/graduate school.
- Appropriate credit for the requested material should be given as follows: "Reprinted (adapted) with permission from (COMPLETE REFERENCE CITATION). Copyright (YEAR) American Chemical Society." Insert appropriate information in place of the capitalized words.
- One-time permission is granted only for the use specified in your request. No additional uses are granted (such as derivative works or other editions). For any other uses, please submit a new request.

If credit is given to another source for the material you requested, permission must be obtained from that source.

Copyright permission for the use and reprint of Figure 2.14 is below.



RightsLink®

My Orders > Orders > All Orders

## License Details

This Agreement between Mohamad Khawaja ("You") and John Wiley and Sons ("John Wiley and Sons") consists of your license details and the terms and conditions provided by John Wiley and Sons and Copyright Clearance Center.

[Get the printable license.](#)

License Number	3637881291998
License date	May 28, 2015
Licensed Content Publisher	John Wiley and Sons
Licensed Content Publication	Advanced Energy Materials
Licensed Content Title	Supercapacitors Performance Evaluation
Licensed Content Author	Sanliang Zhang,Ning Pan
Licensed Content Date	Dec 12, 2014
Licensed Content Pages	1
Type of use	Dissertation/Thesis
Requestor type	University/Academic
Format	Print and electronic
Portion	Figure/table
Number of figures/tables	1
Original Wiley figure/table number(s)	Figure 1
Will you be translating?	No
Title of your thesis / dissertation	Synthesis and Fabrication of Graphene/Conducting Polymers/Metal Oxides Nanocomposite Materials for Supercapacitor Applications
Expected completion date	Jun 2015
Expected size (number of pages)	100
Requestor Location	Mohamad Khawaja 4202 E Fowler Ave. ENB 118 None TAMPA, FL 33620 United States Attn: Mohamad Khawaja
Billing Type	Invoice
Billing address	Mohamad Khawaja 4202 E Fowler Ave. ENB 118 None TAMPA, FL 33620 United States Attn: Mohamad Khawaja
<b>Total</b>	<b>0.00 USD</b>

Copyright permission for the use and reprint of Table 2.1 is below.



RightsLink®

[My Orders](#)

[My Library](#)

[My Profile](#)

Welcome mkhawaja@mail.usf.edu

[Log out](#) | [Help](#)

[My Orders](#) > [Orders](#) > [All Orders](#)

## License Details

This is a License Agreement between Mohamad Khawaja ("You") and Springer ("Springer"). The license consists of your order details, the terms and conditions provided by Springer, and the [payment terms and conditions](#).

[Get the printable license.](#)

License Number	3637890115116
License date	May 28, 2015
Order Content Publisher	Springer
Order Content Publication	Journal of Solid State Electrochemistry
Order Content Title	Double-layer and pseudocapacitance types of electrochemical capacitors and their applications to the development of hybrid devices
Order Content Author	B. E. Conway
Order Content Date	Jan 1, 2003
Volume number	7
Issue number	9
Type of Use	Thesis/Dissertation
Portion	Figures
Author of this Springer article	No
Original figure numbers	Table 2
Title of your thesis / dissertation	Synthesis and Fabrication of Graphene/Conducting Polymers/Metal Oxides Nanocomposite Materials for Supercapacitor Applications
Expected completion date	Jun 2015
Estimated size(pages)	100
<b>Total</b>	<b>0.00 USD</b>

Copyright permission for the use and reprint of Table 2.2 is below.



RightsLink®

[My Orders](#)

[My Library](#)

[My Profile](#)

Welcome mkhawaja@mail.usf.edu

[Log out](#) | [Help](#)

[My Orders](#) > [Orders](#) > [All Orders](#)

## License Details

Thank you very much for your order.

This is a License Agreement between Mohamad Khawaja ("You") and Elsevier ("Elsevier"). The license consists of your order details, the terms and conditions provided by Elsevier, and the [payment terms and conditions](#).

[Get the printable license.](#)

License Number	3637890722956
License date	May 28, 2015
Order Content Publisher	Elsevier
Order Content Publication	International Journal of Hydrogen Energy
Order Content Title	Progress of electrochemical capacitor electrode materials: A review
Order Content Author	Yong Zhang,Hui Feng,Xingbing Wu,Lizhen Wang,Aiqin Zhang,Tongchi Xia,Huichao Dong,Xiaofeng Li,Linsen Zhang
Order Content Date	June 2009
Licensed content volume number	34
Licensed content issue number	11
Number of pages	11
Type of Use	reuse in a thesis/dissertation
Portion	figures/tables/illustrations
Number of figures/tables/illustrations	1
Format	both print and electronic
Are you the author of this Elsevier article?	No
Will you be translating?	No
Original figure numbers	Table 2
Title of your thesis/dissertation	Synthesis and Fabrication of Graphene/Conducting Polymers/Metal Oxides Nanocomposite Materials for Supercapacitor Applications
Expected completion date	Jun 2015
Estimated size (number of pages)	100
Elsevier VAT number	GB 494 6272 12
Price	0.00 USD
VAT/Local Sales Tax	0.00 USD / 0.00 GBP
Total	<b>0.00 USD</b>

Copyright permission for the use and reprint of Table 2.4 is below.



RightsLink®

My Orders > Orders > All Orders

## License Details

Thank you very much for your order.

This is a License Agreement between Mohamad Khawaja ("You") and Elsevier ("Elsevier"). The license consists of your order details, the terms and conditions provided by Elsevier, and the [payment terms and conditions](#).


[Get the printable license.](#)

License Number	3637891386286
License date	May 28, 2015
Order Content Publisher	Elsevier
Order Content Publication	Nano Energy
Order Content Title	Graphene/metal oxide composite electrode materials for energy storage
Order Content Author	Zhong-Shuai Wu,Guangmin Zhou,Li-Chang Yin,Wencai Ren,Feng Li,Hui-Ming Cheng
Order Content Date	January 2012
Licensed content volume number	1
Licensed content issue number	1
Number of pages	25
Type of Use	reuse in a thesis/dissertation
Portion	figures/tables/illustrations
Number of figures/tables/illustrations	1
Format	both print and electronic
Are you the author of this Elsevier article?	No
Will you be translating?	No
Original figure numbers	Table 1
Title of your thesis/dissertation	Synthesis and Fabrication of Graphene/Conducting Polymers/Metal Oxides Nanocomposite Materials for Supercapacitor Applications
Expected completion date	Jun 2015
Estimated size (number of pages)	100
Elsevier VAT number	GB 494 6272 12
Price	0.00 USD
VAT/Local Sales Tax	0.00 USD / 0.00 GBP
Total	<b>0.00 USD</b>



Copyright permission for the use and reprint of Table 2.8 (The ion size portion only) and

Table 2.9 is below.



My Orders   My Library   My Profile   Welcome mkhawaja@mail.usf.edu   [Log out](#) | [Help](#)

My Orders > Orders > All Orders

## License Details

Thank you very much for your order.

This is a License Agreement between Mohamad Khawaja ("You") and Elsevier ("Elsevier"). The license consists of your order details, the terms and conditions provided by Elsevier, and the [payment terms and conditions](#).

[Get the printable license.](#)

License Number	3637891084793
License date	May 28, 2015
Order Content Publisher	Elsevier
Order Content Publication	Journal of Power Sources
Order Content Title	Carbon materials for electrochemical capacitors
Order Content Author	Michio Inagaki,Hidetaka Konno,Osamu Tanaike
Order Content Date	15 December 2010
Licensed content volume number	195
Licensed content issue number	24
Number of pages	24
Type of Use	reuse in a thesis/dissertation
Portion	figures/tables/illustrations
Number of figures/tables/illustrations	1
Format	both print and electronic
Are you the author of this Elsevier article?	No
Will you be translating?	No
Original figure numbers	Table 1
Title of your thesis/dissertation	Synthesis and Fabrication of Graphene/Conducting Polymers/Metal Oxides Nanocomposite Materials for Supercapacitor Applications
Expected completion date	Jun 2015
Estimated size (number of pages)	100
Elsevier VAT number	GB 494 6272 12
Price	0.00 USD
VAT/Local Sales Tax	0.00 USD / 0.00 GBP
Total	<b>0.00 USD</b>